

**CHARACTERIZATION OF THE EFFICACY OF  
STENT GRAFT TREATMENT IN PATIENTS WITH  
AORTIC DISSECTION USING COMPUTATIONAL  
FLUID DYNAMICS ANALYSIS**

**WAN NAIMAH BINTI WAN AB NAIM**

**THESIS SUBMITTED IN FULFILMENT OF THE  
REQUIREMENTS FOR THE DEGREE OF DOCTOR OF  
PHILOSOPHY**

**FACULTY OF ENGINEERING  
UNIVERSITY OF MALAYA  
KUALA LUMPUR**

**2018**

**UNIVERSITY OF MALAYA**  
**ORIGINAL LITERARY WORK DECLARATION**

Name of Candidate: Wan Naimah Wan Ab Naim

Matric No: KHA 130076

Name of Degree: Doctor of Philosophy

Title of Project Paper/Research Report/Dissertation/Thesis (“this Work”):

Characterization of the efficacy of stent graft treatment in patients with aortic dissection using computational fluid dynamics analysis.

Field of Study: Biomedical engineering

I do solemnly and sincerely declare that:

- (1) I am the sole author/writer of this Work;
- (2) This Work is original;
- (3) Any use of any work in which copyright exists was done by way of fair dealing and for permitted purposes and any excerpt or extract from, or reference to or reproduction of any copyright work has been disclosed expressly and sufficiently and the title of the Work and its authorship have been acknowledged in this Work;
- (4) I do not have any actual knowledge nor do I ought reasonably to know that the making of this work constitutes an infringement of any copyright work;
- (5) I hereby assign all and every rights in the copyright to this Work to the University of Malaya (“UM”), who henceforth shall be owner of the copyright in this Work and that any reproduction or use in any form or by any means whatsoever is prohibited without the written consent of UM having been first had and obtained;
- (6) I am fully aware that if in the course of making this Work I have infringed any copyright whether intentionally or otherwise, I may be subject to legal action or any other action as may be determined by UM.

Candidate’s Signature

Date:

Subscribed and solemnly declared before,

Witness’s Signature

Date:

Name:

Designation:

**CHARACTERIZATION OF THE EFFICACY OF STENT GRAFT  
TREATMENT IN PATIENTS WITH AORTIC DISSECTION USING  
COMPUTATIONAL FLUID DYNAMICS ANALYSIS**

**ABSTRACT**

Aortic dissection (AD), characterized by separation of the layers of the aortic wall, poses a significant challenge for clinicians. While Stanford Type A AD patients are normally managed using surgical treatment, the optimal treatment strategy for Stanford Type B AD remains controversial. Recently, stent graft treatment for Stanford Type B AD has become more common. The primary aim of placing the stent graft in AD patients is to occlude the primary entry tear so as to restore true lumen (TL) flow and induce false lumen (FL) thrombosis. Even though FL thrombosis indicates a better long term prognosis, many studies have documented that the FL was not completely thrombosed distal to the stent graft. By improving understanding on which group of patients are most likely to benefit from stent graft treatment; a better assessment can be achieved. This project aims to evaluate the progression of Stanford Type B AD after stent grafting using clinical and using computational fluid dynamics (CFD) studies in order to predict the cause of incomplete FL thrombosis. To achieve this aim, analysis of computed tomography angiography (CTA) images for thirteen AD patients who underwent stent graft treatment was performed. The distribution of thrombus was identified, while both diametric and volumetric measurements of the TL and FL at the thoracic and abdominal levels were calculated to investigate their changes after stent graft implantation as well as during the follow-up periods. Next, a preliminary study to predict the formation of thrombus in a Stanford type B AD patient was carried out using CFD. Further extension of the CFD approach was performed to investigate factors leading to the formation of thrombus and aortic remodelling in AD patients implanted with stent grafts using the longitudinal CTA images obtained from five AD patients. In

comparison to the dimensional and volumetric measurements, volume measurement was shown to provide supportive information in terms of the morphological changes of aortic dissection after stent grafting repair. Patients with dissection up to the abdominal vicinity, no re-entry tears, and branches partially supplied by the FL at the end of the dissection, were more likely to develop complete FL thrombosis. The morphological results were further supported by the CFD analysis, where patients with more than 80% FL thrombosis had concentrated short distance communications around the abdominal branches, while less than 80% FL thrombosis patients had re-entry tears spreading out along the dissection, which created continuous flow activities inside the FL that disrupted thrombosis. Besides tear distributions, thrombosis was also affected by the number of re-entry tears and the presence of abdominal branches being supplied by the FL. Blood flow inside the FL which affected the formation of thrombus, increased with the number of re-entry tears and when only small amounts of blood that entered the FL exited through the branches. Based on low time-averaged wall shear stress (TAWSS) and high relative residence time (RRT) distributions, all patients showed thrombus formation at the upper FL region, particularly at the vicinity of the closed primary entry tear.

**Keywords:** Aortic dissection, stent graft, thrombosis, computational fluid dynamics

**PENCIRIAN KEBERKESANAN RAWATAN STENT GRAFT DI KALANGAN  
PESAKIT BELAHAN AORTA DENGAN MENGGUNAKAN KAEDAH  
PENGIRAAN BERKOMPUTER DINAMIK BENDALIR**

**ABSTRAK**

Belahan aorta (AD), dicirikan sebagai belahan pada dinding aorta, memberikan cabaran besar kepada pengamal perubatan. Walaupun pesakit Stanford Jenis A AD biasanya dirawat dengan menggunakan cara pembedahan, strategi rawatan yang optimum untuk pesakit Stanford Jenis B AD masih kontroversi. Baru-baru ini, rawatan *stent graft* bagi pesakit Stanford Jenis B AD telah menjadi biasa. Tujuan utama meletakkan *stent graft* pada pesakit AD adalah untuk menutup lubang bukaan utama bagi memulihkan pengaliran darah di lumen yang benar (TL) dan mendorong *thrombosis* atau pembekuan darah di lumen yang palsu (FL). Walaupun pembekuan darah di FL menunjukkan prognosis yang lebih baik dalam jangka masa panjang, banyak kajian telah merekodkan bahawa darah di bahagian FL tidak sepenuhnya membeku di bahagian hujung *stent*. Dengan meningkatkan pemahaman kumpulan pesakit yang mana yang mungkin mendapat manfaat daripada rawatan *stent*; penilaian yang lebih baik boleh dibuat. Justeru itu, kajian ini bertujuan untuk menilai perkembangan pesakit Stanford Jenis B AD selepas rawatan *stent* untuk meramalkan kepada punca tidak lengkapnya pembekuan darah di dalam FL. Untuk mencapai tujuan ini, analisis *computed tomography angiography* (CTA) dilakukan untuk tiga belas pesakit AD yang menjalani rawatan *stent graft*. Pengagihan darah beku dikenal pasti, manakala pengukuran diameter dan isi padu TL dan FL di peringkat toraks dan abdomen dikira bagi menyiasat perubahan pada bahagian ini selepas rawatan *stent* serta semasa tempoh susulan. Seterusnya, kajian awal untuk meramalkan pembentukan darah beku pada pesakit Stanford Jenis B telah dijalankan menggunakan kaedah pengiraan berkomputer dinamik bendalir/ *computational fluid dynamics* (CFD). Pendekatan lanjut menggunakan kaedah

CFD telah dijalankan untuk menyiasat faktor-faktor yang membawa kepada pembentukan darah beku dan pembentukan semula aorta pada pesakit dengan rawatan *stent graft* menggunakan CTA imej yang diperolehi daripada lima pesakit. Bagi perbandingan antara ukuran diameter dan isi padu, isi padu telah memberi maklumat sokongan dari segi perubahan morfologi selepas rawatan. Pesakit dengan FL sehingga ke bahagian abdomen tanpa lubang bukaan semula, serta terdapat arteri yang sebahagiannya dibekalkan oleh FL di akhir bahagian FL, lebih cenderung untuk mempunyai pembekuan darah di dalam FL yang lengkap. Penemuan ini disokong oleh analisis daripada CFD, di mana pesakit dengan lebih daripada 80% pembekuan darah di dalam FL mempunyai sekelompok komunikasi/lubang bukaan semula jarak dekat di sekitar kawasan abdomen manakala pesakit yang mempunyai pembekuan darah di dalam FL kurang daripada 80%, lubang bukaan semula tersebar di sepanjang FL, yang akhirnya menghasilkan aliran aktiviti yang berterusan di dalam FL yang mengganggu pembentukan darah beku. Selain daripada pengagihan lubang bukaan semula di sepanjang FL, pembekuan darah juga dipengaruhi oleh bilangan lubang bukaan semula dan kehadiran abdominal arteri yang dibekalkan oleh FL. Aliran darah di dalam FL yang mempengaruhi pembentukan darah beku, meningkat dengan peningkatan jumlah lubang bukaan masuk semula dan apabila hanya sejumlah kecil darah yang masuk ke dalam FL keluar ke abdominal arteri. Berdasarkan *time-averaged WSS* (TAWSS) yang rendah dan *relative residence time* (RRT) yang tinggi, semua pesakit menunjukkan pembentukan darah beku di bahagian atas FL terutamanya pada bahagian lubang masuk utama yang telah ditutup.

Kata kunci: Belahan aorta, stent graft, pembekuan darah, pengiraan berkomputer dinamik bendalir

## ACKNOWLEDGMENTS

Firstly, I would like to express my sincere gratitude to all my PhD supervisors, Assc. Prof. Ir. Dr. Lim Einly, Assc. Prof. Dr. Poo Balan Ganesan and Prof. Dr. Zhonghua Sun for their continuous supports throughout my PhD journey. Special thanks to Assc. Prof. Ir. Dr. Lim Einly for her persistent guidance. She is a caring and kind-hearted supervisor. My special thanks also go to Assc. Prof. Dr. Poo Balan Ganesan for his sincere advice and guidance. Not to forget, Prof. Sun, he is a kind-hearted and caring supervisor. I really enjoy my stay in Perth during the attachment days. I also would like to thank all my colleagues who always listened to my story and given a good advice, so that I can always climb to the top again.

Very special thanks to my beloved husband who is very understandable and helping me with a lot of things particularly on taking care of our daughter. We managed to handle problems together throughout these years of my study. To my daughter, you are my strength for me to finish my work till the end. To my parents and siblings, thanks for always being there and thanks for your prayers.

## TABLE OF CONTENTS

Abstract .....	iii
Abstrak .....	v
Acknowledgments.....	vii
Table of Contents.....	viii
List of Figures .....	xii
List of Tables .....	xv
List of Symbols and Abbreviations.....	xvii
<b>CHAPTER 1: INTRODUCTION.....</b>	<b>1</b>
1.1 Background.....	1
1.2 Therapeutic approaches to AD .....	4
1.2.1 Medical treatment.....	4
1.2.2 Surgical intervention .....	5
1.2.3 Percutaneous intervention: Aortic fenestration and stent graft placement ..	6
1.3 Problem Statement.....	6
1.4 Aim and Objectives .....	9
1.5 Thesis Scope .....	10
1.6 Thesis Outlines .....	11
<b>CHAPTER 2: LITERATURE REVIEW.....</b>	<b>13</b>
2.1 Patient progression after stent graft treatment: Clinical Perspective.....	13
2.2 Quantitative measurements to quantify AD progression.....	16
2.3 Numerical simulation in AD cases .....	17
2.3.1 Tear initiation in AD .....	19
2.3.2 Progression of AD .....	20

2.3.3	Numerical simulation after stent grafting procedure.....	24
2.4	Summary.....	29
<b>CHAPTER 3: RECONSTRUCTION AND MEASUREMENT OF 3D GEOMETRY OF STANFORD TYPE B AD PATIENTS .....</b>		<b>31</b>
3.1	Introduction.....	31
3.2	Methodology.....	31
3.2.1	Study population.....	31
3.2.2	Ethics application .....	31
3.2.3	CTA images selection .....	32
3.2.4	CTA images segmentation and 3D reconstruction.....	32
3.2.5	Diameter measurements .....	33
3.2.6	Volume measurements .....	33
3.3	Results and Discussion .....	35
3.4	Summary.....	45
<b>CHAPTER 4: MORPHOLOGICAL STUDY OF STANFORD TYPE B AD PATIENTS AFTER STENT GRAFT REPAIR.....</b>		<b>46</b>
4.1	Introduction.....	46
4.2	Methodology.....	46
4.2.1	Thrombus identification and volume calculation .....	46
4.2.2	Length of the dissection and aorta, identification of re-entries tears and branches off from the FL.....	48
4.3	Results and Discussion .....	50
4.3.1	The relationship between FL thrombosis and aortic remodelling .....	50
4.3.2	Relationship between aortic morphology and thrombus formation .....	53
4.4	Limitations.....	56
4.5	Summary.....	56

**CHAPTER 5: PREDICTION OF THROMBUS FORMATION IN STANFORD  
TYPE B AD PATIENT: A PRELIMINARY STUDY USING CFD APPROACH .57**

5.1	Introduction.....	57
5.2	Methodology.....	57
5.2.1	Model geometry .....	57
5.2.2	Model settings .....	59
5.2.3	Boundary conditions.....	61
5.2.4	Numerical methods.....	62
5.2.5	Mesh Independence and Time Step Sensitivity Studies.....	63
5.2.6	Eduction Method for the Identification of Vortical Structures .....	64
5.3	Results and Discussion .....	65
5.3.1	Flow patterns and pressure distribution.....	65
5.3.2	Evolution of vortical structures in the FL region throughout a cardiac cycle.....	67
5.3.3	Effect of non-Newtonian (Carreau-Yasuda) property on vortical structures and WSS.....	72
5.3.4	Effect of FL size on vortical structures and WSS using Carreau-Yasuda model.....	73
5.4	Limitations.....	77
5.5	Summary.....	78

**CHAPTER 6: FLOW PATTERN ANALYSIS IN STANFORD TYPE B AD  
PATIENTS AFTER STENT-GRAFTING REPAIR.....79**

6.1	Introduction.....	79
6.2	Methodology.....	80
6.2.1	Model geometry .....	80
6.2.2	Model Settings.....	81

6.2.3	Boundary conditions.....	82
6.2.4	Numerical methods.....	83
6.2.5	Mesh independence and time step sensitivity studies .....	84
6.2.6	Geometrical and haemodynamics parameters for analysis .....	85
6.3	Results and Discussion .....	86
6.3.1	Geometric features .....	86
6.3.2	Blood flow pattern.....	88
6.3.3	The distribution of re-entry tears.....	88
6.3.4	Blood flow rate .....	90
6.3.5	The distribution of TAWSS, RRT and thrombus formation within one year .....	93
6.3.6	Thrombosis between tears.....	96
6.3.7	Vortical structures .....	97
6.4	Significance of this study.....	100
6.5	Limitations.....	100
6.6	Summary.....	101
<b>CHAPTER 7: CONCLUSIONS AND RECOMMENDATIONS .....</b>		<b>103</b>
7.1	Summary and conclusion.....	103
7.2	Directions for future research .....	107
References	.....	109
List of Publications and Papers Presented	.....	122
Appendix A	.....	123

**LIST OF FIGURES**

Figure 1.1: Aortic structure and its components in the human body (Juang *et al.*, 2008).1

Figure 1.2: Aortic wall layer. Adapted from Juang *et al.* (2008)..... 1

Figure 1.3:(A) Stanford Type A AD and (B) Stanford Type B AD. Adapted from Golledge and Eagle (2008).....2

Figure 2.1: (A) The highest Von Mises stress across the wall of a descending aorta; (B) the axisymmetric idealized three-layered model of a descending aorta. Adapted from Khanafer and Berguer (2009) ..... 20

Figure 2.2: Pressure contour plots adapted from Tse *et al.* (2011);..... 25

Figure 2.3: (A) Factors that affecting the drag force on stent graft; (B) The created mesh elements for the fluid domain. Adapted from Fung *et al.* (2008). ..... 28

Figure 2.4: Model of fluid dynamics velocity and vector plot in a thoracic stent graft before (A) and after (B) remodeling. Adapted from Cheng *et al.* (2008). ... 28

Figure 3.1: Visualization of workflow: (A) 3D reconstructed geometry of segmented AD aorta (TL and FL) during pre-treatment and post-treatment, (B) Axial Plane (X-Y Plane), (C) centroid points at TL and FL, (D) Diameter of TL and FL. .... 34

Figure 3.2: Boxplots showing the differences of: (A) TL volume;(B) TL maximal diameter;(C) FL volume; and, (D) FL maximal diameter changes in three segments of the aorta before and after stent graft repair. .... 36

Figure 3.4: Selected axial slices from three different regions (proximal, mid and distal) along Segment 1 for Patient 6 pre- and post-treatment..... 42

Figure 4.1: The TL (indicated by the green circle) and FL (indicated in blue). ..... 47

Figure 4.2: FL is the area defined by the blue line and patent FL is the lighter area marked by the red circle within the FL. The remaining darkest area within

the blue line indicates thrombosis. The area marked by the green line is the TL.....	47
Figure 4.3: Centroids at each axial slice of TL aorta.....	49
Figure 4.4: CTA images of Patient 10 pre-and post-treatment at the descending aortic region.....	51
Figure 5.1: (a) 3D reconstructed model of the AD with labeling of Plane A, Plane B and Plane C; (b) cross sectional image of Geometry 1 at Plane A; (b) cross sectional image of Geometry 2 (red) overlapped with Geometry 1 (white) at Plane A; and (d) cross sectional image of Geometry 3 (white) overlapped with Geometry 1 (brown) at Plane A.....	59
Figure 5.2: Inlet and outlet boundary conditions: (a) pulsatile inlet velocity profile; (b) pulsatile outlet pressure profile. Adapted from references Olufsen <i>et al.</i> (2000); Tse <i>et al.</i> (2011).....	62
Figure 5.3: Comparison of jet flow passing through the entry tear for (a) this work; (b) Cheng <i>et al.</i> (2013).....	66
Figure 5.4: Pressure distribution in the TL and FL regions at (a) peak systole and (b) early diastole for this work; (c) Tse <i>et al.</i> (2011); (d) Cheng <i>et al.</i> (2010).....	67
Figure 5.5: Vortical structures ( $\lambda_{2,t}$ equal to $-12.5 \text{ s}^{-2}$ ) distribution and contour of WSS for Newtonian model at (a) early systole; (b) peak systole; (c) late systole and (d) early diastole.....	70
Figure 5.6: (a) WSS contour superimposed on vortical structures; (b) Contour of WSS and (c) Vortical structures distribution during early diastole.....	71
Figure 5.7: Vortical structures distribution for Carreau-Yasuda model and Newtonian model at early systole and peak systole; .....	73
Figure 5.8: (a) Predicted location of thrombus extension (measured from the entry tear location) and (b) percentage of flow entering the FL for 3 different	

geometries with varying FL diameters (measured at plane A as shown in Figure 5.1).	76
Figure 5.9: The distributions of WSS for Geometries 2 and 3 at peak systole.	76
Figure 6.1: 3D reconstruction of Stanford Type B AD patients' geometry after SG repair.	82
Figure 6.2: A flow rate waveform of a typical Stanford Type B AD patient when applied at the ascending aorta.	83
Figure 6.3: Blood flow pattern of five patients. The results were obtained during peak systole. The dashed red line is the FL.	90
Figure 6.4: The relationship between percentage of total blood flow circulating inside the FL and number of re-entry tears during peak systole.	92
Figure 6.5: TAWSS distributions and RRT contours with subsequent areas of the FL thrombus formation.	94
Figure 6.6: RRT contours with subsequent areas of the FL thrombus forming up to 60 months in Patient 2.	96
Figure 6.7: Patient 3's vortical structures and WSS contour distribution from side view at (A) early systole; (B) peak systole; (C) late systole and (D) early diastole. (E) from anterior view at early diastole. (F) Area of the FL thrombus formation within one year of follow-up after the repair.	99

## LIST OF TABLES

Table 3.1: Percentage changes of the TL maximal diameter and volume from the baseline for each of the 13 patients .....	38
Table 3.2: Percentage changes of the FL maximal diameter and volume from the baseline for each of the 13 patients .....	39
Table 3.3: The agreement between maximal diameter and volume for all comparisons at each segment for both TL and FL .....	40
Table 4.1: The thrombus percentage distribution at Segments 1, 2 and 3 .....	52
Table 4.2: Morphology of the aorta after stent graft repair.....	54
Table 5.1: The dimensions of the aorta and the FL at three different planes for the original (Geometry 1) and modified geometries (Geometries 2 and 3). .....	59
Table 5.2: Carreau-Yasuda model symbol denotation.....	60
Table 5.3: The maximum and critical Reynolds number, as well as Wormersley number for Geometries 1, 2 and 3. ....	61
Table 5.4: Results of mesh independent test of comparison of average velocity and maximum pressure between meshes .....	64
Table 5.5: Comparison of the $\lambda_2$ intensity ( $m^3/s^2$ ) in the whole blood domain between the Newtonian (New) model and the Carreau-Yasuda (C-Y) model .....	73
Table 5.6: Comparison of the $\lambda_2$ intensity ( $m^3/s^2$ ) in the whole blood domain for Carreau-Yasuda model for Geometry 1 (G1), Geometry 2 (G2) and Geometry 3 (G3) .....	76
Table 6.1: The peak Reynolds number, mean Reynolds number and Wormersley number for each patient.....	83
Table 6.2: Geometric features and stent graft length .....	87

Table 6.3: Percentage of the total blood flow and TL to FL volume flow rate ratio during post treatment for each subject at peak systole..... 92

Table 6.4: Maximum WSS and TAWSS values ..... 93

University of Malaya

## LIST OF SYMBOLS AND ABBREVIATIONS

AD	:	Aortic dissection
FL	:	False Lumen
TL	:	True Lumen
CFD	:	Computational Fluid Dynamics
CT	:	Computed Tomography
TEE	:	Transoesophageal Echocardiography
MRI	:	Magnetic Resonance Imaging
CTA	:	Computed Tomography Angiography
3D	:	Three-Dimensional
2D	:	Two-dimensional
SINE	:	Stent graft-induced new entry
WSS	:	Wall Shear Stress
TAWSS	:	Time Averaged Wall Shear Stress
FSI	:	Fluid-structure interaction
ILT	:	Intra-luminal Thrombus
AAA	:	Abdominal Aortic Aneurysm
ROI	:	Region of interest
% of change	:	Percentage of maximal axial diameter and volume changes from the baseline
$\% L_{\text{dissection}}/L_{\text{aorta}}$	:	Percentage of dissection length over aortic lumen length up to bifurcation
$\% \text{Thrombus}_{\text{before}}/\text{FL}$	:	Percentage of thrombosis over false lumen volume before stent-graft repair
$\% \text{Thrombus}_{\text{after}}/\text{FL}$	:	Percentage of thrombosis over false lumen volume after stent-graft repair
$\text{TL}/\text{FL}_{\text{before}}$	:	Ratio of true lumen to false lumen volume flow rate

before supplying to the abdominal branches that partially or fully supplied by the false lumen

$TL/FL_{\text{after}}$	:	Ratio of true lumen to false lumen volume flow rate after supplying to the abdominal branches that partially or fully supplied by the false lumen
SMA	:	Superior mesenteric artery
TKE	:	Turbulent kinetic energy
RRT	:	Relative Residence Time
PISO	:	Pressure Implicit with Splitting of Operators
OSI	:	Oscillatory shear index
D	:	Maximal diameter (mm)
V	:	Volume (ml)
L	:	Length (mm)
$\vec{v}$	:	Velocity Vector (m/s)
$\rho$	:	Density ( $\text{kg/m}^3$ )
$\mu$	:	Viscosity (Pa.s)
D	:	Scalar shear rate
$\mu_0$	:	Zero shear rate limit (0.16 Pa.s)
$\mu_\infty$	:	Infinite shear rate limit (0.0035 Pa.s)
$\lambda$	:	Relaxation time (8.2 s)
n	:	Power index (0.2128)
a	:	Transition region (0.64)
$Re_{\text{max}}$	:	Maximum Reynolds number
$Re_c$	:	Critical Reynolds number
$\omega$	:	Vorticity

## CHAPTER 1: INTRODUCTION

### 1.1 Background

The largest artery in the human body is the aorta. Aorta carries the blood to the whole body (Juang *et al.*, 2008). Aorta consists of an ascending aorta, aortic arch, descending aorta and the abdominal aortic region as shown in Figure 1.1. Meanwhile, the aortic wall consists of three layers which are the intima, media, and adventitia as shown in Figure 1.2 (Juang *et al.*, 2008). The intima is in the inner side of the layer followed by the media and finally the outer layer, adventitia. All the layers are made up of connective tissue and elastic fibers (Juang *et al.*, 2008). This will cause the aorta to stretch from the pressure produced by the blood flow (Juang *et al.*, 2008).

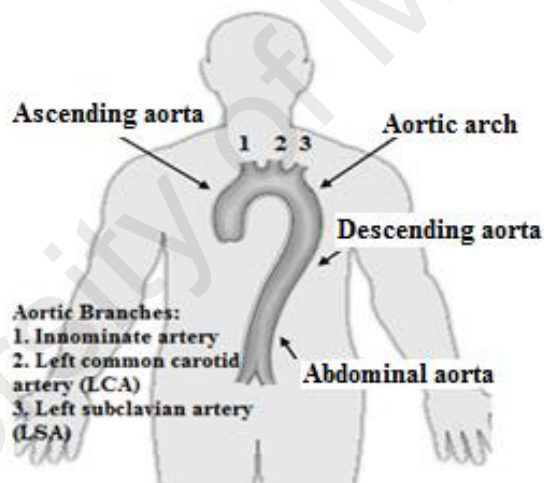


Figure 1.1: Aortic structure and its components in the human body (Juang *et al.*, 2008).

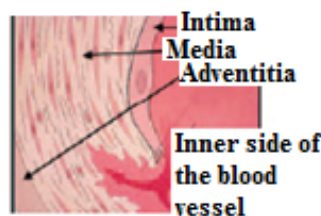


Figure 1.2: Aortic wall layer. Adapted from Juang *et al.* (2008).

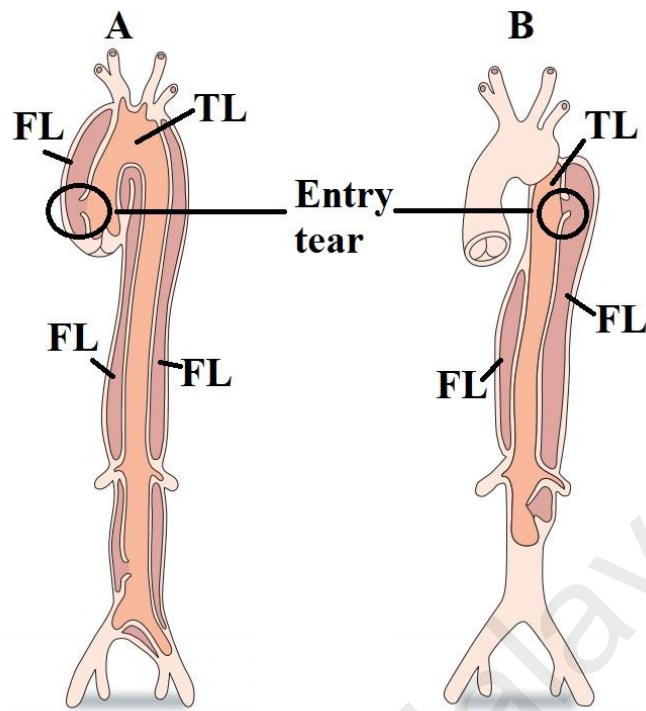


Figure 1.3: (A) Stanford Type A AD and (B) Stanford Type B AD. Adapted from Golledge and Eagle (2008).

Aortic dissection (AD) is characterized by splitting of the aortic wall causing blood to enter the media layer through an entry tear, subsequently divides the layer into true lumen (TL) and false lumen (FL) (Figure 1.3) (Czermak *et al.*, 2004). TL is the actual passageway for the blood to pass through while FL is the newly created passageway (Karthikesalingam *et al.*, 2010). The layer that separates TL and FL is known as intimal flap while the additional tears along the dissection line are known as re-entry tears. The dissections may propagate either distally or proximally from the entry tear and may involve vessel branches (Czermak *et al.*, 2000; Tsai *et al.*, 2005). AD can be categorized into two systems which are defined as DeBakey and Stanford systems (Karthikesalingam *et al.*, 2010). In the DeBakey system, AD was classified into three types; Type I; involves both ascending and descending aorta, Type II; involves ascending aorta only, and Type III; only restricted to the descending aorta (Karthikesalingam *et al.*, 2010). The Type III AD is further classified into Type IIIA

AD; the dissection is above the diaphragm and type IIIB AD; the dissection extends below the diaphragm (Rodriguez *et al.*, 2008). As compared to DeBakey, the Stanford system, which categorizes AD into Type A (involves the ascending aorta) and Type B (involves both the descending and the ascending parts of aorta), have been widely used by the physicians (Czermak *et al.*, 2000; Erbel *et al.*, 2001; Golledge & Eagle, 2008; Karthikesalingam *et al.*, 2010).

Several factors have been associated with the development and progression of AD, including hypertension (Thrumurthy *et al.*, 2012; Tsai *et al.*, 2005; Tse *et al.*, 2011), race and gender (Thrumurthy *et al.*, 2012), genetic factors and connective tissue disease (Thrumurthy *et al.*, 2012; Tse *et al.*, 2011), aging, and previous repair of aortic aneurysm or dissection (Golledge & Eagle, 2008). Among these, hypertension constitutes the highest risk, as chronic exposure to high pressure leads to wall thickening, fibrosis, calcification and extracellular fatty acid deposition (Czermak *et al.*, 2000; Tsai *et al.*, 2005). On the other hand, genetic factors such as Marfan's syndrome, vascular Ehlers-Danlos syndrome, bicuspid aortic valve, and familial AD contribute to a compromised intima and AD through differentiation of the vascular smooth muscle cells and enhanced elastolysis of the aortic wall components (Tsai *et al.*, 2005).

AD may lead to serious complications, including aortic rupture, cardiac failure, hypotension/shock as well as end-organ ischemia (Golledge & Eagle, 2008). Hypotension or shock generally indicates a rupture or impending rupture of the aorta in Stanford Type B AD, and this normally occurs in the elderly patients (Mehta *et al.*, 2004). On the other hand, obstruction of branches arising from the aorta, such as the subclavian artery, coronary arteries, renal arteries may cause malperfusion syndrome (Golledge & Eagle, 2008), leading to serious consequences such as permanent paraplegia (Cooley, 1990). The occurrence of malperfusion syndrome is less common

seen in the elderly compared with the younger patients as they have been reported to have more localized dissection (Mehta *et al.*, 2004). Studies have shown that the effect of dissection on perfusion to a branch artery depends on whether the artery is supplied by the FL or TL, the relative collapse of the TL, and relation of the intimal flap to the branch artery (Golledge & Eagle, 2008).

Numerous methods have been used to diagnose AD in order to develop the best treatment strategies for the patients involved. These include computed tomography (CT) (61% usage), transoesophageal echocardiography (TEE) (33% usage), aortography (4% usage), and magnetic resonance imaging (MRI) (2% usage) (Ince & Nienaber, 2007; Thrumurthy *et al.*, 2012). CT and TEE are commonly used in the initial investigation of suspected acute dissection (Braverman, 2011; Erbel *et al.*, 2001; Golledge & Eagle, 2008; Suzuki *et al.*, 2003), where CT could provide information about the extent of aortic involvement (Braverman, 2011; Golledge & Eagle, 2008; Ince & Nienaber, 2007), whereas TEE has the advantages of defining the mechanism of aortic regurgitation, visualize the coronary ostium and ascertain the functioning of the left and right heart. Apart from the various imaging modalities, biomarkers such as elastin fragments (Shinohara *et al.*, 2003), D-dimers (Golledge & Eagle, 2008; Shinohara *et al.*, 2003) and smooth muscle myosin heavy-chain protein have also started to attract wide interest.

## **1.2 Therapeutic approaches to AD**

### **1.2.1 Medical treatment**

Medical treatment is currently the preferred method of choice for uncomplicated Stanford Type B AD patients (Suzuki *et al.*, 2003; Trimarchi *et al.*, 2006), particularly in patients with stable haemodynamic status, no branch vessel involvement, and no

periaortic hematoma (Mehta *et al.*, 2004; Trimarchi *et al.*, 2006). The primary goals are to prevent the propagation of the FL, prevent rupture, accelerate healing and reduce the risk of complications (Braverman, 2011; Hiratzka *et al.*, 2010; Khan & Nair, 2002) by lowering aortic wall stress. Three parameters have been known to affect aortic wall stress, i.e. velocity of ventricular contraction, rate of ventricular contraction and blood pressure (Hiratzka *et al.*, 2010). In view of this, beta-blocker therapy and vasodilators, which act to reduce heart rate and blood pressure, have commonly been used (Suzuki *et al.*, 2003). Medical treatment has, however, been associated with frequent incidences of organ malperfusion, as a result of the extension of the dissection, expansion of an aneurysm, and compression of the adjacent structures (Khan & Nair, 2002).

### **1.2.2 Surgical intervention**

Surgical intervention is indicated in most patients with Stanford Type A AD (Cooley, 1990), as well as some patients with Stanford Type B AD who show rapid expansion of a dissecting aneurysm, blood leakage, impending rupture, persistent and uncontrollable pain despite medical therapy, recurrent and/or refractory pain and/or impairment of blood flow to an organ or limb (Auer *et al.*, 2000; Elefteriades *et al.*, 1992; Mehta *et al.*, 2004; Palma *et al.*, 1997; Trimarchi *et al.*, 2006). The goals of the surgical therapy are to excise the intimal tear, obliterate the false channel by oversewing the aortic edges and reconstitute the aorta (Braverman, 2011; Khan & Nair, 2002). To date, the high operative mortality rate has been reported to be associated with surgical management. Few predictors of operative mortality have been identified, including the presence of cardiac tamponade, the site of the tear, the time to operation, the presence of renal/visceral ischemia, renal dysfunction, and the presence of pulmonary disease (Khan & Nair, 2002; Palma *et al.*, 1997).

### **1.2.3 Percutaneous intervention: Aortic fenestration and stent graft placement**

In view of the high mortality rate associated with surgical treatment, a less invasive percutaneous intervention such as aortic fenestration and stent graft placement have been increasingly popular (Erbel *et al.*, 2001). Percutaneous fenestration, which involves opening of the intimal flap, aims to provide a re-entry tear for the dead-end FL back into the TL (Erbel *et al.*, 2001).

On the other hand, stent graft facilitates aortic remodelling by covering the primary tear in order to promote FL thrombosis, i.e. blood clotting and subsequently eliminating flow into the FL, at the same time scaffolding the TL (Braverman, 2011; Svensson *et al.*, 2008). Despite its advantages, stent graft placement poses several complications, including migration associated with ventricular ejection, proper size selection, and endoleaks (Won & Lee, 2006).

### **1.3 Problem Statement**

While Stanford Type A AD patients are normally managed using surgical treatment, the optimal treatment strategy for Stanford Type B AD remains controversial (Czermak *et al.*, 2004). Recently, stent graft treatment for the management of Stanford Type B AD has become more common (Czermak *et al.*, 2004). The re-intervention rates after stent graft treatment are higher compared with traditional open surgical repair, and aortic rupture occurs in 1.5% of patients after stent graft treatment during their remaining lifetime (Hogendoorn *et al.*, 2014).

The primary aim of placing a stent graft in AD is to occlude the primary intimal tear so as to restore TL flow and induce blood clotting inside FL, i.e. FL thrombosis (Qin *et al.*, 2012; Stanley *et al.*, 2011). However, these treatment goals may be jeopardized if the target primary entry tear is incompletely covered or additional tears or re-entry tears are left untreated (Qin *et al.*, 2012). It has been shown that aortic rupture after Stanford

Type B dissection occurs at locations devoid of aortic thrombus, indicative of persistent FL flow, even in patients with partial FL thrombosis (Stanley *et al.*, 2011). Residual distal fenestrations allow perfusion in the FL, leading to continuous expansion and fatal rupture of the aorta below the stent graft (Andacheh *et al.*, 2012).

The extent of the dissection, the number of fenestrations and potential compromise of the visceral vasculature and aortoiliac bifurcations, may be important determinants of whether stent graft treatment is feasible (Hogendoorn *et al.*, 2014). A previous study suggested that infrarenal aortic enlargement occurs to a greater degree as well as caused incomplete FL thrombosis in those patients who have pre-intervention evidence of Stanford Type B AD extending below the renal arteries (Andacheh *et al.*, 2012).

Although a patent FL and large maximal FL area have been found to be the principal predictors of adverse outcome after stent graft treatment, there is no method to predict which patients will achieve spontaneous FL thrombosis (Cheng *et al.*, 2013). In the acute-onset cases, the remaining re-entry tears in the descending thoracic aorta were shown to be a critical factor that hampered shrinkage of the thoracic FL, but the remaining re-entry tears in the abdominal aorta were not (Kusagawa *et al.*, 2005). Despite the importance of tear sizes, numbers, and proximity to critical branch arteries in predicting disease progression (Quint *et al.*, 2009), the literature is void with studies describing exact location and frequency of tears (Khoynezhad *et al.*, 2010; Quint *et al.*, 2009; Thrumurthy *et al.*, 2011), and therefore the findings are inconclusive at present. Moreover, Czermak *et al.* (2004), showed that the remaining re-entry tears or branches arising from the FL did not significantly affect thrombus development. Despite the continuous blood flow, the thrombus length continued to grow inside the FL (Czermak *et al.*, 2004).

With regards to the selection of proper size and length of the stent graft, a longer graft has been shown to result in a significantly higher percentage of thrombosis in the FL, as it is believed that it may possibly provide stabilization of a longer length of the dissection flap and thus reducing blood movements in the FL (Qing *et al.*, 2012). However, Stanley *et al.* (2011) reported opposite findings, where the length of aortic coverage was not found to be statistically significant. Improper sizing of the stent graft could lead to endoleaks (undersizing) (Kim *et al.*, 2011) or membrane rupture (oversizing) (Dong *et al.*, 2010). Stent graft-induced new entry (SINE), defined as a new tear caused by the stent graft itself could occur, especially in chronic dissection with a high taper ratio (Dong *et al.*, 2010; Weng *et al.*, 2013). The mismatched shearing stress acting upon the junction between the stented and unstented intima promotes the higher possibility of distal SINE progression (Weng *et al.*, 2013).

Meanwhile, in terms of computational analyses, several studies of ideal geometries and real patient-specific images had been performed to relate the effects of geometrical factors, i.e. tear size, number of tears, location of primary tears and FL size with FL shrinkage or enlargement, as well as thrombus formation (Cheng *et al.*, 2013; Cheng *et al.*, 2010; Fan *et al.*, 2010). These studies worked on AD patients without stent graft treatment (Cheng *et al.*, 2013; Cheng *et al.*, 2010; Fan *et al.*, 2010) and those with simplified stent graft assumptions, where stent graft placement was described as the closure of the primary entry tear in non-stent graft AD patients (Chen *et al.*, 2013a). On the other hand, instead of using simplified stent graft assumptions, Karmonik *et al.* (2011a) had compared the haemodynamics of stent graft AD case (reconstructed from MRI images ) before and after repair and observed the elimination of a large amount of WSS after the insertion of a stent. Their study concurred with a previous clinical study, which found good early post-stenting results after stent graft placement (Karmonik *et al.*, 2011a). However, they only used one patient and the long-term results of

thrombosis and aortic remodelling remained unknown (Sayer *et al.*, 2008). Continuous observation of the entire aorta, especially the FL region after stent graft treatment, is important to detect and monitor complications (Sayer *et al.*, 2008). Follow-up imaging studies on AD patients who went through stent graft treatments would be useful to validate numerical simulation results aimed to predict disease progression and treatment outcomes.

Besides, by increasing the understanding on which group of patients most probably benefits from stent graft treatment; a better assessment can be made. By including computational analysis, more detailed haemodynamic and anatomical factors can be studied thoroughly than with imaging alone, which enable a greater understanding of the evolution of Stanford Type B AD, especially after the stent grafting treatment.

#### **1.4 Aim and Objectives**

This study aims to evaluate the progression of Stanford Type B AD patients after the stent grafting procedure in order to predict patients' outcomes. To achieve this aim, four objectives have been identified as detailed below:

- 1) To quantitatively assess the luminal changes based on the maximal axial diametric and volumetric measurements of computed tomography angiography (CTA) images of patients with Stanford Type B AD who underwent stent graft placement.
- 2) To evaluate the progression of Stanford Type B AD patients after stent graft treatment based on CTA image analysis and identify morphological characteristics that are related to FL thrombosis.
- 3) To carry out a preliminary investigation using computational fluid dynamics (CFD) approach in order to clarify the mechanism behind the formation of

thrombus and to predict its location in Stanford Type B AD patients without stent graft treatment.

- 4) To investigate the haemodynamics effect and predict thrombus formation location on Stanford Type B AD patient after stent graft treatment using CFD approach.

## **1.5 Thesis Scope**

This work focuses on the patients with Stanford Type B AD treated with a stent graft treatment. Thirteen patients' CTA images with follow-up data after the repairs are collected from Sir Charles Gairdner Hospital, Perth, Western Australia. The 2D CTA images are reconstructed into 3D geometries and volumetric measurements are performed in order to calculate for a percentage of FL thrombosis for each patient. The morphological characteristics that are related to FL thrombosis at the long-term follow-up are examined. Five patients based on identified morphological characteristics (number and location of re-entry tears, presentation of branches that off from the FL and length of dissection) with different percentage of FL thrombosis are used for CFD simulation. The rigid wall assumption is used for all simulations. The main difficulty in assuming the wall of AD to be elastic is that the vessel wall contains both healthy and diseased tissues with additional stent graft presentation, for which the exact material properties are difficult to be ascertained. The flow pattern analysis is used to explain how the identified morphological characteristics influence the flow distributions that eventually affect the thrombus formation and location. The simulated results of post-stenting geometries are compared to one-year CTA follow-up images.

## 1.6 Thesis Outlines

This thesis has evaluated the progression of Stanford Type B AD patients after stent grafting repair using both CTA image analysis and CFD approaches. Each chapter, except Chapter 2 (Literature review) and Chapter 7 (Conclusions and recommendations) starts with an introduction, followed by methodology, results, discussion and conclusion.

Chapter 2 systematically reviews the previous clinical studies that have been performed to evaluate the long-term results of AD after the stent grafting procedure. Further, reviews on numerical simulation on AD, including tear initiation, AD progression before and after the treatment have also been studied.

Chapter 3 focuses on the ethics application, CTA data collection, and selection with inclusion and exclusion criteria. The images are then segmented and generated into 3D geometries. Both the maximal axial diametric and volumetric measurements in different segments along the aortic region of TL and FL are measured from the 3D geometries. These methods of measurements are later compared.

Chapter 4 focuses on the evaluation of the TL and FL changes and the measurement of thrombus volume within two years after the stent grafting procedure. The similar method as shown in Chapter 3 is used to measure the maximal axial diameter and volume. The relationship of geometric features with FL thrombosis is examined.

In Chapter 5, a preliminary investigation using a Stanford Type B AD patient without a stent grafting treatment is conducted to discuss the formation of thrombus. Vortical structures analysis of the CFD result is used as a potential parameter to describe the mechanism behind the formation of thrombus and to predict its location in AD patients.

Chapter 6 discusses the effects of geometrical factors of the complete and incomplete FL thrombosis after stent graft repair. Five patients from Chapter 4 with a different number of re-entry tears and abdominal branches supplied by the FL are selected to be used in CFD simulation. The simulated results of post-stenting patients' geometries are compared to those during the one year follow-up.

In Chapter 7, the conclusions and recommendations for future works are provided.

University of Malaya

## CHAPTER 2: LITERATURE REVIEW

### 2.1 Patient progression after stent graft treatment: Clinical Perspective

The success of the stent graft treatment relates to the expanding of the TL as well as shrinkage of the FL which leads to overall decreasing or stabilization of the aortic dimension (Ameli-Renani *et al.*, 2015). Stent graft closes the proximal tear in order to re-build normal blood flow in the TL and eliminate the FL perfusion, thus induces thrombosis in the FL and eventually, the thrombus will regress and lead to aortic remodelling (Ameli-Renani *et al.*, 2015).

Previous works have reported that FL thrombosis also has become one of the primary outcome measures for stent graft treatment (Stanley *et al.*, 2011). Complete FL thrombosis indicates a better long term prognosis, while patent FL may lead to worse outcomes (Qin *et al.*, 2016; Stanley *et al.*, 2011). Many studies have documented that the FL was not completely thrombosed after stent graft treatment (Andacheh *et al.*, 2012; Qin *et al.*, 2012; Tolenaar *et al.*, 2014). The definition of complete thrombosis varied between studies (Czermak *et al.*, 2004; Lee *et al.*, 2013; Stanley *et al.*, 2011). Stanley *et al.* (2011) described complete thrombosis along the stented segment as a complete FL thrombosis. On the other hand, the most accurate explanation to describe FL thrombosis was reported by Lee *et al.* (2013) where the thrombosis was defined in three ways:

- i) Stent graft length FL thrombosis was defined when there was no patent blood flow in the FL from the proximal end of the AD to the distal end of the stent graft.
- ii) Thoracic FL thrombosis was defined when the thrombus happened to be along stent graft length FL and there was no patent FL down to the distal end of thoracic aorta.

iii) Complete FL thrombosis was defined as no patent blood flow in the FL of the thoracic and abdominal aorta.

Volumetric data showed significantly more reduction of the thoracic FL in the presence of FL thrombosis compared with non-FL thrombosis and also a tendency of less volume increase in the abdominal segment (Tolenaar *et al.*, 2014).

There were several causes that might be the factors that contributed to incomplete FL thrombosis. One of them was the timing of the dissection (acute vs chronic) (Rodriguez *et al.*, 2008). Chronic dissection was correlated with incomplete FL thrombosis because of the occurrence of persistent retrograde flow (Rodriguez *et al.*, 2008).

Furthermore, the other factor that contributes to incomplete FL thrombosis was the anatomical structure of the diseased blood vessel. Those anatomical structures were presented of the re-entry tears distal to the stent graft location (at the distal of descending aorta and abdominal region), the presence of the abdominal branches that were partially or fully supplied by the FL (Qin *et al.*, 2012; Schoder *et al.*, 2007; Steingruber *et al.*, 2008; Tolenaar *et al.*, 2014), the maximal size of the abdominal aortic region (Qin *et al.*, 2012), the extension of the dissection length (Rodriguez *et al.*, 2008) as well as the pre-operative size of the thoracic aortic diameter (Stanley *et al.*, 2011). Presentation of the re-entry tears, as well as branches that were supplied by the FL caused persistent FL perfusion (Ameli-Renani *et al.*, 2015). This persistent FL perfusion preserves pressurization of the thin, weaken FL wall leading to aneurysmal dilatation and potentially aortic rupture (Stanley *et al.*, 2011).

However, due to different definitions and levels of FL thrombosis, Czermak *et al.* (2004) and Stanley *et al.* (2011) found that the presentation of re-entry tears and/or abdominal branches arising from the FL did not contribute to incomplete FL thrombosis, since they did observe the continuous development of the thrombosis over

time. Furthermore, they found that thrombus length inside the FL might influence the patients' outcome. For example, patients who developed 80% of FL thrombosis would probably have better long-term results compared with those who developed 40% of the condition. Therefore, the study of thrombus distribution should be based on certain range and it should be monitored in separate regions of the aorta. This would make it easier to monitor which region would develop the least thrombosis, which could be influenced by various factors, such as blood flow and aorta structure.

In addition to those factors, the length of the thoracic aorta covered by the stent graft could also contribute to incomplete FL thrombosis. Medical practitioners have different opinions when performing stent graft repair, where some believed that only the primary entry tear should be closed, while others thought the best results could only be gained by closing the whole thoracic aorta. Sayer *et al.* (2008) suggested the use of a long stent to repair the aorta as they observed a poor rate of FL thrombosis at the distal end of the stent graft. However, Czermak *et al.* (2004) and Stanley *et al.* (2011) observed that the length of the stent-graft insertion did not affect thrombus development inside the FL.

Further, there were questions raised about whether long grafting should be used, particularly in the cases of re-entry tears or a number of abdominal branches originating from the FL (Steingruber *et al.*, 2008). In addition, other issue regarding the stent graft was, the stent graft-induced new entry tear (SINE) that might present challenge for the FL to have complete FL thrombosis because of the continuous flow through the newly created tear (Steingruber *et al.*, 2008).

Meanwhile, using volumetric analysis to calculate size changes in the TL and FL, Czermak *et al.* (2004) found that the stent graft length did not cause the FL volume to increase, whereas Qin *et al.* (2012) observed that changes in aortic volume were associated with the placement of a longer stent graft. Therefore, if the factors affecting

thrombosis could be identified and monitored, a better assessment could be made to optimise stent graft repairs to the benefit of AD patients (Tolenaar *et al.*, 2014).

## **2.2 Quantitative measurements to quantify AD progression**

Stanford Type B AD progression after stent graft repair have been measured based on several measurement methods which were; based on volumetric analysis (Andacheh *et al.*, 2012; Czermak *et al.*, 2004; Kamman *et al.*, 2016; Kim *et al.*, 2011; Kim *et al.*, 2014; Qing *et al.*, 2012; Steingruber *et al.*, 2008), diametric analysis (Conrad *et al.*, 2009; Leshnower *et al.*, 2013; Schoder *et al.*, 2007) as well as derivative from either diameter or volumetric measurements (Rodriguez *et al.*, 2008; Stanley *et al.*, 2011). Due to different methods used, it is hard to compare the results of all the studies (Czermak *et al.*, 2004; Schoder *et al.*, 2007).

In clinical practice, the degree of lumen enlargement or shrinkage in AD patients after a stent graft procedure is measured from the maximal axial diameter in the respective lumens from the stack of 2D CT slices. Considering the irregular shape of the lumen in AD patients, Patterson *et al.* (2015) compared the absolute values of lumen diameter and area in assessing the degree of aortic remodelling in Stanford Type B AD patients before and after treatment. As good correlation was observed between the diameter and area, they concluded that diameter measurements using multiplanar reconstructions based on a central luminal line are adequate in evaluating aortic remodelling.

Due to the complex morphology of the aorta, the maximal axial diameter and area may be located at different positions and blood vessel remodelling based on their measurements may be prone to error. In addition, along with the extension of the aortic lumen, some parts may shrink while others may be dilated or remain stable (unchanged). Consequently, it is difficult to assess changes along the lumen using axial

diameter or area measurements. In view of this, volumetric measurement at different segments along the vessel (for example, above and below the stent region) may be the preferred method (Czermak *et al.*, 2004) as it presents a method that is sensitive enough to monitor significant changes in TL and FL after stent grafting procedure (Parr *et al.*, 2011).

The feasibility of using maximal axial diameter and volume changes to indicate blood vessel remodelling have been studied in abdominal aortic aneurysms (AAAs) (Bargellini *et al.*, 2005; Parr *et al.*, 2011; Wever *et al.*, 2000). In one of the AAAs studies, Parr *et al.* (2011) compared both axial and orthogonal diameter measurements with volumetric analysis. They concluded that blood vessel volume can provide supportive information on the expansion of AAAs because its values are not affected by changes in the diameter (Parr *et al.*, 2011). In contrast to AAAs cases, the relationship between maximal axial diametric and volumetric changes in Stanford Type B AD after stent grafting is complicated as the aorta morphology is more complex. In particular, while AAAs involve a single lumen, AD cases involve TL and FL, which can significantly change shape after treatment (Steingruber *et al.*, 2008). Furthermore, the dissection usually extends over a long distance, with several major branches extending from the main vessel (Litmanovich *et al.*, 2009).

### **2.3 Numerical simulation in AD cases**

The numerical simulation method, particularly CFD approach involves the study and analysis of blood flow patterns as well as other haemodynamic variables. It provides the means through which reproducible numerical experiments can be produced under identical conditions. Over the years, it has emerged as a reliable tool which serves to enhance the understanding of the pathophysiology and progression of the aortic disease, as well as a predictive tool for treatment outcomes. Extensive studies have been

performed to investigate changes in the flow dynamics in a normal thoracic aorta (Shahcheraghi *et al.*, 2002; Wen *et al.*, 2010), dissected aorta (Cheng *et al.*, 2008; Cheng *et al.*, 2010; Doyle & Norman, 2016; Fan *et al.*, 2010; Fung *et al.*, 2008; Hou *et al.*, 2010; Karmonik *et al.*, 2011a; Karmonik *et al.*, 2010; Karmonik *et al.*, 2011b; Karmonik *et al.*, 2012; Lam *et al.*, 2008; Midulla *et al.*, 2012; Rudenick *et al.*, 2010; Tang *et al.*, 2012; Tse *et al.*, 2011) and aortic aneurysm (Borghi *et al.*, 2008; Tan *et al.*, 2009), as well as predict outcomes of stent graft and surgical treatments. Evolving from early CFD techniques using simplified geometries (Fan *et al.*, 2010; Gao *et al.*, 2006; Hou *et al.*, 2010; Khanafer & Berguer, 2009; Liffman *et al.*, 2001; Mohan *et al.*, 2002; Morris *et al.*, 2006; Rudenick *et al.*, 2010; Tang *et al.*, 2012), more recent studies have utilized patient-specific geometry reconstructed from MRI and CT data (Alimohammadi *et al.*, 2015; Cheng *et al.*, 2008; Cheng *et al.*, 2013; Cheng *et al.*, 2010; Dillon-Murphy *et al.*, 2016; Fung *et al.*, 2008; Karmonik *et al.*, 2011a; Karmonik *et al.*, 2010; Karmonik *et al.*, 2011b; Lam *et al.*, 2008; Menichini *et al.*, 2016; Midulla *et al.*, 2012; Rudenick *et al.*, 2010; Shahcheraghi *et al.*, 2002; Tse *et al.*, 2011; Wen *et al.*, 2010). In the recent years, fluid-structure interaction (FSI) models that take into account the interaction between the blood flow and the vessel wall have been developed (Alimohammadi *et al.*, 2015; Borghi *et al.*, 2008; Gao *et al.*, 2006; Khanafer & Berguer, 2009).

Compared to information provided by state-of-the-art imaging diagnostic tools, numerical simulation approach further provides haemodynamic variables such as blood flow dynamics, pressure distribution, wall stress, wall shear stress/rate, mass transport and recirculation region. As a result, it has been extensively used to investigate pathological flow in the blood vessel and evaluate the efficacy of various treatment strategies. Existing studies that applied numerical simulations in studying AD cases are discussed below.

### 2.3.1 Tear initiation in AD

AD started with a tear in the intima layer from the underlying media, dividing the initial single lumen of aorta into a TL and a FL (Thrumurthy *et al.*, 2012; Tsai *et al.*, 2005; Tse *et al.*, 2011). In a study utilizing a fully coupled FSI, axisymmetric three-layered wall model of a descending aorta, Khanafer and Berguer (2009) found that the media layer, which has the largest elasticity, showed the highest wall stress and shear stress as shown in Figure 2.1. Turbulent and Newtonian blood flow settings were used, with different thickness ratio (13/56/31) and elasticity (2/6/4 MPa) for the aortic walls. Results showed that the differences in the elastic properties of the different layers may be associated with the occurrence of dissection in the media layer. In a similar numerical study by Gao *et al.* (2006) using a 3D layered aortic arch model, it was reported that the circumferential wall stress is directly related to systolic blood pressure, and this explains the fact that 70 – 90 % of patients with AD have high blood pressure. Furthermore, similar to Khanafer's study, they demonstrated a higher stress in the media layer as compared to the intima and adventitia layers.

Wen *et al.* (2010) performed both numerical simulations and in vitro experiments on thoracic aorta to investigate the correlation of wall shear stress, pressure and oscillatory WSS index with aortic disorders, particularly AD. The geometry of a normal human thoracic aorta for the purpose of in vitro experiments was obtained using the Phase-Contrast MRI through rapid prototyping, while validation of numerical simulations was performed using measurements obtained from the Phase-Contrast MR Velocimetry. They revealed that the maximum wall shear or wall pressure coincides with the initial location of thoracic AD, and subsequently hypothesized that Stanford Type A dissection which originates in the ascending aorta is most likely the result of both higher values of WSS and wall pressure in the aortic arch, while Stanford Type B dissection tends to be caused by higher WSS.

Using a different approach, Beller *et al.* (2004) investigated the correlation between aortic root displacement and tear progression in AD using a finite element model of the human aortic root, aortic arch and supra-aortic vessels. Displacement and twist were applied to the aortic root base, while two different luminal pressures were simulated to represent control and hypertension conditions. Results showed that aortic root displacement and high blood pressure have a significant effect on the longitudinal stress in the ascending aorta, which may explain the frequent occurrence of circumferential intimal tears and AD in this location.

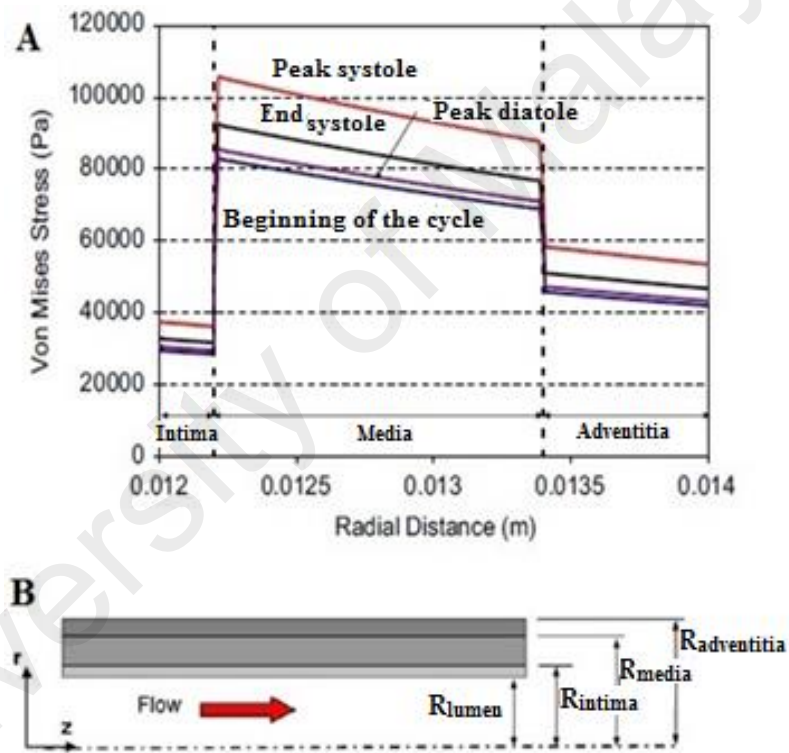


Figure 2.1: (A) The highest Von Mises stress across the wall of descending aorta; (B) the axisymmetric idealized three-layered model of a descending aorta. Adapted from Khanafer and Berguer (2009).

### 2.3.2 Progression of AD

Numerical simulation, which is able to provide physical flow condition through reproducible numerical experiments, plays an important part in predicting the likelihood of disease progression through identifying potential morphological and/or

biomechanical factors (Cheng *et al.*, 2010). Accurate prediction of disease progression, e.g. whether imminent rupture or dilation would occur, has a substantial clinical impact as it helps to determine the timing of surgical/intervention treatment for a patient (Sun & Chaichana, 2016; Tang *et al.*, 2012). In a clinical study performed on 101 patients with Stanford Type B acute dissection without complications, Marui *et al.* (1999) reported that a maximum aortic diameter of  $> 40$  mm and a patent FL during the acute phase serve as important predictors for aortic enlargement in the chronic phase. Therefore, these patients should undergo surgery before the enlargement of the aorta, while those with a maximum aortic diameter of  $<40$  mm should continue with hypotensive therapy. Tang *et al.* (2012). did a CFD study using a 3D aortic model reconstructed from CT images of a patient with thoracic AD to investigate the effect of six biomechanical factors, i.e. (i) size of the dissecting aneurysm, (ii) blood pressure, (iii) geometry around the distal tear, (iv) partial thrombosis, (v) distance between the tears, and (vi) shear stress on force on the walls of the FL in order to predict chances of rupture. Results are consistent with the clinical findings by Marui *et al.* (1999), who showed that an increase in the size of the dissection, as well as blood pressure increases the force acting on the FL wall.

Although aortic diameter has been clinically used as a guideline to predict AD dilation, it is believed that haemodynamic parameters (e.g. pressure and WSS), geometrical factor, as well as mechanical properties of the aorta wall played a key role in disease progression (Tse *et al.*, 2011). Patency of the FL and partial thrombosis, as well as prolonged high WSS, has been listed as markers for the prediction of dilation (Cheng *et al.*, 2013; Cheng *et al.*, 2015; Rudenick *et al.*, 2010). In a CFD study using patient-specific dissecting aneurysmal aortas before and after the formation of the luminal aneurysm, Tse *et al.* (2011) found that high-pressure difference between the true and FLs in the pre-aneurismal aorta coincides with the false luminal aneurysm in

the descending aorta as shown in Figure 2.2. Furthermore, a region of elevated time-averaged WSS (TAWSS) was found at the entry tear and is believed to cause the extension of the tear. Apart from that, Tse *et al.* (2011) inferred from their results that the wrapping of the FL around the TL may be associated with the helical nature of haemodynamic flow in the human aorta.

The highly disturbed flow pattern in Stanford Type B AD was likely to induce turbulent zones, and this led to the use of transitional, turbulence flow model by Cheng *et al.* (2010) in their numerical simulation. Results showed that the dissected aorta was dominated by highly disturbed (involving helical flows) and possibly turbulent flow with strong recirculation within both the FL and TL, particular in the region surrounding the tear. High levels of TAWSS were found at the coarctation throat and the edge of the tear, increasing the likelihood of tear expansion and reduction of aortic distensibility. Around the region near the tear, high turbulence intensity values were found. Although both laminar and turbulent flow simulations produce a qualitatively similar distribution of WSS, the significantly higher magnitude was obtained with the transitional turbulence model.

In another study, Karmonik *et al.* (2012) employed CFD simulations to identify haemodynamic changes associated with disease progression, using patient-derived geometries derived from a 3D contrast-enhanced MRI study at the initial examination and a CTA study at 10-month follow-up. Using geometrical data from the patient, they were able to reproduce the haemodynamic changes caused by FL dilatation. It was shown that FL dilatation occurring during the period between initial and follow-up studies led to lower blood flow velocities at the FL, thus reducing total pressure and overall WSS.

Meanwhile, in term of FL thrombosis, recent studies have reported an increase in the risk of death i.e. by a factor of 2.7 in AD patients with partial thrombosis in the FL (Sueyoshi *et al.*, 2009; Trimarchi *et al.*, 2013). Despite evidences showing a close correlation between FL thrombosis and the progression of FL aneurysm (Trimarchi *et al.*, 2013), mechanisms behind FL thrombosis remains unclear and there is no definitive method in predicting spontaneous FL thrombosis (Cheng *et al.*, 2013).

To date, limited simulation studies have attempted to relate slow and recirculating flow (Fan *et al.*, 2010; Karmonik *et al.*, 2012) as well as long particle residence time (Cheng *et al.*, 2013) with FL thrombosis in uncomplicated AD patients. However, the assumption that thrombus would form in regions with low velocity or negligible fluid motion is contradicted by Biasetti *et al.* (2011), who reported that despite having low flow velocities and WSS, intra-luminal thrombus (ILT) is seldom observed in the aneurysmatic bulge of the saccular AAA cases. To the contrary, Biasetti *et al.* (2011) applied the particle laden flow theory to prove the importance of vortical structures in analyzing platelet motion and explaining the formation of ILT (Biasetti, 2013) in patients with AAA. A series of numerical as well as experimental studies using digital particle image velocimetry on stenosed carotid artery have also been performed by another group (Bluestein *et al.*, 1999; Kamman *et al.*, 2016; Raz *et al.*, 2007), which quantitatively depicted the process by which fluid dynamic mechanisms, i.e. involving vortices and shear stress led to platelet activation, aggregation and deposition, and the subsequent formation of thrombin. In these studies, the platelet activity state assay was used to measure flow-induced platelet activation. Compared to AAA and carotid artery, the shape of the dissected aorta is much more complex, with the presence of FL which initiated from the entry tear, extended proximally to the arch, forming a coarctation proximal to the tear, and spiraled distally around the TL (Cheng *et al.*, 2010). This complicated geometrical feature resulted in complex flow phenomenon, including

substantive recirculating and disturbed flow, especially in the FL region (Cheng *et al.*, 2010).

In a study performed on fifty-five consecutive patients with acute Stanford Type B AD, Chang *et al.* (2008) reported that maximal FL area and branch-vessel involvement were independent predictors of in-hospital complications. In relation to this, Trimarchi *et al.* (2013) revealed that AD patients with larger initial aortic diameter have an increased chance of thrombosis in the FL region. Although several simulation studies have been performed to investigate the variations in haemodynamics brought about by FL dilatation (Karmonik *et al.*, 2012; Tse *et al.*, 2011), conflicting results have been obtained. Using CFD study, Karmonik *et al.* (2012) demonstrated a significant reduction in the average total pressure and WSS at the thoracic posterior FL wall due to FL aneurismal dilatation during follow-up. Contradictory findings were observed by Tse *et al.* (2011), who reported higher pressure in the FL region in the post-aneurismal aorta as compared to the pre-aneurismal aorta, and they attributed this to false luminal dilation and a reduction in the velocity value. The differences in these simulation results may be explained by the fact that geometries obtained through a longitudinal study (at initial examination and follow-up scans) may not only involve a change in the FL diameter, but also variations in the tear configurations which were reported to affect overall haemodynamics (Cheng *et al.*, 2013).

### **2.3.3 Numerical simulation after stent grafting procedure**

Owing to its minimally invasive procedure which reduces the mortality rate and fastens the recovery time, stent-graft placement has become one of the major treatment strategies for AD. In view of this, numerical simulations aimed to investigate the efficacy of stent graft treatment and evaluate various stent graft designs have attracted wide interest.

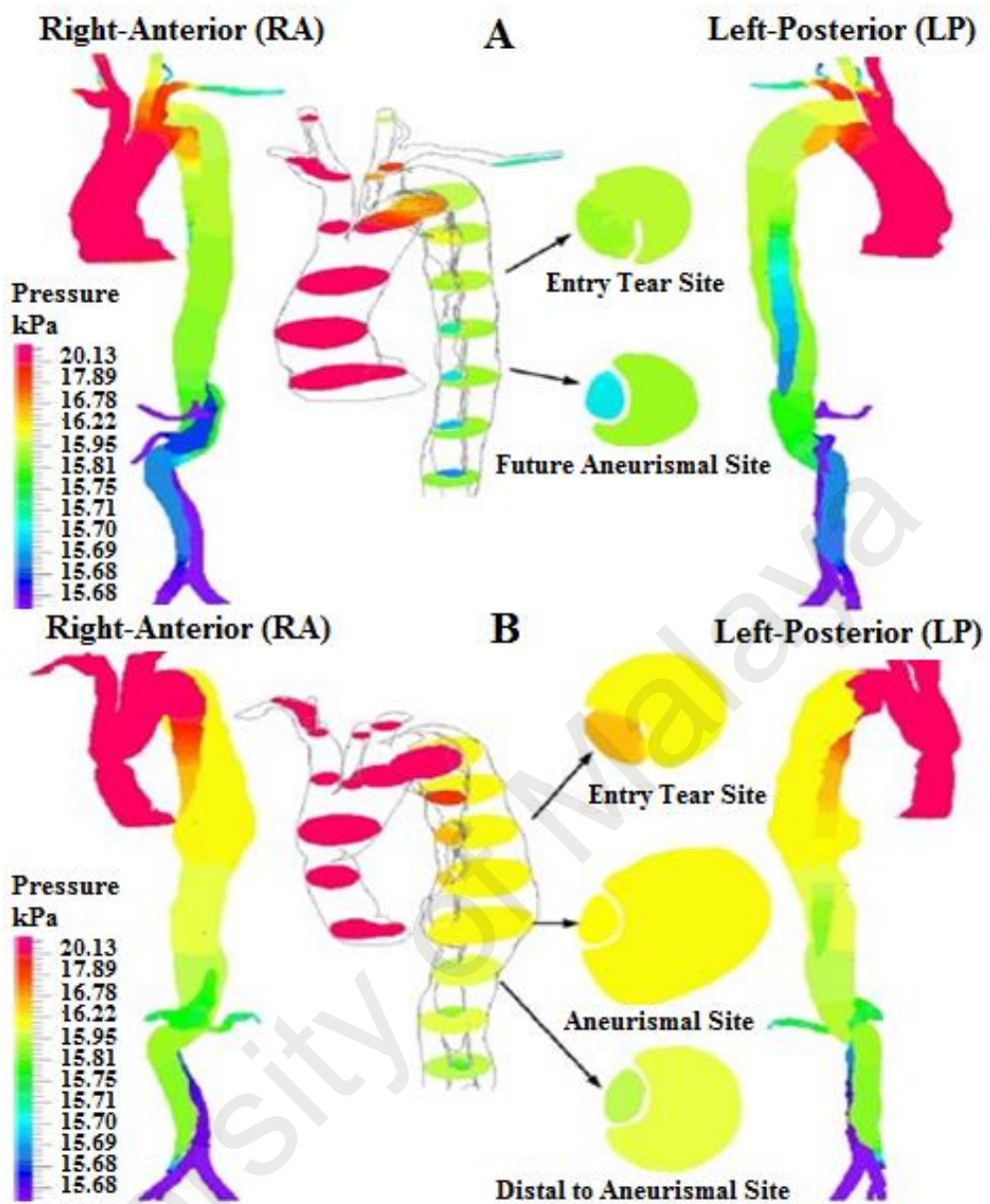


Figure 2.2: Pressure contour plots adapted from Tse *et al.* (2011); (A) The pre-aneurismal aorta (before formation of the luminal aneurysm); (B) The post-aneurismal aorta (after formation of luminal aneurysm). In the middle, an interior view of random axial cross-sections shows pressure difference in TL and FL.

Karmonik *et al.* (2011a); Karmonik *et al.* (2011b) and Simon *et al.* (2016) performed a series of simulation studies on the effect of endovascular stent graft placement in AD. CFD was performed with aortic geometry derived from MR angiographic images and inflow conditions, (i.e. aortic flow waveform) measured with 2D phase contrast MRI. The entrance tear was virtually occluded to simulate endovascular stent graft treatment, by eliminating inflow into the FL. Their results agreed with that reported by Tsai *et al.*

(2008), who found a decrease in both systolic and diastolic FL pressure with entry occlusion, despite a low variability for TL systolic pressures. One interesting results in their study was the occurrence of a reversal in the pressure difference between TL and FL at end systole. They further extended their study to quantify WSS and dynamic pressure changes after endovascular treatment with dynamic MRI measurements obtained from a patient pre and post (1 week) stent graft placement, as well as at one-year follow-up. It was observed that the large WSS and dynamic pressure found at the entrance tear and a stenotic region in the TL was significantly reduced, i.e. by more than a factor of two, after the endovascular graft treatment. Only a small posterior section of the FL remained after the treatment, and the antegrade flow within the lumen was eliminated. Two regions of elevated dynamic pressure were found within the stent graft, which may lead to stent graft failure.

Although endovascular treatment has proven to be a promising strategy, issues still remain on the effect of the degree of thrombosis (or in another term the level of FL patency) on potential rupture of the FL post-operatively, and whether a secondary procedure should be undertaken. Fan *et al.* (2010) who used idealized geometry employed CFD to assess the effect of three features, i.e. (i) the ratio of the area of the FL to that of the TL, (ii) the size of the re-entry tear, and (iii) the position of the re-entry tear, on the extent of thrombosis in the FL after endovascular stent graft treatment. Results showed that increasing the area ratio of the TL to the FL lower the risk of FL rupture, as it creates a larger domain of stagnant fluid in the FL. On the other hand, a patient with a larger reentry tear is at a higher risk, as this increases blood flow motion into the FL through the re-entry tear. Lastly, the position of the re-entry tear along the descending aorta has a negligible effect on the formation of thrombosis.

Apart from studies aiming to investigate the effect of endovascular stent graft placement, several researches have also looked into the effect of various biomechanical

factors on stent graft remodeling and migration using numerical simulations. As reported by Lam *et al.* (2008), an inappropriate proximal landing zone, a lack of a healthy distal attachment site and minimal oversizing could lead to stent graft instability in the long term. Three factors affecting the drag force on a stent graft were analyzed using CFD techniques, (Cheng *et al.*, 2008; Lam *et al.*, 2008) i.e. (i) the internal diameter of the stent graft,  $d$ , (ii) the starting position of the graft,  $\theta$  and (iii) the diameter of curvature of the aortic arch,  $D$  as shown in Figure 2.3. A stent graft template was determined on the basis of contrast enhanced transaxial thoracic CT scan images of a patient by fitting the cubic spline curve through the luminal cross-sections. Results showed that drag force increases linearly with increase in the internal diameter, due to an increase in the mass flow rate. On the other hand, the drag force decreases considerably with the starting position shifting downwards, i.e. from the proximal end to more distal end of the aortic arch. Flow separation and secondary flows occur at the aortic arch due to the effect of curvature, leading to substantial energy dissipation. To the contrary, the diameter of curvature of the aortic arch plays a less significant effect on drag force, thus poses minimal risk of migration to the stent grafts.

In a subsequent study, Cheng *et al.* (2008) followed up 12 patients with Stanford Type B ADs implanted with thoracic stent graft for more than 12 months. Serial CT scans of patients showed that there was a general increase in both inlet and outlet graft areas after endovascular stent graft treatment as in Figure 2.4. Furthermore, substantial remodeling of the stent graft was observed in these patients. The increase in the area of the stent graft is associated with an increase in the resultant drag force on the stent graft. Apart from geometrical factors, the same research group also extended their study to investigate the effect of dynamic factors (Fung *et al.*, 2008), i.e. blood pressure level and waveform, as well as blood viscosity on drag force. It was shown from their results that increasing blood pressure level and systolic slope of the pressure waveform

substantially increased the drag force, which contributes to stent graft failure. On the other hand, blood viscosity had a milder effect on drag force.

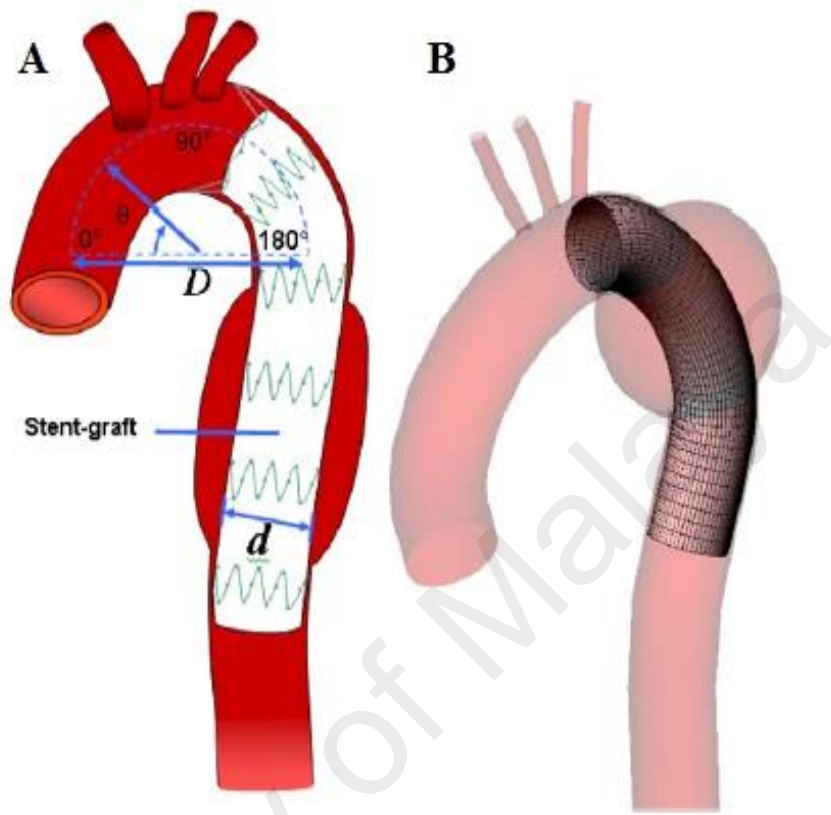


Figure 2.3: (A) Factors that affecting the drag force on stent graft; (B) The created mesh elements for the fluid domain. Adapted from Fung *et al.* (2008).

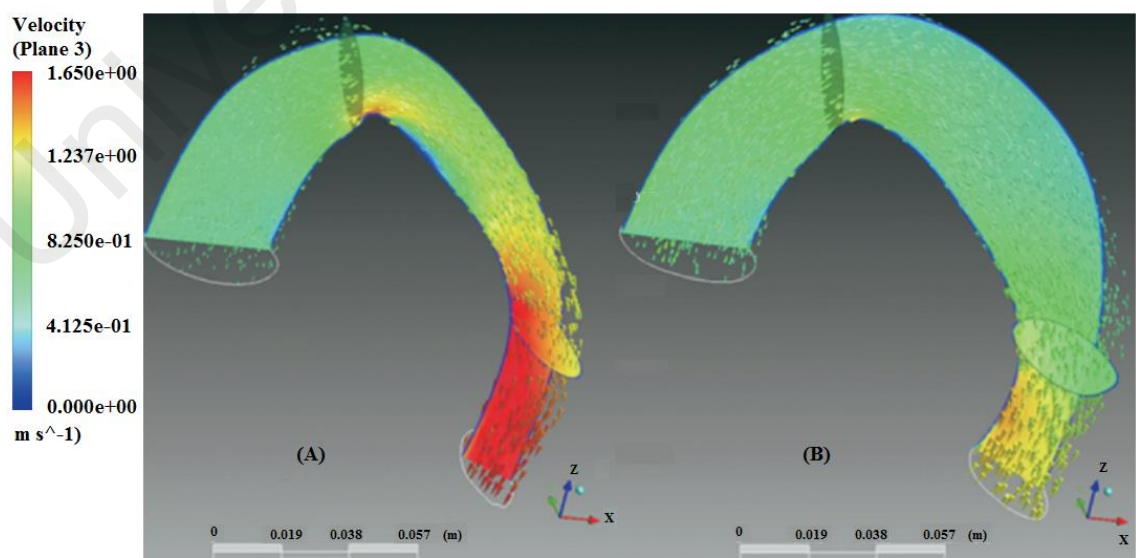


Figure 2.4: Model of fluid dynamics velocity and vector plot in a thoracic stent graft before (A) and after (B) remodeling. Adapted from Cheng *et al.* (2008).

Apart from endovascular stent graft therapy, fenestration and thromboexclusion are alternative surgical treatment strategies for AD. Using patient-specific geometry derived from MR images, Karmonik *et al.* (2011a) performed a simulation study examining the effect of fenestration on flow patterns and pressures in aortic dissection by completely removing the intraarterial septum. Results showed that surgical fenestration reduces the systolic pressure from 2400 to 800 Pa in the combined lumen. As reported by Panneton *et al.* (2000), surgical fenestration helped to relieve organ or limb ischemia.

Surgical thromboexclusion involves bypassing the dissected aorta and creating flow reversal in the dissected segment (Carpentier *et al.*, 1981; Elefteriades *et al.*, 1992). Researchers from Beijing University of Technology (Guan *et al.*, 2009; Guan *et al.*, 2010; Qiao *et al.*, 2008) performed numerical simulation on idealized 2D geometric models for Stanford Type B AD to investigate the effect of bypass graft on pressure and flow patterns. It was shown from their results that bypass graft operation reduces pressure and blood flow activities in the FL, and this is believed to alleviate the propagation of AD and promoting thromboexclusion in the dissecting channel.

## **2.4 Summary**

Continuous assessment of the entire aorta after the stent graft treatment is crucial to monitor the progression of the disease and to detect possible complications (Kusagawa *et al.*, 2005). Patient progression is monitored by the level of thrombosis in the FL, with complete thrombosis of FL is expecting to have beneficial outcomes while patent FL and partial thrombosis are associated with late outcomes (Qin *et al.*, 2012). Reported rates of FL thrombosis differ between studies, and aorta-related complications were frequent during follow-up (Manning *et al.*, 2009). Questions regarding the best strategy for stent-graft procedure, remain unanswered (Manning *et al.*, 2009).

Meanwhile, numerical simulation greatly contributes to diagnosis and medical planning by providing clinicians and surgeons a better insight on the disease through revealing various haemodynamic factors that are difficult to be measured in vivo. However, due to different limitations, these simulations are always done with underlying assumptions which may affect the accuracy of the simulation results. As such, result validation is of utmost importance, where matched outcome between simulated results and findings from in vitro experiments or imaging modalities is desired.

With the advancement of imaging technologies, patient-specific models have become increasingly popular. To increase the robustness of the model, numerical simulations involving a large number of patient-specific geometries with various configurations should be performed, taking into consideration the complexity of the AD geometries and the huge variability across patients. Apart from that, follow up imaging studies on AD patients who went through stent graft treatments would be useful to validate numerical simulation results with the aim of predicting disease progression and treatment outcomes.

## **CHAPTER 3: RECONSTRUCTION AND MEASUREMENT OF 3D GEOMETRY OF STANFORD TYPE B AD PATIENTS**

### **3.1 Introduction**

Based on the review in Section 2.2, this chapter aims to examine the maximal axial diametric changes in different segments of TL and FL and determine if it can be used in the aortic remodelling of AD patients after undergoing stent grafting procedure. The results may have potential to predict the recovery outcome of patients and facilitate decision-making when further intervention is needed. The maximal axial diametric results and volumetric measurements are analysed for a concordance to provide supportive information on morphological changes in the clinical aspect.

### **3.2 Methodology**

#### **3.2.1 Study population**

The study population comprised of 13 Stanford Type B AD patients who underwent computed CTA before and after treatment. CTA scan images of patients with Stanford Type B AD were collected at Sir Charles Gairdner Hospital, Perth, Western Australia between 2004 and 2015. CTA images were retrieved from the imaging database (picture archiving and communication system) in a hospital with patient's details being de-identified.

#### **3.2.2 Ethics application**

The study was approved by the Curtin University, Perth, Western Australia (Approval number: SCI-31-14) and Sir Charles Gairdner Hospital, Perth, Western Australia (HREC No: 2014-115).

### **3.2.3 CTA images selection**

Initially, the numbers of patients obtained from the hospital were 30 patients. After proper selection, only 13 patients were suitable to be used. Below criteria were used for patients' selection:

Inclusion criteria:

- Patients with Stanford Type B AD.
- Treated with endovascular stent grafts
- Routine CTA follow-ups (6 months, 12 months and yearly thereafter).

Exclusion criteria:

- Patients with Stanford Type A AD
- Treated with open surgery
- Incomplete CTA follow-ups or follow-up with other imaging modalities

For this chapter, the follow-up scans were performed on the sixth and 12th month after the stent-grafting procedure. 30 datasets from 13 patients were processed, where two patients had three datasets (post-treatment, six and 12 months), while the rest had two datasets (either post-treatment and six months, or post-treatment and 12 months).

### **3.2.4 CTA images segmentation and 3D reconstruction**

The patients' CTA images were transferred to the ScanIP software (Simpleware, Ltd, Exeter, UK), whereby the region of interest (ROI), including the TL and FL of the ascending aorta (starting at slices distal to the coronary artery), aortic arch, descending thoracic aorta and abdominal aorta (ending at slices proximal to the aortic bifurcation), were identified and segmented on each axial slice.

### **3.2.5 Diameter measurements**

The segmented ROI from the ScanIP software (Simpleware, Ltd, Exeter, UK) were imported into the MATLAB software (version r2012a, The Mathworks Inc, Natick, MA) for analysis. Axial diameter calculations were performed for the TL and FL regions from the start of the descending aorta (distal to the left subclavian artery) to the bifurcation (Figure 3.1(A)). At each axial plane (Figure 3.1(B)), the centroids of both TL and FL were calculated (Figure 3.1(C)). The axial diameter of TL and FL were measured along the line interconnecting the two centroids as shown in Figure 3.1(D). In non-dissected aorta, diameter was measured perpendicular to the maximum elliptic diameter (Manning *et al.*, 2009).

### **3.2.6 Volume measurements**

The TL and FL volumes were calculated by multiplying the corresponding area of ROI at each axial slice with the slice spacing, to estimate the ROI volume, and summing the corresponding ROI volume across all slices. The algorithms for calculating TL and FL volumes were also programmed using the MATLAB software.

In this study, we have divided the aorta into three segments of interest (Figure 3.1(A)), i.e. the stented segment (Segment 1), the aortic segment extending from the distal end of the stent graft to the origin of the celiac artery (Segment 2), and the segment between the origin of the celiac artery and the bifurcation (Segment 3). The TL and FL volumes for these three segments were measured separately. Apart from volume measurements, the maximum axial diameters of TL and FL at each segment were also determined by selecting the largest diameter measurement from each segment.

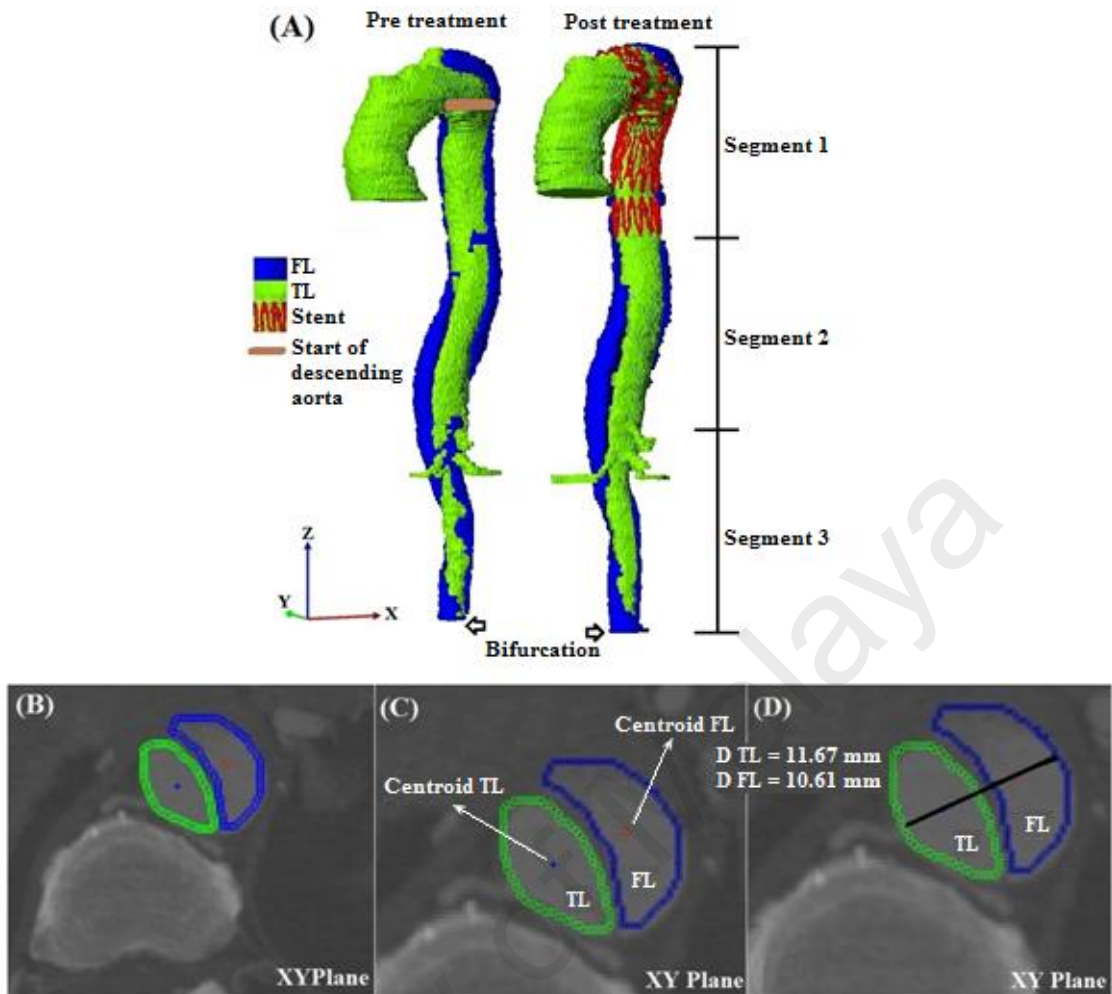


Figure 3.1: Visualization of workflow: (A) 3D reconstructed geometry of segmented AD aorta (TL and FL) during pre-treatment and post-treatment, (B) Axial Plane (X-Y Plane), (C) centroid points at TL and FL, (D) Diameter of TL and FL.

Aortic remodelling was subsequently quantified by calculating the percentage of maximal axial diameter and volume changes from the baseline as shown in the Equation 3.1 below:

$$\% \text{ of change} = \frac{\text{post-treatment volume} - \text{pre-treatment volume}}{\text{pre-treatment volume}} \times 100 \quad (3.1)$$

where % represents the percentage.

Lumen changes were identified based on a 10% cut-off point which is based on previously reported studies (Czermak *et al.*, 2004; Steingruber *et al.*, 2008), in which an increase in lumen maximal axial diameter and volume was defined as >10% increase from the baseline value;  $\pm 10\%$  from baseline defined a stable maximal axial diameter

and volume, and a decreased lumen maximal axial diameter and volume was defined as > 10% decline from the baseline value (Czermak *et al.*, 2004; Steingruber *et al.*, 2008).

### 3.3 Results and Discussion

As shown in Figure 3.2, at Segments 1 and 2, the TL diameter and volume increased throughout the study period (Segment 1: mean volume =  $132.83 \pm 97.06$  ml; mean maximal axial diameter =  $43.71 \pm 9.95$  mm. Segment 2: mean volume =  $47.65 \pm 10.93$  ml; mean maximal axial diameter =  $31.12 \pm 9.63$  mm). For Segment 3, both TL maximal axial diameter and volume showed a slight increase from pre-stenting to six months, but slightly declined at the 12th month.

The changes between maximal axial diameter and volume were also noticed in the FL regions as shown in Figure 3.2 (C) and (D). As opposed to TL, the FL of Segment 1 decreased from pre-stenting (mean volume =  $129.62 \pm 150.52$  ml; mean maximal axial diameter =  $42.98 \pm 15.82$  mm) until the sixth month of follow-up, (mean volume =  $57.90 \pm 89.83$  ml; mean maximal diameter =  $22.68 \pm 21.77$ mm), and but increased again at the 12th month (mean volume =  $72.33 \pm 95.88$  ml; mean maximal axial diameter =  $27.71 \pm 6.23$  mm). The increment at the 12 months' follow-ups might be due to the effect of reducing patient number; FL in certain patients was completely gone and there was no follow-up taken during 12 months for some patients. On the other hand, there was no consistent trend in the mean maximal axial diameter and volume of FL in Segments 2 and 3, even though the FL mean volume at Segment 2 showed the most fluctuation.

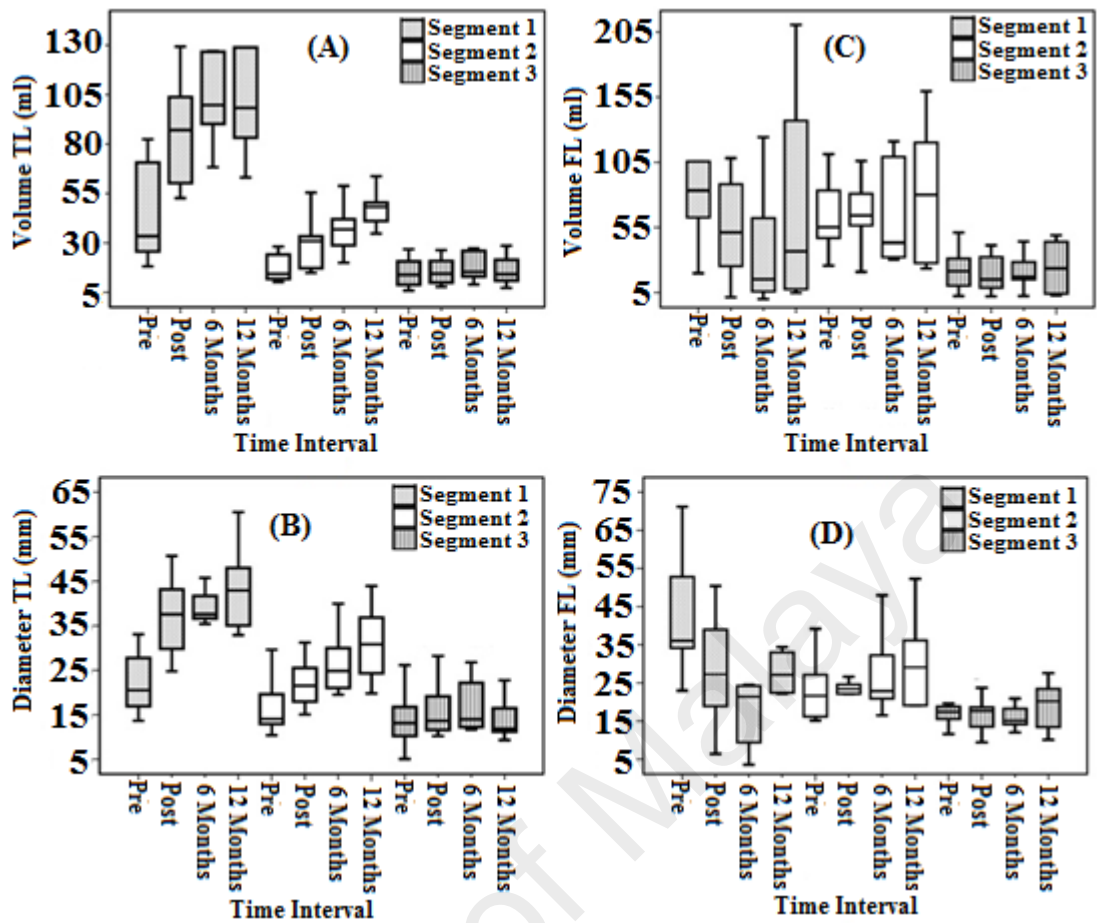


Figure 3.2: Boxplots showing the differences of: (A) TL volume;(B) TL maximal diameter;(C) FL volume; and, (D) FL maximal diameter changes in three segments of the aorta before and after stent graft repair, with 12 months' follow-up.

The values and trends of mean maximal diameter and volume within 12 months of follow-up at each TL and FL segment concurred with the results reported by Schoder *et al.* (2007) and Czermak *et al.* (2004), respectively.

Detailed changes in the percentage of maximal axial diameter and volume from the baseline, i.e. pre-treatment of each patient were analysed at post-treatment, and follow-ups after six and 12 months for Segments 1, 2 and 3 of the TL and FL. The percentages of change in each patient were shown in Table 3.1 for TL and Table 3.2 for FL. A positive value indicated expansion, whereas negative showed shrinkage. There were 153 comparisons between the maximal axial diameter and volume of patients for all segments throughout the follow-up period (Table 3.3). In Segment 1 TL (Table 3.1),

both maximal axial diameter and volume for patients showed a drastic increase from pre-treatment/baseline with 100% concordance.

Meanwhile, in Segment 2 TL, both maximal axial diameter and volume appeared to increase in the whole 12 months except for Patient 1 (post-treatment), Patient 5 (post-treatment) and Patient 9 (post-treatment and six months) (Table 3.1). Patients 1 and 9 showed volume increase but stable maximal diameter, while Patient 5, whose scan image was presented in Figure 3.3, showed an increase in maximal axial diameter, but had stable volume (Table 3.1). These differences had a discordance value of 18% (Table 3.3).

Unlike segments 1 and 2 TL, which demonstrated an increase in size for most patients, there was less reduction in both maximal axial diameter and volume for Segment 3 TL. Several patients showed different trends between the diameter and volume, i.e. Patients 1, 9 and 10 at post-treatment, Patients 1 and 4 at the sixth month, and Patients 1, 6 and 10 at the 12 months and these differences represented 29% of the discordance (Table 3.3).

As opposed to Segment 1 TL, Segment 1 FL in most patients (Table 3.2) showed drastic shrinkage for both maximal axial diameter and volume from the baseline. Two out of 25 comparisons (8% in Table 3.3) in Segment 1 FL showed discordance between the diameter and volume. However, Patient 6 showed stable diameter but a reduction in volume during post-treatment (Figure 3.4), while Patient 7 showed stable diameter but increase in volume after 6 months (Table 3.2).

The changes in Segment 2 FL had a discordance value of 32% (Table 3.3). It was represented by Patients 2, 6 and 8, who showed stable maximal diameters but increased volume, and Patient 9, whose diameter increased but the volume was reduced (Table 3.2).

Table 3.1: Percentage changes of the TL maximal diameter and volume from the baseline for each of the 13 patients

ID	Post-treatment		6 months		12 months	
	Maximal Diameter, D (%)	Volume, V (%)	Maximal Diameter, D (%)	Volume, V (%)	Maximal Diameter, D (%)	Volume, V (%)
Segment 1						
1	65.77	81.89	64.70	106.10	57.66	90.37
2	55.23	145.18	98.81	220.81	84.88	227.16
3	72.72	94.06	122.15	180.63		
4	171.36	416.42	169.57	484.08		
5	42.41	191.71	69.88	400.55	64.15	517.68
6	73.76	194.23			110.96	307.34
7	76.22	181.04	122.20	235.87		
8	105.65	57.48	97.27	123.22	89.38	153.44
9	37.25	76.15	27.88	91.69		
10	57.35	76.81			87.81	90.40
11	83.37	73.34	100.41	144.74		
12	65.31	122.92	75.85	130.64		
13	41.36	33.30	26.61	79.79		
Segment 2						
1	5.50	31.36	35.16	74.75	48.46	98.82
2	52.52	220.28	60.49	171.33	40.60	237.06
3	34.19	44.92	73.45	133.05		
4	70.58	146.03	62.93	138.89		
5	27.93	-4.44	116.72	92.78	162.52	128.33
6	44.95	113.92			134.53	240.88
7	27.37	90.00	31.86	156.79		
8	43.12	129.78	50.65	144.30	57.03	164.62
9	-2.34	26.46	3.74	50.53		
Segment 3						
1	-0.06	12.19	1.45	14.39	4.19	25.38
2	178.67	98.33	142.69	116.67	142.68	81.67
3	24.30	13.95	14.98	22.09		
4	-7.46	-1.37	7.23	22.12		
5	4.65	1.88	5.39	5.00	21.74	34.38
6	18.27	26.26			7.61	20.38
7	-4.22	-1.46	-1.43	2.09		
8	-34.97	-46.20	-25.30	-27.65	-27.00	-15.33
9	8.07	19.60	52.97	64.25		
10	29.02	-9.53			13.79	-16.05
11	-1.56	-4.72	-1.32	-0.22		
12	30.96	31.29	59.08	20.63		

Table 3.2: Percentage changes of the FL maximal diameter and volume from the baseline for each of the 13 patients

ID	Post-treatment		6 months		12 months	
	Maximal Diameter, D (%)	Volume, V (%)	Maximal Diameter, D (%)	Volume, V (%)	Maximal Diameter, D (%)	Volume, V (%)
Segment 1						
1	-43.64	-67.42	-59.52	-81.83	-57.22	-93.98
2	-19.88	-45.74	-61.05	-25.33	-64.69	-23.89
3	-26.89	-66.48	-80.67	-99.72		
4	-59.89	-74.37	-67.02	-90.62		
5	6.73	-4.62	-21.09	-46.38		
6	6.67	-11.89			-19.42	-84.58
7	11.76	31.50	8.01	20.06		
8						
9	-44.77	-37.67	-89.43	-99.45		
10	-46.19	-55.75			-48.71	-64.89
11	-19.38	-69.39	-59.18	-93.38		
12	-34.05	-40.28	-32.78	-31.37		
13	-81.40	-92.22				
Segment 2						
1	2.40	7.83	22.32	23.19	33.26	22.28
2	-38.26	-23.61	-4.55	7.90	1.02	43.36
3	-24.64	-18.60	29.07	24.81		
4	13.45	20.34	8.15	-6.40		
5	39.47	61.43	4.20	5.20	20.41	-32.57
6	-1.99	16.42			7.15	15.09
7	17.33	17.46	44.77	52.02		
8	-8.03	36.77	-12.70	-31.52	-24.94	-40.93
9	42.23	-25.82	39.41	-41.43		
Segment 3						
1	4.84	-15.68	-1.89	-48.93	-13.05	-50.95
2	-64.70	-52.99	-54.26	-35.04	-62.10	-45.73
3	-13.22	-15.70	21.68	40.50		
4	36.00	27.95	19.81	37.58		
5	13.13	28.84	-4.03	32.56	13.59	61.40
6	-3.94	-0.70			19.54	27.99
7	-0.90	-15.98	1.67	-15.59		
8	19.07	5.31	27.49	41.72	46.10	62.52
9	-3.34	-35.37	-1.43	-64.16		
10	-9.46	23.43			-12.00	25.94
12	-39.58	-54.28	-33.29	-46.40		

Compared with Segments 1 and 2 FL, Segment 3 FL showed the most discordance (38%). Six patients showed different trends of lumen changes: Patients 1, 7 and 9 had stable maximal axial diameter but the volume was reduced during post-treatment and 6 months; Patients 5 and 10 showed stable diameter but volume increased at post-treatment and six months; and, Patient 8 showed insignificant change in volume but had increased maximal axial diameter during post-treatment (Table 3.2).

Table 3.3: The agreement between maximal diameter and volume for all comparisons at each segment for both TL and FL

		Volume			Percentage of Maximal Diameter and Volume concordance	Percentage of Maximal Diameter and Volume discordance	
		Decrease	Stable	Increase			
TL							
Segment 1	Maximal Diameter	Decrease	-	-	-	100%	-
		Stable	-	-	-		
		Increase	-	-	30		
Segment 2		Decrease	-	-	-	82%	18%
		Stable	-	-	3		
		Increase	-	1	18		
Segment 3		Decrease	3	-	-	71%	29%
		Stable	-	7	6		
		Increase	1	1	10		
		Total	4	9	67		
FL							
Segment 1	Maximal Diameter	Decrease	21	-	-	92%	8%
		Stable	1	1	1		
		Increase	-	-	1		
Segment 2		Decrease	4	-	-	68%	32%
		Stable	-	4	4		
		Increase	3	0	7		
Segment 3		Decrease	7	-	1	62%	38%
		Stable	6	1	2		
		Increase	-	1	8		
		Total	42	8	23		

Notes: The grey colour box indicates the concordance results between maximal diameter and volume.

Even though the maximal axial diameter and volume changes have been compared previously in AAAs (Bargellini *et al.*, 2005; Parr *et al.*, 2011), no similar study was reported for AD. Due to the presence of TL and FL in AD cases, the implantation of stent grafts in these patients aims to achieve the following results:

- (i) To expand the diameter and increase the flow in TL; and,
- (ii) To reduce the FL size and, ideally, exclude its flow and pressure to enable long-term aortic remodelling and prevent aneurysmal expansion.

Unlike AAAs, which generally affects the infrarenal aorta, the entire region from the thorax to the bifurcations were analysed as these were the affected regions in AD patients.

Most studies monitored aortic remodelling by measuring the whole vessel (from the top of the aortic arch to the lowest renal artery level) as a single unit (Qing *et al.*, 2012). In this work, the descending aorta was separated into three regions in order to distinguish the differences in change along the entire aorta beyond the left subclavian artery.

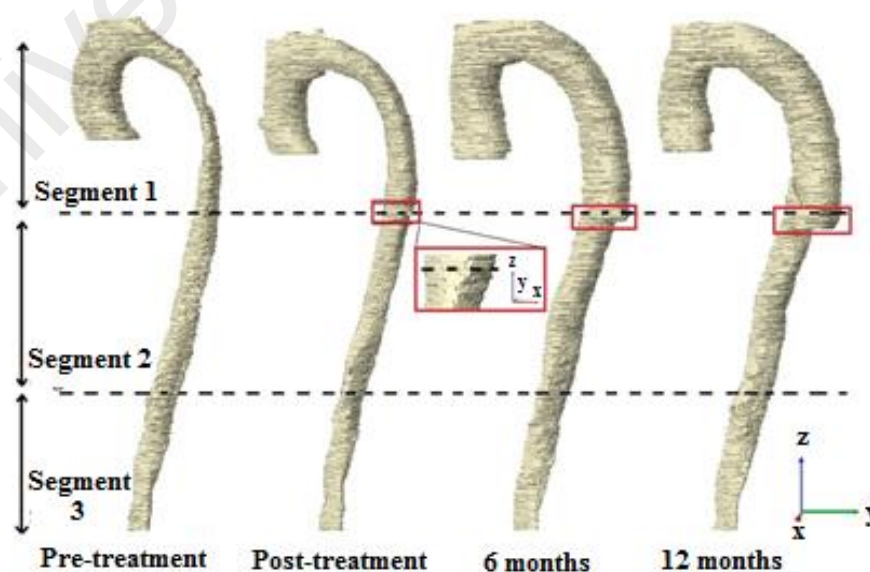


Figure 3.3: Localized expansion (red rectangular box) was observed distal to the stent graft edge (located at Segment 2 TL) during post treatment for Patient 5, which was further amplified during 6 and 12 months follow-up.

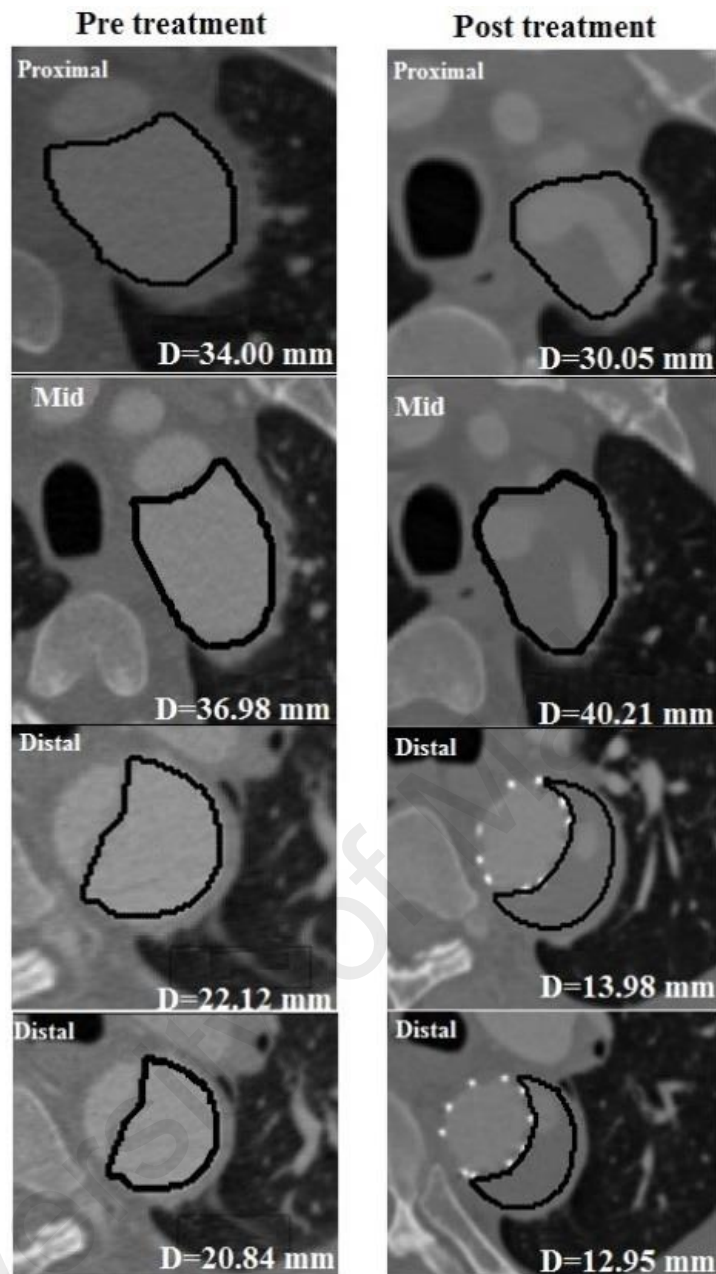


Figure 3.4: Selected axial slices from three different regions (proximal, mid and distal) along Segment 1 for Patient 6 pre- and post-treatment. The solid contours represent the region of interest (ROI) for the FL, while D represents the calculated diameter.

As expected, the findings showed that the shape throughout Segment 1 TL consistently increased in size after stent grafting. The uniformity in size observed throughout Segment 1 from the proximal to the distal regions resulted in 100% concordance between maximal diameters and volumes. Based on this finding, it can be deduced that the maximal axial diameter measurements alone had potential to monitor changes in TL region after the stent-grafting procedure.

Compared with Segment 1 TL, i.e. stented region, the other TL and FL segments showed different degrees of inconsistency with regard to lumen shrinkage or expansion: Segment 1 FL showed 8% discordance between maximal axial diameter and volume, i.e. observed in Patients 6 and 7. As shown in Figure 3.4, the distal part of Segment 1 FL in Patient 6 had significantly shrunk at post-treatment, leading to an overall shrinkage in total volume of Segment 1 FL. On the contrary, the proximal part showed inconsistent changes in size, with some slices showing a slight increase while others showing a slight decrease. As the proximal part was relatively larger than the distal region, the maximal axial diameter was stable for this particular region (Segment 1 FL) at post-treatment. A reduction in vessel dimension could be noticed using maximal axial diameter after 12 months of follow-up when the proximal region began to shrink. Based on this observation, volume data seems to be an efficient indicator of FL shrinkage in this Patient 6. A stable diameter but reduction in volume was also observed in Segment 1 FL of Patient 7 during the sixth month of follow-up. Although both maximal axial diameter and volume decreased after six months, the maximal diameter technique yielded a stable result as the level of reduction fell below the 10% cut-off point. The difference in results was caused by the fact that the small maximal diametric change at the sixth month reflected only a part of the constant expansion of the entire lumen ROI measured by volume.

Compared with Segment 1, Segment 2 showed more discordance between maximal axial diameter and volume. About 14% of TL volume changes and 32% of FL volume changes were apparently not observed using maximal axial diameter measurements in Segment 2. Particularly, stable diameters with an increase in volume were observed in the TL of Patients 1 and 9, and FL in Patients 2, 6 and 8. The expansion of FL volume in Segment 2 has also been reported (Czermak *et al.*, 2004; Steingruber *et al.*, 2008). The ability to precisely identify the expansion of TL and FL after stent-graft repair had

major implications, as a misclassification could cause an underestimation of FL growth that might lead to increased risk of aortic rupture. In several cases, i.e. Patient 5, Segment 2 TL and Patient 9, Segment 2 FL, an increase in maximal axial diameter was observed but the volume remained stable. This situation occurred due to the inconsistency in lumen size changes along the segment, such as the one happening in Patient 9, where the proximal part had shrunk while other regions showed an increment in diameter during post-treatment. Meanwhile, localised expansion was observed distal to the stent graft edge during post-treatment in Patient 5 (Figure 3.3), most probably due to the placement of the stent, as distal stent graft migration was noticed in this particular location during the sixth month of follow-up.

Compared with Segments 1 and 2, Segment 3 showed the most discordance between maximal axial diameter and volume, where the TL showed 29% discordance while FL was 38%. Overall, the expansion or shrinkage of the TL and FL were not detected in maximal axial diameter measurements in over one-third of the cases. The method only measures changes in regions with the largest diameters, but not the overall lumen changes. Depending on disease progression, the location of the greatest diameter might be different from one time to another.

Based on the findings, it is believed that volume measurements provide supportive information on morphologic changes for both TL and FL. However, volume assessment is time-consuming as it requires additional processing, such as image segmentation and reconstruction (Bargellini *et al.*, 2005; Wever *et al.*, 2000). Future work includes the development of an automated segmentation technique to save time. Noteworthy, the automated extraction of the TL and FL volumes using the MATLAB software took an average of 15 minutes.

One limitation of the present study is the use of maximal axial diameter measurements, which has been reported to yield considerably larger error compared with measuring perpendicular to the vessel axis (Wever *et al.*, 2000). Even so, maximal axial diameter measurements have been used in many studies (Evangelista *et al.*, 2012; Kusagawa *et al.*, 2005), and, most importantly, is widely accepted in clinical practice. Lastly, the analysis was performed using one software only, and different software packages may generate variable results due to the characteristics of their tools. Comparison or assessment of intra-software reproducibility should be considered in further research.

### **3.4 Summary**

Based on the results, diameter measurement has the potential to indicate aortic remodelling of the TL at the stented segment, i.e. Segment 1, which showed consistent changes along the stent length. Apart from Segment 1 TL, the other segments showed inconsistent changes between diametric and volumetric measurements. Even though the aorta was divided into three regions, and the results were analysed at each of these regions, it is not easy to interpret morphological change based on maximal axial diameter measurements alone. Thus, volume measurements should provide supportive information to reflect morphologic changes in both TL and FL. As subsequent intervention is indicated in the presence of an expanding lumen to prevent or treat aneurysmal degeneration, and this is currently based on diameter measurement alone, the use of volumetric data may guide clinicians in deciding whether further intervention is warranted in the presence of an increased diameter.

## **CHAPTER 4: MORPHOLOGICAL STUDY OF STANFORD TYPE B AD PATIENTS AFTER STENT GRAFT REPAIR**

### **4.1 Introduction**

Based on the review of factors that caused incomplete FL thrombosis after stent graft repair in Section 2.1, in this chapter, the outcome of stent graft repairs in 13 Stanford Type B AD patients were examined. The TL and FL volumetric changes, as well as percentage of FL thrombosis in the stent segment and the distal end of the stent were evaluated. The morphologic characteristics relating to FL thrombosis were also examined.

### **4.2 Methodology**

The study population comprised of 13 Stanford Type B AD patients, who underwent CTA before and after stent graft repair at Sir Charles Gairdner Hospital in Perth, Western Australia, between 2004 and 2015. The study was approved by the institutional review boards and patient identities were removed. Follow-up scans were performed within 24 months after surgery and 30 datasets were processed.

In this chapter, each patient's FL thrombus volume and its percentage over the total FL volume, the dissection length, aorta length, and percentage of dissection length over lumen length, number of re-entry tears and branches from the FL were measured and calculated, as well as performing aortic remodelling, i.e. expansion and FL shrinkage. The methodology used to calculate and observe the aortic remodelling based on diameter and volume was similar with the one used in Section 3.1.1 to 3.1.6.

#### **4.2.1 Thrombus identification and volume calculation**

Thrombus area in the aorta was identified as below:

- 1) The TL and FL could be seen in Figure 4.1.

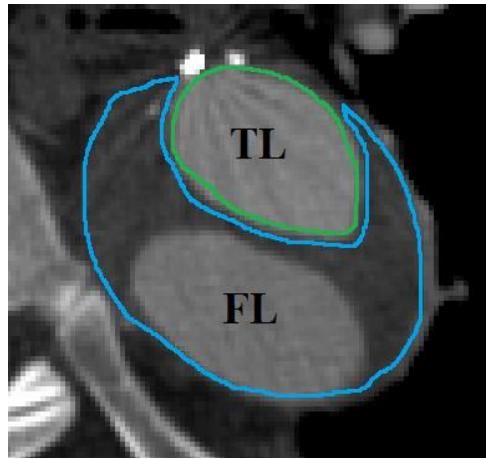


Figure 4.1: The TL (indicated by the green circle) and FL (indicated in blue).

2) The thrombus had darker contrast compared with the patent FL (Figure 4.2).

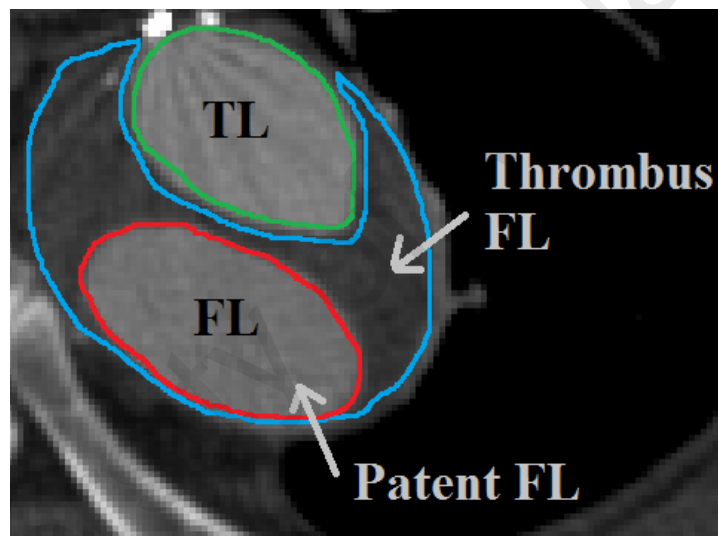


Figure 4.2: FL is the area defined by the blue line and patent FL is the lighter area marked by the red circle within the FL. The remaining darkest area within the blue line indicates thrombosis. The area marked by the green line is the TL.

The total FL volume (patent FL and thrombus area) of each patient was calculated by multiplying the corresponding ROI at each axial slice with the slice spacing, and summing the corresponding ROI volumes across all slices. The patent FL volume was also calculated using the same method. The thrombus volume was calculated from Equation 4.1:

$$\text{Thrombus volume} = \text{Total FL volume} - \text{Patent FL volume} \quad (4.1)$$

Similar to Chapter 3, the aorta was divided into three segments which comprises the stent segment (Segment 1), the aortic segment extending from the distal end of the stent graft to the origin of the celiac artery (Segment 2) and the segment between the celiac artery origin and the bifurcation (Segment 3). The thrombus volumes of these three segments were measured separately.

The percentage of thrombus volume over FL volume at each segment and the summation of these three segments were calculated using Equation 4.2:

$$\text{Percentage of thrombus volume} = \text{Thrombus volume} / \text{FL volume} \times 100 \quad (4.2)$$

#### 4.2.2 Length of the dissection and aorta, identification of re-entries tears and branches off from the FL

The dissection, aorta (the summation of the length of thoracic and abdominal aorta up to the bifurcation region) and stent graft lengths were measured based on the centroid of each axial slice (Figure 4.3) according to Equation 4.3:

$$L = \sqrt{(x1 - x2)^2 + (y1 - y2)^2 + (z1 - z2)^2} \quad (4.3)$$

where  $L$  represents the length.

The above equation was multiplied with the pixel spacing value of the X- and Y-axis in order to obtain the results in mm.

After obtaining the dissection and aorta lengths, the percentage of dissection length over lumen length up to the bifurcation ( $\% L_{\text{Dissection}}/L_{\text{Aorta}}$ ) was calculated using Equation 4.4:

$$\% \frac{L_{\text{Dissection}}}{L_{\text{Aorta}}} = \frac{L_{\text{Dissection}}}{L_{\text{Thoracic aorta}} + L_{\text{Abdominal aorta (up to bifurcation)}}} \times 100 \quad (4.4)$$

where  $L$  represents the length and  $\%$  represents the percentage.

The algorithms for calculating FL volume, patent FL volume, thrombus volume, dissection length, aortic length and stent graft length were programmed using the MATLAB software. The re-entry tears and FL branches were identified with the help of radiologists (Dr Lei Jing from Kunming Hospital, China, and Professor Zhonghua Sun from Curtin University, Perth, Western Australia).

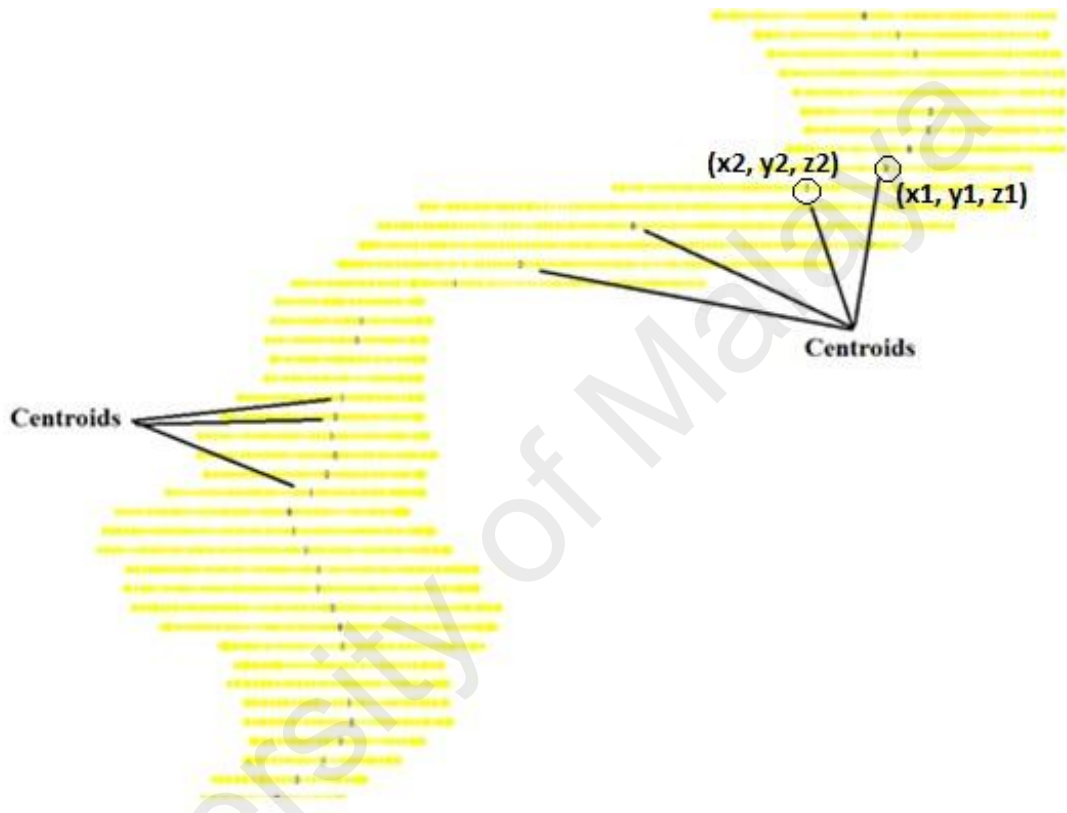


Figure 4.3: Centroids at each axial slice of TL aorta.

Based on Chapter 3, it was difficult to determine the morphological changes based on maximal axial diameter measurements alone. Therefore, volumetric measurements were used to analyse thrombosis in the FL.

## 4.3 Results and Discussion

### 4.3.1 The relationship between FL thrombosis and aortic remodelling

As shown in Table 4.1, most of the patients, except in Segment 1 of Patients 7 and 13, showed thrombus percentage increasing within 24 months of follow-up. Overall, more than 50% of the FL in Segment 1 developed thrombosis during the follow-up period. All patients showed a decrease in FL size in Segment 1, and the results were comparable with the findings by Czermak *et al.* (2004).

Compared with Segment 1, FL thrombosis was less apparent in Segment 2. Most of the results in Segment 2 showed more than 50% thrombus development during follow-up except for Patient 3. The SINE formed at the distal edge of the stent in Patient 3, causing continuous blood perfusion to the FL in Segment 2. Generally, all patients showed an increase of thrombosis post-treatment. Meanwhile, the FL volumetric changes varied between patients, with four of them showing an increase, four others showing a decrease, while one patient had little change. Previously, Czermak *et al.* (2004) had reported insignificant increase in the FL volume of Segment 2 in approximately half of their patients, and the results were comparable with their findings. The FL in the segment immediately next to the stent graft appeared to be a weak region (Czermak *et al.*, 2004). The weakness of Segment 2 FL might show that the stent grafts had caused changes in wall stress at this location (Czermak *et al.*, 2004). These changes might result in morphological disorders of the aorta, especially in diseased vessels (Czermak *et al.*, 2004).

Unlike Segments 1 and 2, Segment 3 showed the least sign of thrombosis. This circumstance could be explained by the presence of re-entry tears and branches partially supplied by the FL within the segment (Schoder *et al.*, 2007). However, thrombus formation significantly increased during follow-up for Patients 7, 8, 11 and 12.

Substantial FL volume changes were observed in Segment 3, where six out of 10 patients showed an increase in FL size. These results were consistent with those reported by Schoder *et al.* (2007). This significant volume increase in this segment is a cause for concern as it could lead to aortic expansion and rupture. On the contrary, Czermak *et al.* (2004) had noticed that only a small number of their patients had volume changes and they were less pronounced. Due to this reason, Czermak *et al.* (2004) concluded that Segment 3 was of minor importance in the follow-up of patients.

Patient 10 was excluded from analysis since his geometry was more complicated with the presentation of two TLs and one FL in (Figure 4.4).

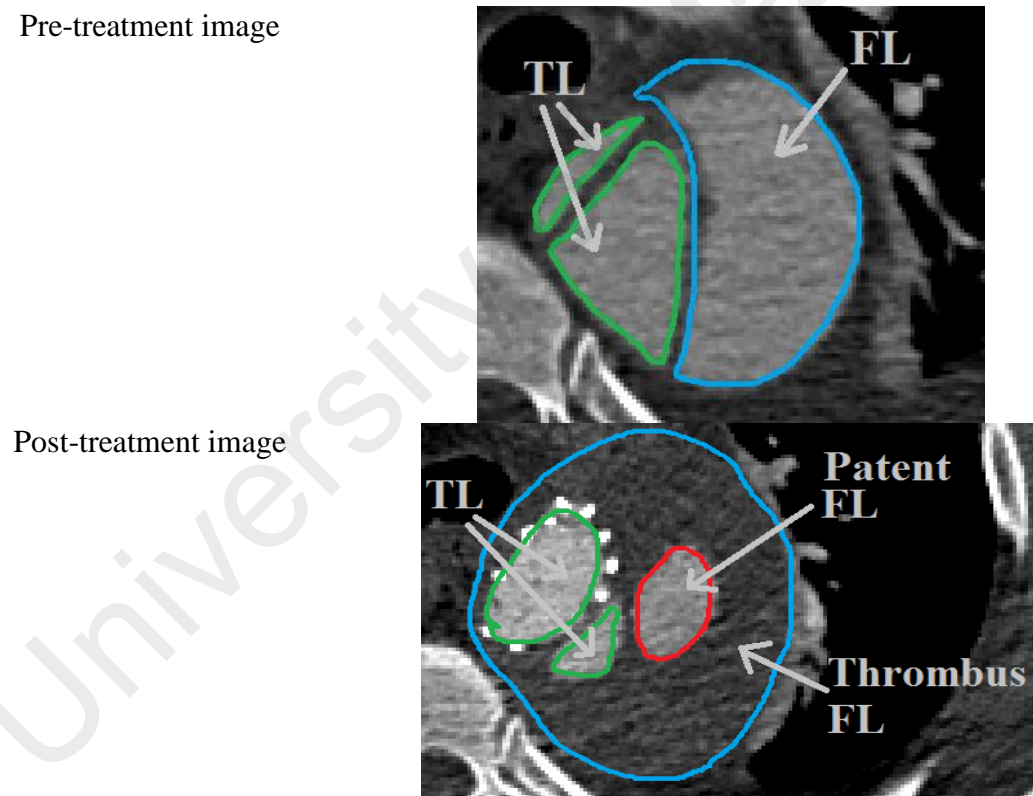


Figure 4.4: CTA images of Patient 10 pre-and post-treatment at the descending aortic region.

Table 4.1: The thrombus percentage distribution at Segments 1, 2 and 3

Patient	Percentage of thrombosis in Segment 1				FL size changes	Total FL thrombosis across all segments
	Post-treatment	6 months	12 months	24 months		
SEGMENT 1						
1	100.0	-	-	-	Decrease	88.5
2	75.9	98.2	93.1	100.0	Decrease	84.3
3	93.0		98.9	100.0	Decrease	40.5
4	14.8	90.4	-	-	Decrease	54.2
5	62.2	-	47.3	50.4	Decrease	34.7
6	70.9	100.0	-	100.0	Decrease	100.0
7	95.9	90.6	-	-	Decrease	69.5
8	97.2	100.0	-	-	Decrease	72.3
9	77.8	-	82.0		Decrease	42.7
11	-	-	-	-	-	45.1
12	43.0	48.8	-	64.3	Decrease	54.0
13	98.7	73.1	-		Decrease	70.1
SEGMENT 2						
1	-	54.9	-	88.5	Decrease	
2	20.8	73.5	84.4	87.3	Increase	
3	9.2	-	16.1	35.1	Increase	
4	0.0	81.8	-		Increase	
5	-	-	-	-	-	
6	-	-	-	-	-	
7	75.1	81.6	-		Stable	
8	84.6		87.8	91.1	Decrease	
9	44.4	-	60.7		Increase	
11	69.3	-	93.8	-	Decrease	
12	--	-	-	-	-	
13	61.0	76.4	-	-	Decrease	
SEGMENT 3						
1	-	-	-	-	-	
2	0.0	3.9	3.2	10.0	Decrease	
3	0.0	0.0	5.5	2.1	Decrease	
4	0.0	1.8	-	-	Increase	
5	3.7	-	0.0	-	Increase	
6	-	-	-	-	-	
7	9.5	51.9	-	-	Increase	
8	11.6	33.9	53.3	63.0	Increase	
9	0.8	-	0.8	-	Increase	
11	0.0	2.3	17.6	-	Increase	
12	13.3	31.0	-	33.7	Decrease	
13	69.7	59.6	-	-	Decrease	

### 4.3.2 Relationship between aortic morphology and thrombus formation

After analysing thrombus formation at each segment, the total thrombus formation was analysed. Based on two years of follow-up, the thromboses inside the FL were classified into three categories in Table 4.2. They comprised of more than 80% FL thrombosis (Group 1), more than 50% but less than 80% FL thrombosis (Group 2) and 50% FL thrombosis or less (Group 3).

Based on Table 4.2, three patients, i.e. Patients 1, 2 and 6 showed more than 80% FL thrombosis in Group 1. Patient 6 showed 100% complete FL thrombosis, while Patients 1 and 2 demonstrated 88.5% and 84.3% FL thrombosis, respectively (Table 4.1). Among these three patients, Patient 1 had Type IIIA AD, while the rest were Type IIIB AD. Since Patient 1 had Type IIIA AD, by closing the primary entry tear and the whole dissection, Patient 1 obtained complete FL thrombosis during post-treatment. However, there was a SINE occurrence that caused a new dissection to form at the distal edge of the stent graft at the sixth month of follow-up (Segment 2 of Table 4.1). However, Patient 1 then developed 88% thrombosis at the 18th month of follow-up.

In comparison to the other Type IIIB AD patients, Patients 2 and 6 in Group 1 had the lowest percentage of  $\% L_{\text{Dissection}}/L_{\text{Aorta}}$  with no re-entry tears along the dissection. Another similarity between Patients 2 and 6 was the presence of branches that were partially supplied by the FL at the end of their dissections. Hughes *et al.* (2014) concluded that complete FL thrombosis after stent graft repair appeared to occur only in the setting of all branches arising from the TL. However, based on these two patients, i.e. Patients 2 and 6, in a condition of no re-entry tears, no occurrence of endoleaks and with dissection length up to only the abdominal branches vicinity, patients that had branches that were partially supplied by the FL at the end of the dissection could also generate more than 80% FL thrombosis. The communications connecting between the TL and the FL, i.e. branches partially supplied by both TL and FL would eventually act

as an extension of the branches (Qin *et al.*, 2012). It might be a kind of pathophysiology during the development of the FL and branches supplied by the FL, since the FL would shrink after the primary tear had been closed up by the stent (Qin *et al.*, 2012). Compared with Patient 2, the stent implanted in Patient 6 was longer (320 mm). The long stent insertion might hinder blood flow inside the FL, which could lead to a faster rate of thrombosis (Sayer *et al.*, 2008). Segment 1 in Patient 1 had completely developed FL thrombosis (100%) within six months of follow-up, while the same condition was seen in Patient 2 24 months later.

Table 4.2: Morphology of the aorta after stent graft repair

Patient	% $L_{Dissection}/L_{Aorta}$	Number of arteries partially of fully perfused by the FL	Number of re-entry tears	Length of implanted stent graft (mm)	Maximal FL diameter at abdominal region during pre- treatment (mm)	Acute vs Chronic
Group 1: More than 80 per cent complete FL thrombosis						
1	24	-	-	170	-	Acute
2	84	3	-	120	15.45	Acute
6	72	1	-	320	-	Acute
Group 2: More than 50 per cent but less than 80 per cent FL thrombosis						
4	100	1	3	170	11.62	Acute
7	100	1	3	180	17.43	Acute
8	100	1	9 (post- treatment), 3 (follow- up)	150	15.60	Acute
11	100	-	5	135	15.48	Acute
12	84	-	-	220/340 (Re- intervention)	17.98	Chronic
13	100	-	3	200	17.23	Acute
Group 3: Less and equal to 50 per cent FL thrombosis						
3	100	1	5	160	26.56	Acute
5	100	2	-	480	31.31	Chronic
9	100	3	7	130	19.62	Acute

Meanwhile, there were six patients who showed more than 50%, but less than 80% FL thrombosis, i.e. Group 2. All patients in this group had more than 100%  $\% L_{Dissection}/L_{Aorta}$ , except for Patient 12. Patient 12 had less than 100%  $\% L_{Dissection}/L_{Aorta}$ , and developed 54% of FL thrombosis only two years later. This patient's condition was not stable because of the presentation of ulcers. Moreover, the thrombosis formed approximately 60% only along the stent region (Table 4.1). The other five patients in Group 2 had more than three re-entry tears within Segments 2 and 3, which caused continuous perfusion in the FL (Czermak *et al.*, 2004). Thromboses hardly formed because of high blood flow inside the FL. However, the number of branches partially or fully supplied by the FL, stent graft length and maximum FL diameter at the abdominal section were varied among patients in the group.

Only three patients, i.e. Patients 3, 5 and 9 showed 50% FL thrombosis or less (Group 3). They were Type IIIB AD patients and had 100%  $L_{Dissection}/L_{Aorta}$ . Compared with Group 1 and Group 2 patients, Group 3 patients showed higher maximum FL diameter in Segment 3 that ranged between 19.62 mm and 26.56 mm, and also had more re-entry tears except for Patient 5. As noticed in a numerical simulation study by Fan *et al.* (2010), a bigger FL would have a smaller domain of stagnant fluid, which could result in a smaller region of thrombosis. In Table 4.1, no thrombus or very little thrombosis could be seen in Segment 3. Patient 5 did not have re-entry tears at the FL despite having a long stent implanted. He had chronic Stanford Type B AD before treatment, therefore, the flap was hardly moved by the stent because it was probably not mobile (Sayer *et al.*, 2008). Thrombosis was rarely observed along the stent region in Patient 5 (Table 4.1). Similar to Group 2 patients, the number of branches that were partially or fully supplied by the FL and stent graft length was varied among patients.

#### **4.4 Limitations**

Due to the small number of patients and short follow-up time, robust conclusions on the efficacy of stent graft placement for Stanford Type B AD could not be drawn. However, the results reflected the feasibility of stent graft repair in stabilising the TL of Stanford Type B AD patients. Further studies based on a large cohort with longer follow-up data are desirable.

#### **4.5 Summary**

A good outcome in stent graft repair can be achieved with TL expansion and FL shrinkage in Segment 1. Continuous blood flow in the FL at Segments 2 and 3 would cause the volume to increase in some patients, leaving these segments an area of concern. In addition, good outcomes could also be achieved with complete FL thrombosis. This study characterises thrombus formation into three groups. The first group is Group 1, where the patients have more than 80% FL thrombosis. Patients in this group have shorter dissection length (up to celiac artery branches) without re-entry tears; and contain abdominal branches that were partially supplied by the FL at the end of the dissection. The second group is Group 2, where the patients have more than 50% but less than 80% FL thrombosis. The patients in this group have longer dissection length with three and more re-entry tears along the dissection in Segment 2 and 3. The third group is Group 3, where the patients have 50% FL thrombosis or less. The patients in this group have higher maximal FL diameter at the abdominal region before stent graft repair. Other circumstances hindered the complete FL thrombosis are the occurrence of SINE, ulcers and chronic Type B AD.

# **CHAPTER 5: PREDICTION OF THROMBUS FORMATION IN STANFORD TYPE B AD PATIENT: A PRELIMINARY STUDY USING CFD APPROACH**

## **5.1 Introduction**

Based on the review of Section 2.3.2, a preliminary investigation which uses vortical structures as a potential parameter to describe the mechanism behind the formation of thrombus and to predict its location in AD patients, using patient-specific geometry of a Stanford Type B AD patient was carried out. Detailed distributions of vortical structures as well as WSS in the FL region were analyzed throughout a cardiac cycle, both qualitatively and quantitatively. In order to investigate the effect of FL size on the haemodynamic variables and the subsequent effect to thrombosis, the original geometry was modified by varying the diameter of the FL region. Furthermore, the Carreau-Yasuda model, representing non-Newtonian fluid property was used to study the difference between Newtonian and non-Newtonian fluid settings on vortical structures. This work had been published in the Journal of Applied Mathematical Modelling.

## **5.2 Methodology**

### **5.2.1 Model geometry**

CTA images of a Stanford Type B AD patient were manually segmented to generate a 3D model, (i.e. Geometry 1), as shown in Figure 5.1 and Table 5.1. The FL ended at the descending aorta region. This study was approved by the Curtin University Human Research Ethics Committee. Diameters of the descending aorta (including both TL and FL) at planes A, B, and C as illustrated in Figure 5.1 and Table 5.1 were 37.9, 56.0 and 41.8 mm, respectively. On the other hand, diameters of the FL at planes A, B, and C were 25.2 mm, 24.8 mm and 26.0 mm respectively. To investigate the effect of FL size

on the haemodynamic variables, the original geometry was modified by increasing (Geometry 2) and decreasing (Geometry 3) the diameter of the FL region. The FL in Geometry 1 has been separated from the TL using Boolean operation function (subtract) in ScanIP image processing software (Simpleware Ltd, Exeter, Devon, UK). Then, two copies of FL were generated. For Geometry 2, the 'Segmentation' tool was used to 'paint' separated FL approximately 1-2 pixel (1 mm per pixel)  $\pm 0.57$  at each of cross sectional images. Meanwhile, the separated FL was unpainted approximately 2-3 pixels  $\pm 0.17$  mm at each of cross sectional images for Geometry 3. Irregular shapes of the geometry as well as limited geometry orientation cause some limitations for geometry modification. Therefore, the increment size is varying between 5-10% while the decrement size varying between 10-15% along the FL. Based on Chen *et al.* (2013b), an increase in the total aortic diameter (up to 4 mm) is likely to happen during the follow up periods for patients with Stanford Type B AD. Later, in both cases, the modified FL reunited (Boolean operation) with the TL and become complete sets of AD geometry (Geometry 2 and Geometry 3). Measurements of the diameter at Plane A, Plane B and Plane C were obtained at perpendicular to the line of the intimal flap. The respective sizes of the FL as well as the descending aorta at the three different planes for the original and modified geometries are listed in Table 5.1. The height and width of the entry tear were 18.4 mm and 44.6 mm respectively.

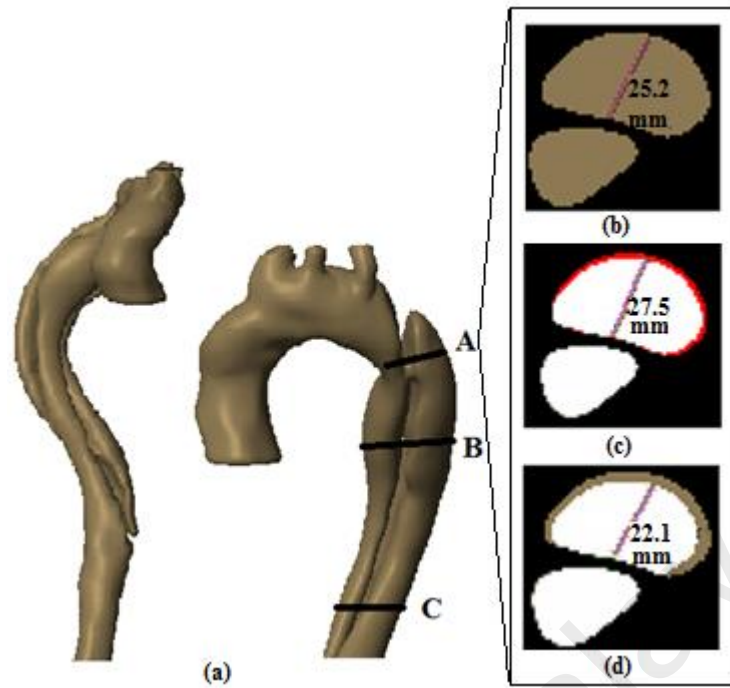


Figure 5.1: (a) 3D reconstructed model of the AD with labeling of Plane A, Plane B and Plane C; (b) cross sectional image of Geometry 1 at Plane A; (c) cross sectional image of Geometry 2 (red) overlapped with Geometry 1 (white) at Plane A; and (d) cross sectional image of Geometry 3 (white) overlapped with Geometry 1 (brown) at Plane A.

Table 5.1: The dimensions of the aorta and the FL at three different planes for the original (Geometry 1) and modified geometries (Geometries 2 and 3).

Geometry	Plane	Diameter (mm)	
		Aorta	FL
Geometry 1	A	37.9	25.2
	B	56.0	24.8
	C	41.8	26.0
Geometry 2	A	40.2	27.5
	B	57.1	25.8
	C	44.0	28.1
Geometry 3	A	34.8	22.1
	B	53.5	22.1
	C	39.0	23.0

### 5.2.2 Model settings

The aortic wall was assumed to be rigid, based on in vivo data obtained from 32 Stanford Type B AD patients which showed a significant reduction (12%) in the vessel wall distensibility (Ganten *et al.*, 2009). No-slip boundary condition was applied at the aortic wall, whereby the fluid near the wall boundary has zero velocity relative to the

boundary. Two different fluid properties, i.e. Newtonian and Carreau-Yasuda (representing non-Newtonian) models were used in the present study. The Carreau-Yasuda model was chosen, as previous experimental studies (Gijssen *et al.*, 1999) have shown that its shear thinning properties match that of the blood, and it is able to predict velocity distribution in the carotid bifurcation accurately. For the Newtonian model, blood was assumed to be homogenous and incompressible with a dynamic viscosity of 0.00371 Pa.s and a density of 1060 kg/m<sup>3</sup> (Tse *et al.*, 2011). The Carreau-Yasuda model (Biasetti *et al.*, 2011; Gijssen *et al.*, 1999), on the other hand, is defined as Equation 5.1:

$$\frac{\mu - \mu_{\infty}}{\mu_0 - \mu_{\infty}} = [1 + (\lambda\gamma)^a]^{\frac{n-1}{a}} \quad (5.1)$$

where  $\gamma = \sqrt{2D}$ . The symbol denotation was listed in Table 5.2.

Table 5.2: Carreau-Yasuda model symbol denotation

Symbol	Definition
D	The scalar shear rate
$\mu_0$	The zero shear rate limit (0.16 Pa.s)
$\mu_{\infty}$	The infinite shear rate limit (0.0035 Pa.s)
$\lambda$	The relaxation time (8.2 s)
n	The power index (0.2128)
a	The width of the transition region (0.64)

Similar to previously published simulation studies for AD (Tse *et al.*, 2011), the flow was assumed to be laminar in the present study. For a pulsatile and unsteady flow, turbulence occurs at a Reynolds number that is much higher than that expected for a steady flow due to a more stable accelerating flow and a more unstable decelerating flow (Tse *et al.*, 2011). According to Morris *et al.* (2005), flow can be considered to be laminar if the maximum Reynolds number ( $Re_{max}$ ) is less than the critical Reynolds number ( $Re_c$ ). The critical Reynolds number ( $Re_c$ ), or also called the transition Reynolds number, for unsteady flow takes the form of  $Re_c = k \times$  Wormersley number (Nerem *et al.*, 1972), where  $k$  ranges between 250 to 1000. As shown in Table 5.3, the

maximum Reynolds numbers,  $Re_{max}$  for all three geometries adopted in this study were lower than their respective minimum critical Reynolds number,  $Re_c$ .

The continuity and momentum equations (Equation 5.2 and Equation 5.3) were used to govern blood flow in the present study, as follows:

$$\frac{\partial}{\partial t}(\rho v) + \rho(v \cdot \nabla)v = -\nabla p + \nabla \cdot \tau \quad (5.2)$$

$$\nabla \cdot v = 0 \quad (5.3)$$

The symbol  $\vec{v}$  represents the velocity vector,  $p$  represents the pressure,  $\rho$  represents the density and  $\tau$  represents the stress.

Table 5.3: The maximum and critical Reynolds number, as well as Wormersley number for Geometries 1, 2 and 3.

	Geometry 1	Geometry 2	Geometry 3
Maximum Reynolds number, $Re_{max}$	4570	3826	4533
Average Wormersley number	20.8	21.3	20.0
Minimum Critical Reynolds number, $Re_c$	5193	5325	5016

### 5.2.3 Boundary conditions

A pulsatile flow as illustrated in Figure 5.2(a), with a flat velocity profile, was applied at the entrance of the ascending aorta and this is consistent with that used in previous studies (Olufsen *et al.*, 2000; Tse *et al.*, 2011). The use of a flat velocity profile at the aortic inlet was justified based on in-vivo measurements using the hot film anemometry technique on animal models (Nerem *et al.*, 1972). Although a recent study by Van Doormaal *et al.* (2012) showed that the usage of a flat velocity profile could not capture the WSS at the ascending aorta accurately; they found that the effect of the inlet velocity profile in the descending aorta region, which is the focus of the present study, was negligible. Based on previous studies (Olufsen *et al.*, 2000; Tse *et al.*, 2011), 5% of

the flow volume was diverted to each branch outlet, which are left subclavian artery, left common carotid artery, and brachicephalic artery. A pulsatile pressure waveform as shown in Figure 5.2(b) was applied at the exit of the descending aorta. As patient-specific measurements of flow and pressure were not obtained in this project, the above-mentioned boundary conditions (at the inlet and outlet), which have been used extensively in studies on diseased aorta (Chen *et al.*, 2013b; Lam *et al.*, 2008; Tse *et al.*, 2011), were applied in our simulations.

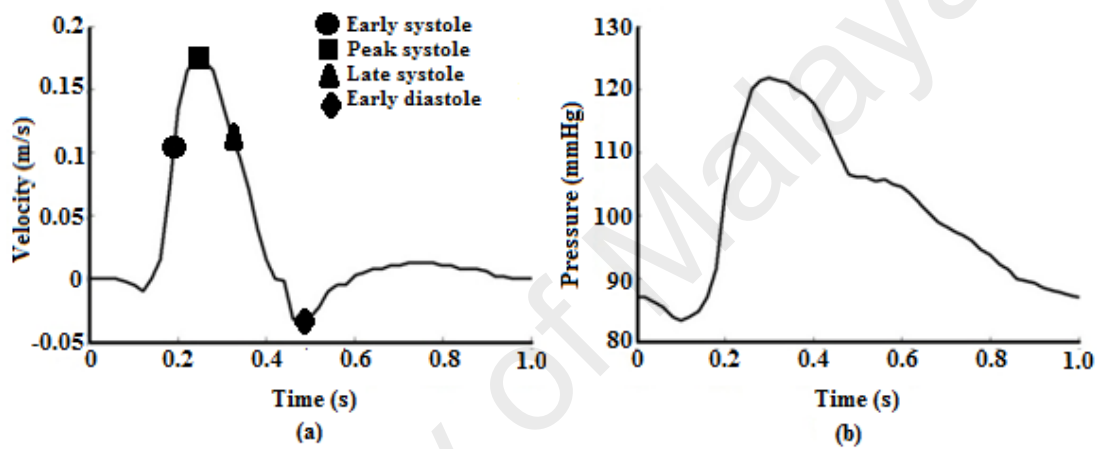


Figure 5.2: Inlet and outlet boundary conditions: (a) pulsatile inlet velocity profile; (b) pulsatile outlet pressure profile. Adapted from references Olufsen *et al.* (2000); Tse *et al.* (2011).

#### 5.2.4 Numerical methods

The commercial CFD package of ANSYS FLUENT 14.0 (ANSYS, Inc., Canonsburg, PA, USA) was used, which is based on the finite volume method. The Second Order Upwind Scheme was used to discretize the governing equations. The PISO (Pressure Implicit with Splitting of Operators) algorithm was used for the coupling of the pressure-velocity terms. A steady state solution at the maximum flow rate during peak systole was first obtained and this solution was used as an initial condition, for unsteady pulsatile flow simulation. Five cardiac cycles were simulated for each model. After four complete cycles, cycle to cycle variations were less than 1 %.

Therefore, all results presented in the current study were taken from the 5<sup>th</sup> cardiac cycle. During the post processing stage, the results were taken at four time instants (reported with reference to the beginning of the 5<sup>th</sup> cardiac cycle), i.e. at  $t = 0.20$  s (early systole),  $0.25$  s (peak systole),  $0.38$  s (late systole) and  $0.47$  s (early diastole).

### 5.2.5 Mesh Independence and Time Step Sensitivity Studies

ICEM CFD, ANSYS 14.0 Inc. was used for meshing of the domain. The meshes consist of prism cells near the boundary wall and tetrahedral cells at the core region. In a simulation study investigating the mesh requirements for flow within the dissected aorta, Chen *et al.* (2013b) revealed that laminar simulations with near-wall mesh refinement using the prismatic boundary layer elements resulted in similar flow patterns, including WSS and other quantities, to the  $k-\omega$  SST model, with discrepancies less than 1.3% for both velocity and pressure. Thus, 15 prismatic layers were used for the near-wall mesh refinement at the boundary layer in the present study. Meanwhile, mesh dependency tests were carried out by creating three different meshes consisting of 1.92 million, 2.62 million and 3.52 million total cells, respectively, for Geometry 2. The average velocity and pressure at the entry tear region, which is both the region of interest and location with a high numerical sensitivity (due to substantial changes in the area and diversion of flow from the true lumen to the false lumen), were analyzed and shown in Table 5.4. The difference between the chosen mesh (2.62 million) and finer mesh (3.52 million) for both average velocity and average pressure was less than 5% and therefore, 2.62 million cell was deemed adequate for this simulation. Meanwhile, the number of elements being used was comparable with Cheng *et al.* (2010), which used 2.69 million elements in their simulation for AD. The number of elements used for Geometries 1 and 3 were 2.65 M and 2.66 M, respectively.

Apart from the grid independence study, a test concerning the time step sensitivity of the unsteady simulation was also conducted. Three temporal discretization settings were tested: 0.01 s (large time step), 0.005 s and 0.001 s. Reducing the time step from 0.005 s to 0.001 s has only resulted in a small difference in the velocity distribution (less than 5%) but significantly increased the computational cost. Thus, a time step of 0.005 s was used in the present study for computational efficiency.

Table 5.4: Results of mesh independent test of comparison of average velocity and maximum pressure between meshes

Number of cells	Average velocity (m./s)	Differences (%)	Average pressure (Pa)	Differences (%)
1 915 996	0.26		1105.65	
2 628 175	0.23	12.3	1093.95	1.1
3 521 903	0.24	3.9	1147.12	4.7

### 5.2.6 Eduction Method for the Identification of Vortical Structures

For a quantitative representation of vortical structures,  $\lambda_2$  method defined by Jeong and Hussain (1995) was used as it is recommended to be the most suitable method for problems related to biological fluid such as blood (Biasetti *et al.*, 2011). To determine the local pressure minimum due to vortical motion, the eigenvalues of the  $S^2 + \Omega^2$  tensor (the symmetric (S) and antisymmetric ( $\Omega$ ) parts of the velocity gradient tensor) were calculated (Pierakos & Vlachos, 2006). Ranking the eigenvalues as  $\lambda_1 > \lambda_2 > \lambda_3$ , the presence of vortical structures was defined as regions with negative  $\lambda_2$  (Biasetti *et al.*, 2011). For the purpose of providing a clearer illustration, a threshold value,  $\lambda_{2,t}$  equivalent to  $-12.5s^{-2}$  was applied to reduce the number of vortical regions (Biasetti *et al.*, 2011; Loerakker *et al.*, 2008). The  $\lambda_2$  intensity in the whole blood domain was calculated using the following Equation 5.4:

$$\int \omega dV_{\text{fluid}} \quad (5.4)$$

where  $dV_{\text{fluid}}$  is the fluid domain and  $\omega$  is the vorticity. In the present study, vortical structures was analyzed by distinguishing spanwise vortices from streamwise vortices, as proposed by Biasetti *et al.* (2011). Vortical structures originate from the shear layer near the wall where a region of high velocity gradient exists (Biasetti *et al.*, 2011). Spanwise vortical structures were formed when this unstable shear layer undergoes a Kelvin-Helmholtz instability, leading to a rolled up layer of vorticity (Biasetti *et al.*, 2011). In contrary, unstable low speed streaks trigger the formation of streamwise vortical structures, where sheets of streamwise vorticity collapse into streamwise vortices by a stretching rather than a roll up mechanism (Biasetti *et al.*, 2011). The nonlinear process of pairing, tearing and reconnection in vortical structures causes them to move, develop and interact among each other (Biasetti *et al.*, 2011).

The breakdown of vortical structures into streamwise substructures released the platelets which would subsequently adhere to low WSS location, leading to the formation of thrombus. Therefore, in order to predict the location of thrombus extension, WSS contour was superimposed on the vortical structures distribution. The location of thrombus extension can be predicted at the regions where vortical structures show break up (due to a lost in strength) with low velocity and WSS ( $< 0.5$  Pa) (Bluestein *et al.*, 1999; Kamman *et al.*, 2016; Raz *et al.*, 2007).

## **5.3 Results and Discussion**

### **5.3.1 Flow patterns and pressure distribution**

Figure 5.3(a) showed the velocity streamline superimposed on the vortical structures in the original geometry at peak systole, using the Newtonian model. Consistent with previously published CFD simulation study by Cheng *et al.* (2013) on AD, strong jet-like flow passed through the entry tear region and impinged onto the posterior region of

the FL wall (Figure 5.3(b)). Recirculation zones with dominant vortical structures were observed around the entry tear, as previously shown in both initial and follow up studies using phase-contrast magnetic resonance images (PC-MRI) (Karmonik *et al.*, 2012) as well as in vitro experimental studies (Rudenick *et al.*, 2013). Consequently, high shear gradient was generated, resulting in high, localized WSS at this region. Both the peak systolic velocity (85 cm/s) and maximum TAWSS (6.73 Pa) coincides with previously published values, (i.e. up to 80 cm/s (Cheng *et al.*, 2013) for large tears and 6.92 – 14.1 Pa at the throat of the coarctation (Tse *et al.*, 2011).

With regards to the pressure distribution, the pressure in the TL was generally higher than that in the FL in the proximal portion but opposite in the distal portion at peak systole (Figure 5.4 (a)), as observed in both in vitro experimental (Tsai *et al.*, 2008) and simulation (Cheng *et al.*, 2010; Tse *et al.*, 2011) studies (Figures 5.4(c) and 5.4(d)). To the contrary, proximal FL pressure was slightly higher as compared to TL during diastole (Figure 5.4(b)).

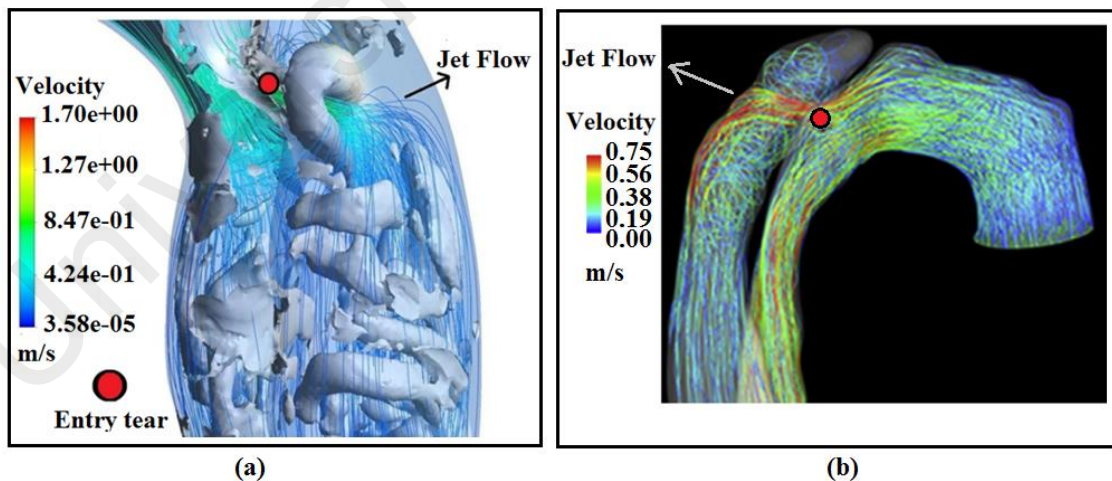


Figure 5.3: Comparison of jet flow passing through the entry tear for (a) this work; (b) Cheng *et al.* (2013).

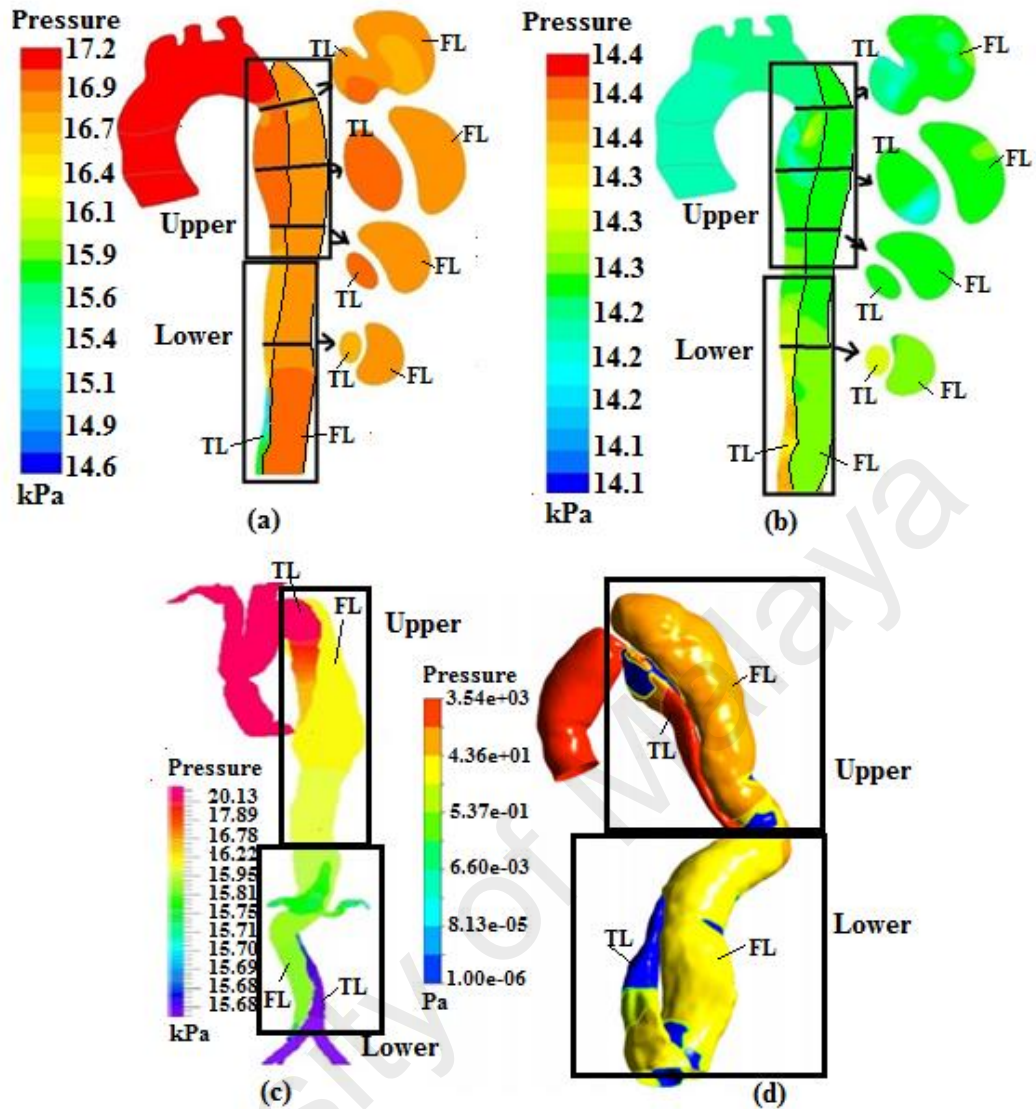


Figure 5.4: Pressure distribution in the TL and FL regions at (a) peak systole and (b) early diastole for this work; (c) Tse *et al.* (2011); (d) Cheng *et al.* (2010).

### 5.3.2 Evolution of vortical structures in the FL region throughout a cardiac cycle

Based on Figure 5.5, the region of interest in this study was the FL region. Region labeled with A was located above the entry tear region while regions labeled with B, C and D were located at the entry tear and below the entry tear region. As shown in Figure 5.5, aggregated vortical structures were found above the entry tear region during early systole (zoom in Label A1) while these vortical structures were found to be slightly reduced in size during peak systole (zoom in Label A2). Below this, i.e. around the

entry tear region, vortical structures observed during early systole (Label B1) were found to develop into a ring-shaped pattern during peak systole (Label B2). Meanwhile, below the entry tear region, vortical structures which exist (Label C1) during early systole were observed to move slightly downstream during peak systole (Label C2). At the distal part of the false lumen, more distinct spanwise vortical structures could be observed during peak systole (Label D1) as compared to early systole, especially at the inner part of the curvature. The interaction between the vortical structures with the boundary layer caused a localized region of high WSS at the coarctation (12.43 Pa during peak systole) and the entry tear region (14.70 Pa during peak systole).

As compared to peak systole, the ring-shaped vortical structures found around the entry tear entrance region (Label B2) expanded and accumulated around and below the region (from approximately 20 mm to 80 mm) during late systole and early diastole (Labels B3 and B4) respectively. Meanwhile, vortical structures that were located downstream of the entry tear (Label C2) during peak systole were found to have broken down into several streamwise substructures during late systole and early diastole (Label C3 and Label C4). Less spanwise vortical structures were found at the distal part of the FL during late systole (Label D2) and early diastole (Label D3).

This is the first study attempting to explain and predict the location of thrombus in AD cases with complicated geometrical feature both qualitatively and quantitatively, based on the evolution of vortical structures and their interaction with the WSS in the FL region throughout a cardiac cycle. In the present study, vortical structures were seen to occupy the entire FL region (except at a few locations) over the whole cardiac cycle (Figure 5.5 – 5.6). The presence of recirculation zones with dominant vortical structures, together with the action of the high WSS surrounding the entry tear, is believed to cause platelet activation (Biasetti *et al.*, 2011). The strong jet-like flow through the entry tear pushed the reattachment point downstream, and contributed to the

growth of the vortical structures (Kamman *et al.*, 2016). The growth and accumulation of the vortical structures around and below the entry tear region continued throughout peak and late systole (label B2 and B3 in Figure 5.5), causing repeated collision of platelets for a long period of time (Ahmed *et al.*, 2016), and is believed to result in the spontaneous formation of the platelet aggregates (Biasetti *et al.*, 2011). During late systole and early diastole, the flow had lost its strength and as a result the vortical structures were seen to have broken down into several streamwise substructures. The breakup of vortical structures released the platelets which were subsequently adhered to the low WSS location.

Figure 5.6 shows the superimposition of the WSS contour and the vortical structures distribution during early diastole to predict the location of thrombus formation. Based on the analysis (from the evolution of vortical structures in Figure 5.5 and Figure 5.6) following the method described in Section 5.2.6 where the thrombus will be formed when the breakdown of vortical structures into streamwise substructures released the platelets which would subsequently adhere to low WSS location (Figure 5.6), thrombus is predicted to form at the posterior region of the FL wall, extending up to 56 mm below the entry tear (Label C4 in Figure 5.5, corresponding to the circular region in Figure 5.6). These results were supported by two separate longitudinal studies (Cheng *et al.*, 2013; Karmonik *et al.*, 2012) who carried out on a chronic dissection patient (Karmonik *et al.*, 2012) as well as sequential follow-up scans on a patient with acute dissection (Cheng *et al.*, 2013). In Karmonik *et al.* (2012) study on a chronic dissection patient, a hypointense region was observed in the MRI images after contrast injection at the posterior thoracic FL wall, which they believed to represent thrombus formation. Cheng *et al.* (2013) performed seven consecutive scans over a year on an acute dissection patient, and they reported the formation of thrombus at the posterior FL region below the entry tear, which extended downward along the wall during follow-up examinations.

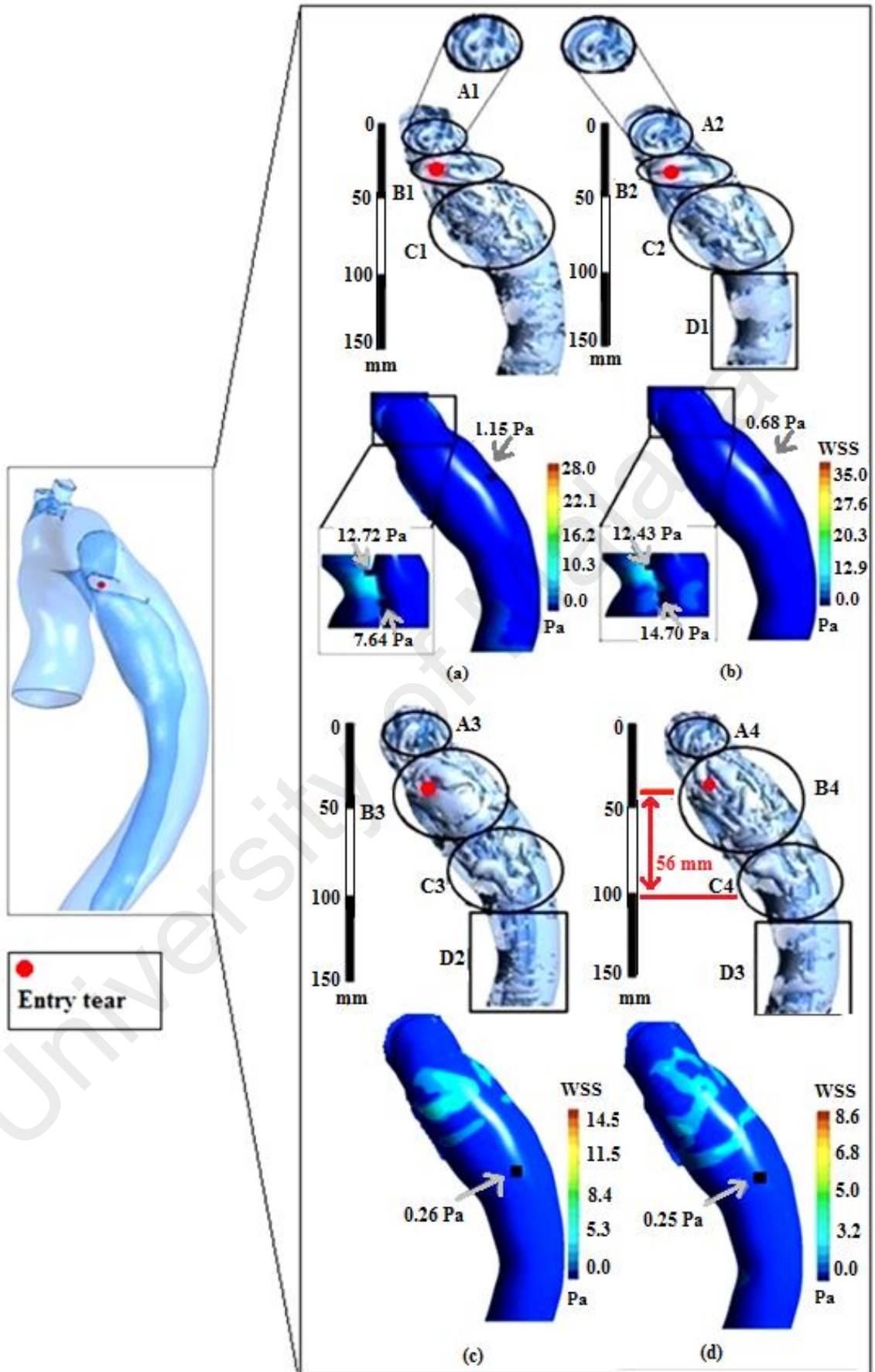


Figure 5.5: Vortical structures ( $\lambda_{2,t}$  equal to  $-12.5 \text{ s}^{-2}$ ) distribution and contour of WSS for Newtonian model at (a) early systole; (b) peak systole; (c) late systole and (d) early diastole.

As reported in previous studies (Trimarchi *et al.*, 2013; Tsai *et al.*, 2007), formation of a partial thrombus in the FL region may occlude distal re-entry tears, leading to high diastolic pressure, increased wall tension and elevated risk of aneurismal dilatation or rupture, particularly at the proximal FL site. Furthermore, intraluminal thrombosis has been reported to cause local inflammation and localized wall weakening (Sueyoshi *et al.*, 2009), in particular in the FL region which already had reduced wall strength. In addition, high WSS observed at the coarctation throat may cause additional injury to the endothelial cells, leading to an expansion of the entry tear (Tse *et al.*, 2011).

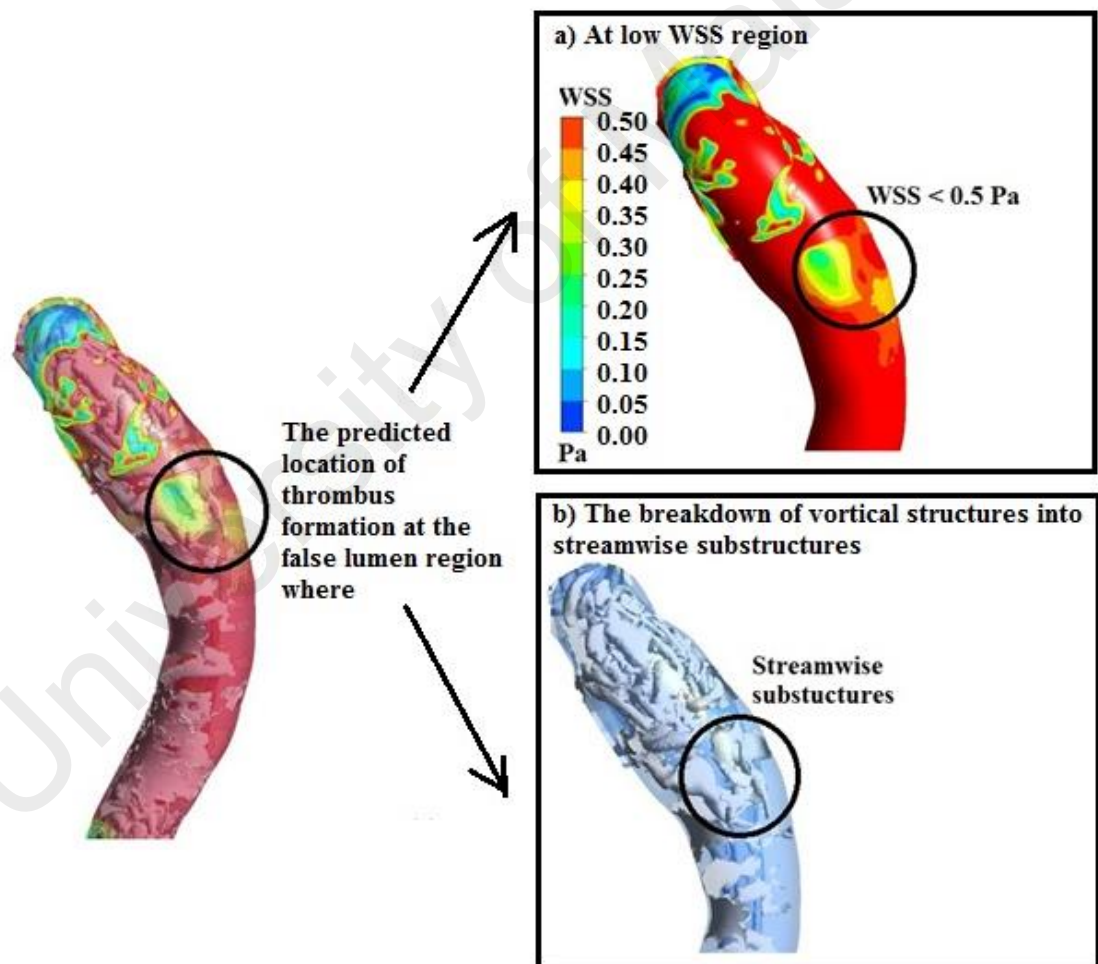


Figure 5.6: (a) WSS contour superimposed on vortical structures; (b) Contour of WSS and (c) Vortical structures distribution during early diastole.

### 5.3.3 Effect of non-Newtonian (Carreau-Yasuda) property on vortical structures and WSS

As compared to the Newtonian model, though the distribution of the spanwise vortical structures for the Carreau-Yasuda model showed no significant difference, a lower number of streamwise vortical structures with smaller sizes were observed in the Carreau-Yasuda model (Figure 5.7). In terms of quantitative representation based on  $\lambda_2$  intensity in the blood vessel domain (Table 5.5), some significant differences were seen between these two models at early systole, peak systole and early diastole. For example, the Newtonian model predicted up to 8.12% more vortical structures per volume of fluid at early systole as compared to the Carreau-Yasuda model. Among the four cardiac phases, minimum percentage difference in  $\lambda_2$  intensity was found during late systole, with the Newtonian model having slightly higher  $\lambda_2$  intensity (2.44%) as compared to the Carreau-Yasuda model.

A non-Newtonian model is known to be able to capture blood rheology more accurately as compared to a Newtonian model (Biasetti *et al.*, 2011). To date, only Cheng *et al.* (2010) have looked at the effect of rheological properties in aortic dissection cases using the Quemada model. Their results revealed that the inclusion of a non-Newtonian model caused a reduction in the maximum WSS value (~8%) and either an extension or reduction in the turbulence intensity at different regions along the vessel. Both graphical and quantitative presentation of vortical structures in this simulation results revealed that the Newtonian model overestimated streamwise vortical structures in the FL. This is in agreement with Biasetti *et al.* (2011) findings, which suggested that streamwise vortical structures might be an artifact of the Newtonian model. The shear thinning behavior of the Non-Newtonian model was able to capture the increase in viscosity in the core flow region, thus suppressing the development of streamwise vortical structures (Biasetti *et al.*, 2011).

Table 5.5: Comparison of the  $\lambda_2$  intensity ( $\text{m}^3/\text{s}^2$ ) in the whole blood domain between the Newtonian (New) model and the Carreau-Yasuda (C-Y) model

Cardiac phase	New	C-Y	Diff New-CY (%)
Early systole	-0.0084	-0.0078	8.12
Peak systole	-0.0192	-0.0180	6.67
Late systole	-0.0303	-0.0311	2.44
Early diastole	-0.0235	-0.0222	5.89

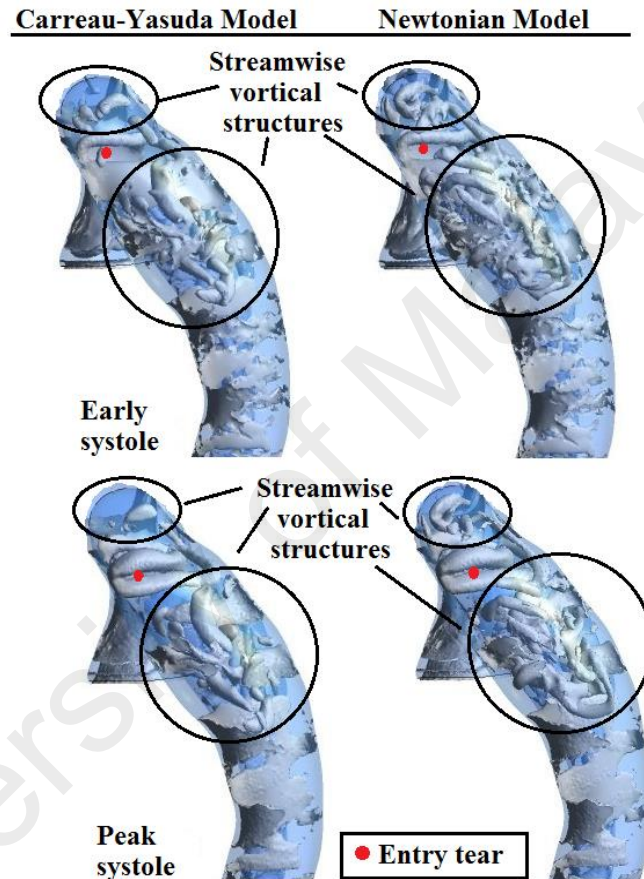


Figure 5.7: Vortical structures distribution for Carreau-Yasuda model and Newtonian model at early systole and peak systole.

### 5.3.4 Effect of FL size on vortical structures and WSS using Carreau-Yasuda model

Since Carreau-Yasuda model is expected to present blood rheology more accurately, it was used in this section. Among the three geometries used in the present study, Geometry 2 has the largest FL diameter, followed by Geometry 1 and 3. Geometry 1

was the original geometry and was used as the reference for modification. Geometry 2 was defined as having the largest dimension among all three geometries, as it was developed by increasing the FL size from the original geometry by 10%. Geometry 3 was developed by decreasing the FL size by 10% from the original geometry. From the analysis, the changes or trend of the vortical structures and WSS results in the simulation study are very much dependent on the changes in the FL sizes.

With regards to the quantitative representation based on the  $\lambda_2$  intensity (Table 5.6), a significant difference can be seen among the different geometries with varying FL sizes, especially during early and peak systole. Higher  $\lambda_2$  intensity was achieved with an increase in the FL size in all cardiac phases. In particular, Geometry 2 with the largest FL diameter predicted up to 51.58% more vortical structures per volume of fluid at early systole as compared to Geometry 1 with a smaller FL diameter. Among the four cardiac phases, minimum percentage difference in  $\lambda_2$  intensity was found during late systole and early diastole. Meanwhile, the simulation results (Figure 5.8) showed that the percentage of flow entering the FL increased with an increase in the FL size. On the other hand, the predicted location of thrombus formation (based on the analysis method (Figure 5.5 (d), label with red lines)) appeared to be extended further away from the entry tear region with increasing FL size.

The distributions of WSS were almost similar in both geometries (Geometries 2 and 3) despite a difference in their relative magnitudes (Figure 5.9). During early systole and peak systole, high WSS was observed at the coarctation region at the exit of the aortic arch and at the entry tear region, coincident with regions accumulated with spanwise vortical structures. Regions of low WSS was observed at the distal region of the posterior FL wall. Geometry 2 with the largest false lumen diameter demonstrated the highest maximum WSS value (21.04 Pa vs. 15.01 Pa for Geometry 3 with the smallest FL diameter at peak systole at the entry tear region, accounting for a difference

of 40.2%), but a lower minimum WSS value (0.42 Pa vs. 0.58 Pa for Geometry 3 at posterior FL region, accounting for a difference of 32.9%).

Although FL size has been recognized as an important risk factor for rapid aneurismal growth and increased chance of thrombosis (Trimarchi *et al.*, 2013), the mechanism behind this remains to be clarified. In the present study, the effect of FL size on the risk of thrombus formation using vortical structures presentation by modifying the original patient specific geometry was investigated. The simulation results demonstrated a more dominant vortical structures and higher  $\lambda_2$  intensity with increasing false lumen size. In addition, consistent with previously published findings (Cheng *et al.*, 2010; Tse *et al.*, 2011), higher maximum WSS value was encountered at the bended throat of coarctation, with an increase in the percentage of flow entering the FL. Based on the interrelationship among vortical structures, WSS and thrombus formation described before, the observations could explain the increased chance of thrombus formation in patients with FL dilatation (Biasseti *et al.*, 2011). Apart from that, the analysis results showed that the predicted location of thrombus formation appeared to be extended further away from the entry tear region with increasing FL size. It is believed that this is caused by an associated increase in the FL flow rate and  $\lambda_2$  intensity, which pushed the vortical structures further downstream. The findings were consistent with a longitudinal study (Cheng *et al.*, 2013), which demonstrated a downward shift of the areas of thrombus formation during sequential follow up scans in a patient with acute dissection, which showed a significant increase in the primary tear size and FL flow rate. Formation of thrombus further away from the entry tear region could increase the chance of dissected aorta with the sac-formation type, i.e. that involves coverage of the distal re-entry tear, which has been shown to cause a substantial increase in the growth rate of the FL (Trimarchi *et al.*, 2013).

Table 5.6: Comparison of the  $\lambda_2$  intensity ( $\text{m}^3/\text{s}^2$ ) in the whole blood domain for Carreau-Yasuda model for Geometry 1 (G1), Geometry 2 (G2) and Geometry 3 (G3)

Cardiac phase	G1	G2	G3	Diff G1-G2 (%)	Diff G1-G3 (%)
Early systole	-0.0078	-0.0128	-0.0069	51.58	12.29
Peak systole	-0.018	-0.0223	-0.0142	21.59	23.94
Late systole	-0.0311	-0.031	-0.026	0.32	18.01
Early diastole	-0.0222	-0.0216	-0.0208	2.74	6.52

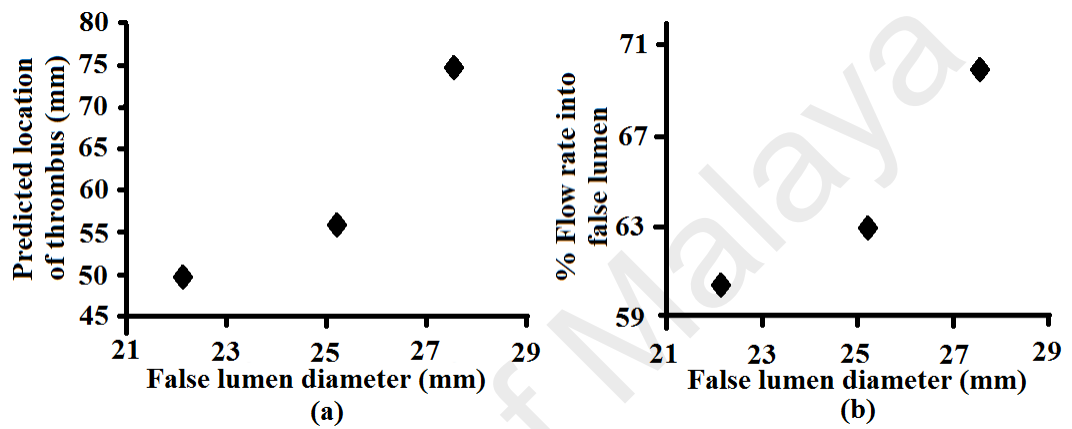


Figure 5.8: (a) Predicted location of thrombus extension (measured from the entry tear location) and (b) percentage of flow entering the FL for 3 different geometries with varying FL diameters (measured at plane A as shown in Figure 5.1).

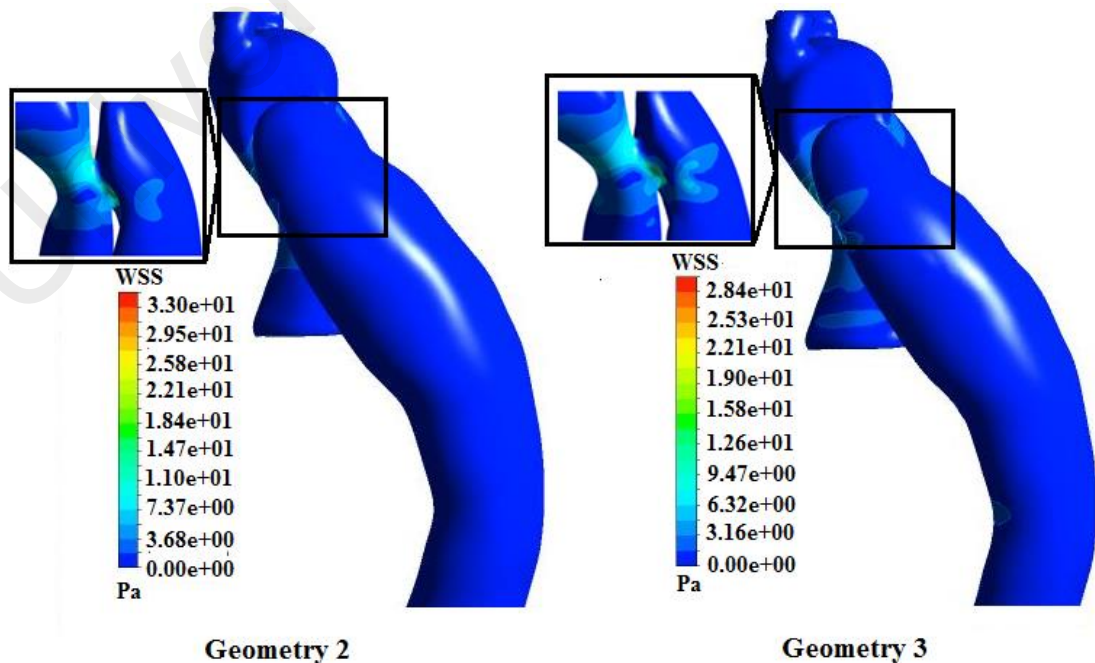


Figure 5.9: The distributions of WSS for Geometries 2 and 3 at peak systole.

#### 5.4 Limitations

As this is a preliminary study to describe the evolution of vortical structures and their interaction with the WSS in AD cases, CT images of only one patient during initial examination were used, and no follow up studies were performed to confirm the predicted location of thrombus formation. In spite of this, the process by which vortices and shear stress influence platelet activity, i.e. activation, aggregation and deposition, which served as the basis of this study, has been well established numerically and validated experimentally in previous publications (Kamman *et al.*, 2016; Raz *et al.*, 2007). Furthermore, as shown in Section 5.3.1, with regards to haemodynamic variables in term of flow pattern and pressure distribution, the simulation results were comparable with previously published clinical and experimental findings. Future studies involving more patients with different AD configurations, obtained at both initial examination and during follow up studies, will be carried out to ascertain the predictive value of the vortical structures on thrombus formation.

The aortic wall was assumed to be rigid. This is justified to be a reasonable assumption given the fact that the compliance of an aneurysmal blood vessel is significantly reduced due to the lack of elastin (Boussel *et al.*, 2009). As described in Section 5.2.2, in vivo data have shown a significant reduction in the vessel wall distensibility in Stanford Type B AD patients, and consequently no appreciable vessel wall movement was observed in the cine MRI images over a cardiac cycle (Ganten *et al.*, 2009). Furthermore, the main difficulty in assuming the wall of aorta and AD to be elastic is that the vessel wall contains both healthy and diseased tissue, for which the exact material properties are difficult to be ascertained.

In the present study, laminar flow model was adopted based on the calculation results which showed that the maximum Reynolds numbers for all three geometries were lower than their respective ranges for critical Reynolds number. Furthermore, near wall mesh

refinement using 15 prismatic boundary layer elements was adopted in the present study, based on simulation findings by Chen *et al.* (2013b) who revealed that a minimum of 10 prismatic layers for the boundary layer was fine enough to yield similar flow patterns as the  $k-\omega$  SST model. While the present study focuses on qualitative presentation of vortical structures, on-going studies using transitional SST model are being carried out.

## 5.5 Summary

In conclusion, this study shows that the evolution of vortical structures throughout a cardiac cycle and their interaction with the WSS provided an insight into the potential mechanism behind the development and progression of thrombus in the FL region. The analysis shows that the formation and thickening of thrombus is likely to occur at the posterior FL wall, distal to the entry tear region. Higher  $\lambda_2$  intensity, associated with higher maximum WSS and lower minimum WSS, was achieved with an increase in the FL size, and it is believed that this increases the risk of thrombus formation and thus aneurismal dilatation. The percentage of the flow entering the FL increased with an increase in the FL size, leading to a downward shift of the areas of thrombus formation along the FL wall.

## CHAPTER 6: FLOW PATTERN ANALYSIS IN STANFORD TYPE B AD PATIENTS AFTER STENT-GRAFTING REPAIR

### 6.1 Introduction

As had been mentioned in Section 2.1, despite the incomplete FL thrombosis caused by communications between the TL and FL, i.e. re-entry tears and/or abdominal branches off from the FL, Czermak *et al.* (2004) and Stanley *et al.* (2011) observed that the FL thrombus length could still grow. Further explanation is required to explain this growth despite having continuous blood flow inside the FL.

Based on Section 2.3.3, several computational analyses of ideal geometries and real patient images with simplified stent graft configuration had been performed to relate the effects of geometrical factors (tear size, number of tears, location of primary tears and FL size) with FL shrinkage or enlargement, as well as thrombus formation (Cheng *et al.*, 2013; Cheng *et al.*, 2010; Fan *et al.*, 2010). These studies worked on CTA images collected from AD patients without stent graft treatment (Cheng *et al.*, 2013; Cheng *et al.*, 2010; Fan *et al.*, 2010), where the primary entry tear in these images were closed to simulate an stent graft placement (Chen *et al.*, 2013a). The complexity of the TL and FL geometry models in AD patients would significantly change after stent insertion, and thrombosis would also develop inside the FL (Kim *et al.*, 2011). Therefore, it is crucial to investigate the geometrical factors and flow pattern in AD patients after stent graft repair in order to predict potential formation and progression of the thrombus.

In view of that, Karmonik *et al.* (2011a) had compared the haemodynamics of stent graft AD cases before and after repair based on a model reconstructed from MRI images. Observing a patient before and after stent-graft repair, they compared the WSS as well as blood flow distribution, and found the elimination of a large amount of WSS after the insertion of a stent (Karmonik *et al.*, 2011a). Their study concurred with a

previous clinical study, which found good early post-stenting results after stent graft placement (Karmonik *et al.*, 2011a). However, the long-term results of thrombosis remained unknown (Sayer *et al.*, 2008). Continuous observation of the entire aorta, especially the FL region after stent graft treatment, is important to detect and monitor complications (Sayer *et al.*, 2008).

There are several factors such as the number of re-entry tears, location of aortic branches, FL diameter and extent of aortic dissection which can influence FL thrombosis and the purpose of this study is to investigate the effects of two geometrical factors; re-entry tears and abdominal branches in patients with Stanford Type B AD, who developed complete and incomplete FL thrombosis after stent graft repair. Using CFD, and geometries reconstructed from CTA images during post-stent graft treatment, this study examined the blood flow pattern, blood flow rate and WSS distribution in Stanford Type B AD patients. Additionally, the relationship of these haemodynamic parameters with the formation of FL thrombosis was also investigated. The simulated results were compared with results of patients obtained within one year of follow-up.

## **6.2 Methodology**

### **6.2.1 Model geometry**

The study was approved by the Curtin University Human Research Ethics Committee. Five extensive acute Stanford Type B AD patients were selected after stent graft repair, and their CTA images were manually segmented to generate 3D models (Figure 6.1). All patients were males aged between 44 and 71 years old. Two patients, i.e. Patients 1 and 2 presented with more than 80% FL thrombosis (Group 1) while three others had less than 80% (Group 2) within one year after endovascular stent graft repair. These five patients with sequential CTA scans, i.e. post treatment, six months and

yearly thereafter were analysed as longitudinal case studies. The upper extremities' vessels were excluded from CFD analysis in all five patients. Flow patterns in regions of interest, which were the descending thoracic aorta and abdominal regions, were unlikely to be affected by the exclusions. On the other hand, four abdominal branches, i.e. celiac, superior mesenteric artery (SMA), left renal and right renal arteries were incorporated in order to identify the influence of these branches on the flow pattern.

### 6.2.2 Model Settings

The aortic wall was assumed to be rigid. This was based on in vivo data obtained from 32 Stanford Type B AD patients who experienced significant reduction (12%) in vessel wall distensibility (Ganten *et al.*, 2009). No-slip boundary condition was applied at the aortic wall, whereby the fluid near the wall boundary had zero velocity relative to the boundary. Newtonian models were used in the present study. Blood was assumed to be homogenous and incompressible with a haemodynamic viscosity of 0.00371Pa.s, and a density of 1060kg/m<sup>3</sup> (Tse *et al.*, 2011).

Instead of using the laminar flow assumption as that described in Chapter 5 on a single patient data (preliminary study done in year 2014), the flow pattern was assumed to be transitional (SST transitional model) in this work. This was because a more recent study which compared the velocity data acquired in vivo using phase-contrast MRI with the CFD results provided by both laminar and SST transitional model of the same patient (Cheng *et al.*, 2014) has demonstrated more accurate velocity results from the SST model (Cheng *et al.*, 2014). The continuity and momentum equations were used to govern blood flow in the present study.

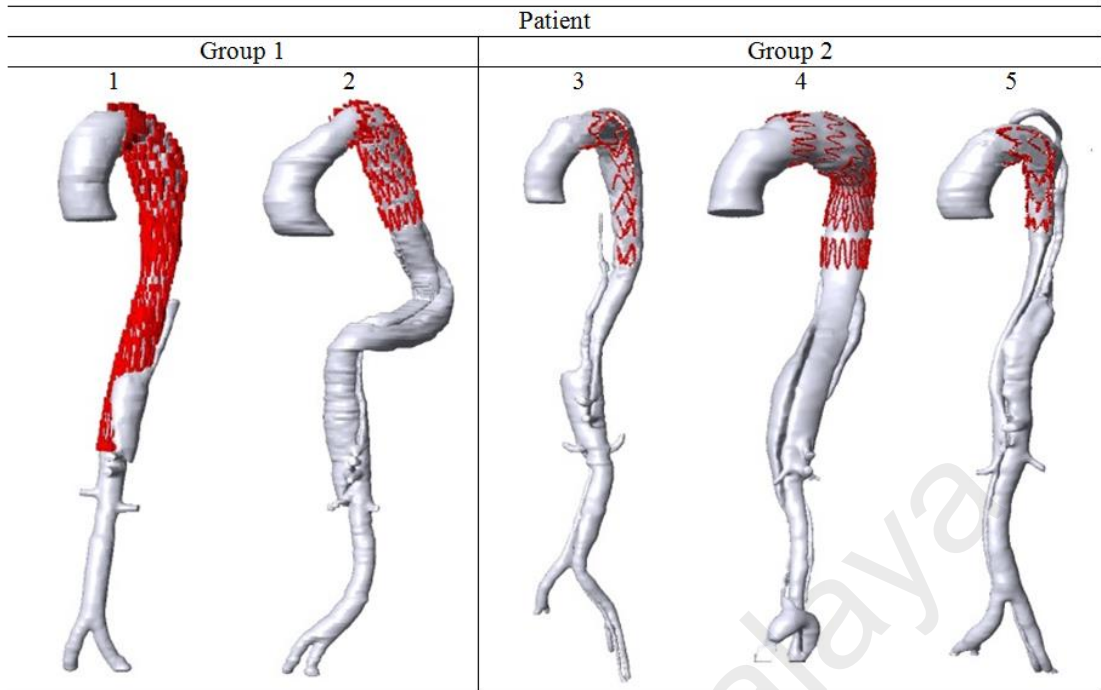


Figure 6.1: 3D reconstruction of Stanford Type B AD patients' geometry after SG repair. The red colour showed the region of SG insertion. The SG will be used for illustration purpose only and will not be incorporated for simulation.

### 6.2.3 Boundary conditions

A flat velocity profile was specified at the inlet of the ascending aorta. Due to the lack of patient-specific flow information, a flow-rate waveform from a typical Stanford Type B AD patient was applied at the inlet of all models of study (Dillon-Murphy *et al.*, 2016). As shown in Figure 6.2, the waveform was derived from the cine phase-contrast MRI data of an acute Type B AD patient (Dillon-Murphy *et al.*, 2016). The cardiac cycle period was one second and cardiac output was 3.64 L/min. The flow rate applied at the inlet was approximately 16% lower than the patient-specific flow extracted at the ascending aorta. The slightly lower flow rate actually helped to offset possible effects caused by removing the upper extremities' branch vessels (Cheng *et al.*, 2010). Based on the inlet area and diameter of the reconstructed aorta models, the peak Reynolds number, mean Reynolds number and Womersley number for each patient were recorded in Table 6.1.

An inlet turbulence level of 1.5% was assumed for all cases as required to start the simulation using the SST-Transitional model. This low inlet turbulent intensity value was confirmed by other numerical studies, and was also applied and validated in flow simulations of AD cases (Cheng *et al.*, 2010). Different pressure profiles were assigned at each of the six abdominal branches (celiac artery, superior mesenteric artery (SMA), left and right renal, and left and right iliac arteries (both internal and external iliac)) (Vignon-Clementel *et al.*, 2006).

Table 6.1: The peak Reynolds number, mean Reynolds number and Wormersley number for each patient.

Patient	Peak Reynolds number	Mean Reynolds number	Wormersley number
1	3157.2	736.7	20.1
2	2756.5	643.2	23.0
3	3503.7	817.6	18.1
4	2463.1	574.8	25.7
5	2801.6	653.7	22.6

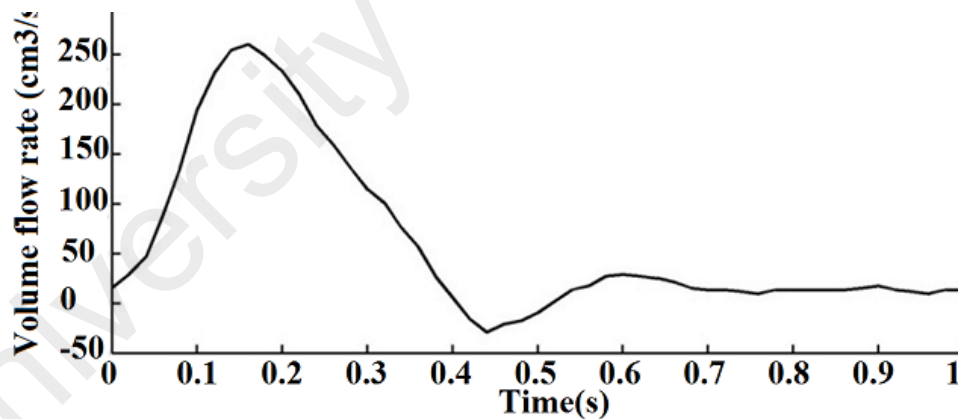


Figure 6.2: A flow rate waveform of a typical Stanford Type B AD patient when applied at the ascending aorta.

#### 6.2.4 Numerical methods

Analysis was performed using the commercial CFD package ANSYS FLUENT 14.0 (ANSYS, Inc., Canonsburg, PA, USA). The Second Order Upwind Scheme was used to make the governing equations discreet. A steady state solution at the maximum flow

rate during peak systole was first obtained, and this solution was used as an initial condition for unsteady pulsatile flow simulation. Three cardiac cycles were simulated for each model. After three complete cycles, cycle-to-cycle variations were less than 1%. Therefore, all results presented in this study were taken from the third cardiac cycle.

### **6.2.5 Mesh independence and time step sensitivity studies**

A hybrid mesh with 3D tetrahedral cells in the core region and prismatic cells in the sheared fluid boundary layer was adopted. Dimensionless distance  $y^+$  was less than two. A minimum of 10 grid nodes for the prismatic cells, which were required to resolve the inner layers of the boundary layer, was applied.

Different mesh sizes were used for the model. Maximum WSS, pressure and turbulence kinetic energy were compared between the meshes, and the differences in each variable were calculated. The meshes were considered sufficient for the simulation when the differences in variables were less than 5% between the adopted meshes and a much fine mesh. The final number of elements used for simulation varied from two to three million, depending on the size and structure of the model geometries.

Apart from the grid independence study, a time-step sensitivity test of unsteady simulation was also conducted. Three temporal settings of discrete were tested: 0.01 s (large time step), 0.005 s and 0.001 s. Reducing the time step from 0.01s to 0.005s and 0.001 s resulted in a small difference (less than 5%) in pressure, maximum WSS and maximum turbulent kinetic energy (TKE), but significantly increased the computational cost. Thus, a time step of 0.01s was used in the present study for computational efficiency.

### 6.2.6 Geometrical and haemodynamics parameters for analysis

In order to perform geometrical analysis based on CTA images, several variables were measured, which include percentage of dissection length over aortic lumen length up to bifurcation ( $\% L_{\text{dissection}}/L_{\text{aorta}}$ ), stent graft length, number of arteries partially or fully supplied by FL, number of re-entry tears, percentage of thrombosis over FL volume before stent-graft repair ( $\% \text{Thrombus}_{\text{before}}/\text{FL}$ ) and percentage of thrombosis over FL volume after stent-graft repair ( $\% \text{Thrombus}_{\text{after}}/\text{FL}$ ). The length of the dissection, length of the aorta (sum of the thoracic and abdominal aorta from the left subclavian artery to the aortic bifurcation) and length of the stent graft were first separately measured. Then,  $\% L_{\text{dissection}}/L_{\text{aorta}}$  was calculated by dividing the length of the dissection with the length of the aorta. The thrombus volumes were obtained by deducting the patent FL volumes from the total FL volumes. Thrombus region was identified based on its darker color as compared to the patent FL.  $\% \text{Thrombus}_{\text{before}}/\text{FL}$  and  $\% \text{Thrombus}_{\text{after}}/\text{FL}$  were obtained by dividing the thrombus volume with the total FL volume before the endovascular SG repair and a year after the repair. The re-entry tears and branches off from the FL were identified with the help of the radiologists.

Several parameters were obtained for blood flow pattern analysis based on the CFD results, which were percentage of total flow entering the FL, percentage of total flow to the abdominal branches that partially or fully supplied by the FL and percentage of total flow circulating inside the FL. Percentage of total flow circulating inside the FL was obtained by deducing percentage of total flow to the abdominal branches that supplied by the FL from percentage total of flow entering the FL. Linear regression analyses were used to calculate the relationship between percentage of total flow circulating inside the FL and the number of re-entry tears.

On the other hand, TAWSS and RRT were calculated using the MATLAB software (version r2012a, The Mathworks Inc, Natick, MA) as well as ANSYS CFD Post.

TAWSS was calculated by averaging the time-varying WSS over one cardiac cycle (Cheng *et al.*, 2013). RRT was calculated as Equation 6.1:

$$RRT = \frac{1}{(1-2\text{ OSI}) * TAWSS} \quad (6.1)$$

where oscillatory shear index (OSI) is related to the azimuthal variation of flow direction during a cardiac cycle and has been shown to be the highest in recirculating flows (Cheng *et al.*, 2013).

## 6.3 Results and Discussion

### 6.3.1 Geometric features

From Table 6.2, AD had different lengths of dissection, different number of abdominal branches that were partially or fully supplied by the FL, and different number of re-entry tears. All these differences might possibly result in different degrees of thrombus formation inside the FL. Group 1 patients had shorter dissection length, i.e. up to abdominal vicinity with no re-entry tears, but had abdominal branches that were partially supplied by the FL. In contrast, Group 2 patients had both re-entry tears and branches.

The %  $L_{\text{Dissection}}/L_{\text{Aorta}}$  length in Group 2 was also longer than that in Group 1. However, previous clinical studies showed neither the %  $L_{\text{Dissection}}/L_{\text{Aorta}}$  nor the stent graft length influenced thrombosis (Czermak *et al.*, 2004; Stanley *et al.*, 2011). This study observed similar results in terms of stent graft length, where no differences were observed between the two groups.

Meanwhile, multiple re-entry tears were observed to be the contributing factor to incomplete FL thrombosis after stent graft repair (Leshnower *et al.*, 2013; Qin *et al.*, 2012; Song *et al.*, 2014; Tolenaar *et al.*, 2014). This work's results were comparable

with literature, where Group 1 patients usually presented with no re-entry tears while Group 2 patients had three or more tears. In addition, the abdominal branches from the FL also interrupted thrombosis (Leshnowar *et al.*, 2013; Qin *et al.*, 2012; Song *et al.*, 2014; Tolenaar *et al.*, 2014). Hughes *et al.* (2014) concluded that complete thrombosis of the FL could occur only when all branches rose from the TL.

However, even though with no re-entry tears and the dissection length was only up to the abdominal branches, patients who had branches partially supplied by the FL also generated more than 80% FL thrombosis. Thus, the reason for thrombus growth, even with the presentation of re-entry tears and/or abdominal branches off from the FL, remains to be elucidated. Details of the CFD flow pattern analysis, coupled with geometrical factors, could be used to predict the formation of thrombosis.

Table 6.2: Geometric features and stent graft length

Parameters	Patient					Clinical studies that concur with the results
	1 Group 1	2	3	4 Group 2	5	
% $L_{Dissection}/L_{Aorta}$	72.0	84.4	100.0	100.0	100.0	(Czermak <i>et al.</i> , 2004)
SG length (mm)	320	120	180	160	130	(Czermak <i>et al.</i> , 2004; Stanley <i>et al.</i> , 2011)
Number of abdominal branches partially or fully supplied by the FL	1	3	1	1	3	(Czermak <i>et al.</i> , 2004; Hughes <i>et al.</i> , 2014; Qin <i>et al.</i> , 2012; Song <i>et al.</i> , 2014; Stanley <i>et al.</i> , 2011; Tolenaar <i>et al.</i> , 2014)
Number of re-entry tears	0	0	3	5	7	(Hughes <i>et al.</i> , 2014; Qin <i>et al.</i> , 2012; Schoder <i>et al.</i> , 2007; Song <i>et al.</i> , 2014)
% $Thrombus_{Before}/FL$	15.7	8.4	3.0	4.4	0.6	
% $Thrombus_{After}/FL$	100	82.2	69.5	37.8	43.3	

### **6.3.2 Blood flow pattern**

Aortic geometry represents an important role in regulating haemodynamic patterns. AD patients have variable flow patterns because of the complexity of their aortic geometry. However, the pattern characteristics in this study were similar inside the TL of all patients as they become organised compared with FL flow (Figure 6.3). Flow in the FL was helical and irregular. A certain volume of blood would enter the FL through re-entry tears or small communicators between the TL and FL (branches partially supplied by the TL and the FL) with high velocity and impinge upon the inner surface of the FL opposite the tear (Figure 6.3). Blood then flowed distally in the FL and some of it would exit through the branches (Figure 6.3). These flow patterns in AD cases with stent graft repairs were similar to those reported by Cheng *et al.* (2013); Cheng *et al.* (2010).

### **6.3.3 The distribution of re-entry tears**

Based on Figure 6.3, Group 1 patients had no re-entry tears and the only communication established was through branches that were partially supplied by the FL, located at the end of the dissection. This created concentrated communications with shorter distance around the abdominal branches (Figure 6.3). The helical flow was hardly seen at the upper section of the FL, and this indicated no active flow occurring within this region, which eventually caused FL thrombosis to develop. For patient 1, who only had one branch (celiac) partially supplied by the FL; the opening to the celiac artery served as an entrance to the FL while the celiac artery itself acted as an exit. For patient 2, who had three branches partially supplied by the FL (celiac, SMA, right renal arteries), the entrance and exit of the flow existed in these abdominal branches.

Unlike Group 1, Group 2 patients had both re-entry tears and abdominal branches partially or fully supplied by the FL, which spread out along the dissection length (Figure 6.3). During peak systole, the proximal re-entry tears would act as entrances to the FL while the re-entry tears at the end of the dissection, as well as the branches supplied by the FL, would serve as exits from the FL (Figure 6.3). These re-entry tears would alternate their roles as entrances and exits to the FL during early diastole (Figure 6.3). Thromboses were unlikely to form inside the FL because of the continuous flow activities inside it.

The roles of re-entry tears as entrances and exits to the FL had been discussed in previous numerical studies (Chen *et al.*, 2013a), and the results of this study were comparable with them. However, those studies focused only on flow distributions and prediction of FL expansion (Chen *et al.*, 2013a), and the re-entry tear distributions and their relationship with FL thrombosis were not analysed. Therefore, in this work, the concentrated tears/communicators distribution were demonstrated to have a high chance to undergo complete FL thrombosis. Although previous clinical work showed that incomplete FL thrombosis was caused by three or more re-entry tears (Hughes *et al.* (2014)), but the short distance between the aggregated tears/communicators in the same location caused only this area to have active flow activity without affecting other FL regions, and eventually, lead to FL thrombosis in the non-active area.

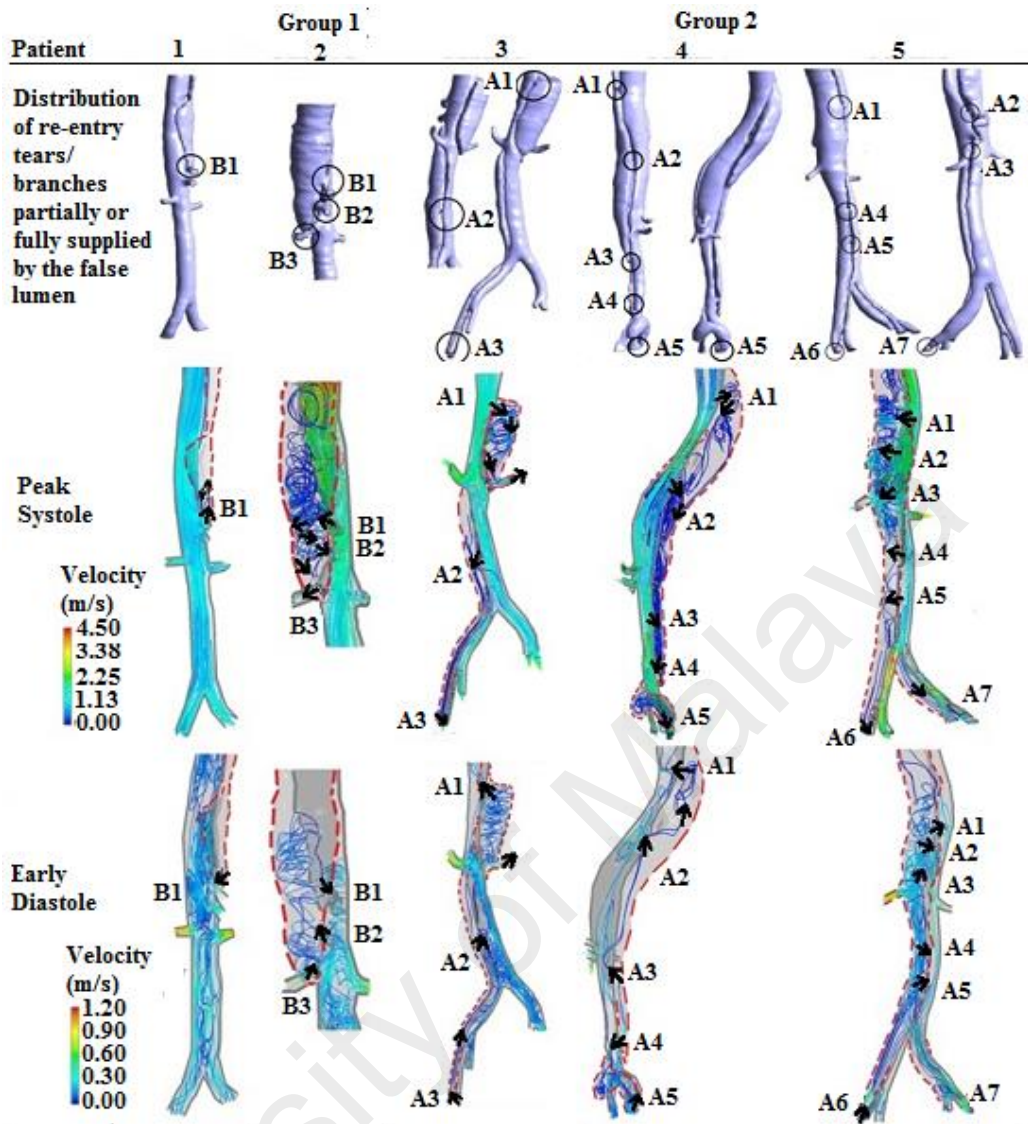


Figure 6.3: Blood flow pattern of five patients. The results were obtained during peak systole. The dashed red line is the FL. The black circles are locations of re-entry tears and abdominal branches partially supplied by the TL and FL.

### 6.3.4 Blood flow rate

From Table 6.3, there were no distinct differences between percentage of total flow entering the FL and percentage of total flow to the abdominal branches that partially or fully supplied by the FL, but there were notable differences of percentage of total flow circulating inside the FL between Group 1 and Group 2 patients. Group 1 patients had the least percentage of total flow circulating inside the FL compared with Group 2 patients. To illustrate the relationship between percentage of total flow circulating inside the FL and the number of re-entry tears, a linear regression plot as used in a previous

study (Cheng *et al.* (2013) was applied. Linear regression analysis demonstrated a significant relationship ( $R^2=0.887$ ) between percentage of total flow circulating inside the FL and the number of re-entry tears (Figure 6.4). The increased number of re-entry tears increased the flow circulating inside the FL, reducing the slow and stagnant blood flow zones, and subsequently reducing FL thrombosis formation (Cheng *et al.*, 2013; Cheng *et al.*, 2010).

Besides the number of re-entry tears, the number of branches that were supplied by the FL also had an important influence on the total flow circulating inside the FL. Even though percentage of total flow entering the FL and percentage of total flow to the abdominal branches that supplied by the FL alone did not show distinct differences between Group 1 and Group 2 patients, but how much percentage of total flow entering the FL that went to the branches would affect how much the remaining flow circulating inside the FL, which in turn, affected FL thrombosis. The situation could be translated into the ratio of TL to FL flow rate before and after deduction of % of flow rate to FL, with the % of flow rate to FL branches ( $TL/FL_{\text{before}}$  and  $TL/FL_{\text{after}}$ ). Results in Table 6.3 showed that the  $TL/FL_{\text{after}}$  ratio increased drastically when more blood flow that entered the FL was flowing to the branches, leaving a little flow circulating inside the FL. Group 1 patients showed the highest  $TL/FL_{\text{after}}$  ratio.

Previously, Cheng *et al.* (2013), who worked on AD cases without stent graft repair, had shown the blood flow that entered the FL could impact the FL expansion and thrombosis. On the contrary, the result showed that FL thrombosis was not influenced by the blood flow that entered the FL (Table 6.3), but by the remaining blood flow inside the FL. The difference of results was probably due to the inclusion of abdominal branches in this study, while Cheng *et al.* (2013) had omitted them in their model. The inclusion of the abdominal branches was essential because the flow that entered the FL might be used to satisfy the required flow demand of the abdominal branch vessels

(Dillon-Murphy *et al.*, 2016). With exception to Dillon-Murphy *et al.* (2016), there were no studies that included the abdominal branches as part of their research on Stanford Type B AD patients. However, different from this study, Dillon-Murphy *et al.* (2016) had observed the aortic geometry before SG repair, but did not highlight the importance of the branches in thrombosis.

Table 6.3: Percentage of the total blood flow and TL to FL volume flow rate ratio during post treatment for each subject at peak systole.

Parameters	Group 1		Group 2		
	1	2	Subject		
			3	4	5
% Thrombus <sub>After</sub> /FL	100.0	82.2	69.5	37.8	43.3
Percentage of total of flow entering the FL	8.30	5.64	6.90	5.60	45.00
TL/FL <sub>before</sub>	11.1	16.7	14.3	17.0	1.2
Percentage of total of flow to the abdominal branches that partially or fully supplied by the FL	8.16	5.41	5.20	1.00	36.14
Percentage of total of flow circulating inside the FL	0.14	0.23	1.70	4.60	8.86
TL/FL <sub>after</sub>	655.0	410.3	81.9	20.7	6.2

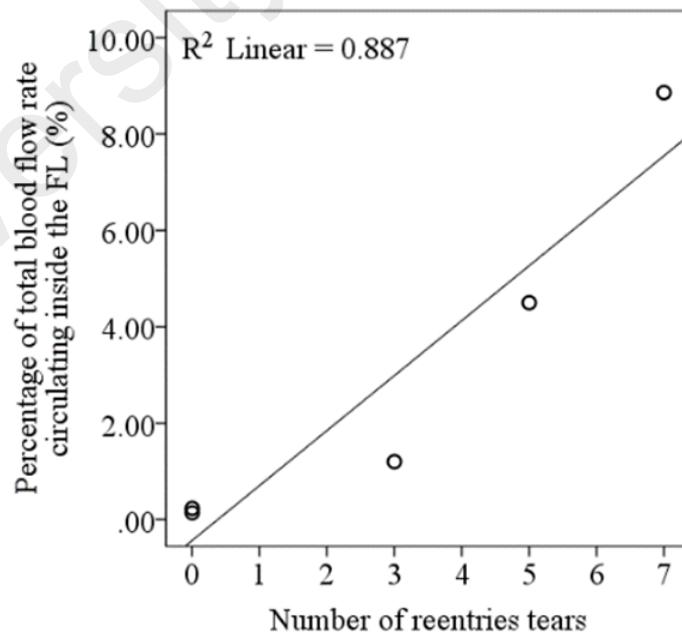


Figure 6.4: The relationship between percentage of total blood flow circulating inside the FL and number of re-entry tears during peak systole.

### 6.3.5 The distribution of TAWSS, RRT and thrombus formation within one year

In this section, local WSS at entry point, global WSS and RRT as well as thrombus growth was discussed.

#### 6.3.5.1 Local WSS at entry point

The values of maximum WSS and TAWSS were shown in Table 6.4. High WSS (>40 Pa) and high TAWSS were observed in the re-entry tear regions and at communicators between TL and FL that partially supplied the branches where jet flow was present (Figure 6.3). The initial activation of platelets that led to FL thrombosis was triggered by high shear stress that reached above 40 Pa (Menichini & Xu, 2016). The peak WSS in all patients of this study were above the defined thrombus activation threshold of 40 Pa.

#### 6.3.5.2 Global WSS and RRT

Based on Figure 6.5, most of the FL regions showed the lowest WSS (<1 Pa). Almost the whole upper part above the abdominal branches and re-entry tears for Group 1 and Group 2 patients had TAWSS less than 0.1 Pa (Figure 6.5). The low TAWSS area was related to the region of stagnancy and flow recirculation, and this was also characterised by the long RRT (Menichini & Xu, 2016). Figure 6.5 showed that the locations of high RRT overlapped with the low TAWSS region for all patients.

Table 6.4: Maximum WSS and TAWSS values

Subject	Max WSS (Pa) at re-entry tear/ communicator	Max TAWSS (Pa)
1	66.5	15.8
2	65.0	11.3
3	85.3	30.5
4	104.0	28.0
5	173.4	44.0

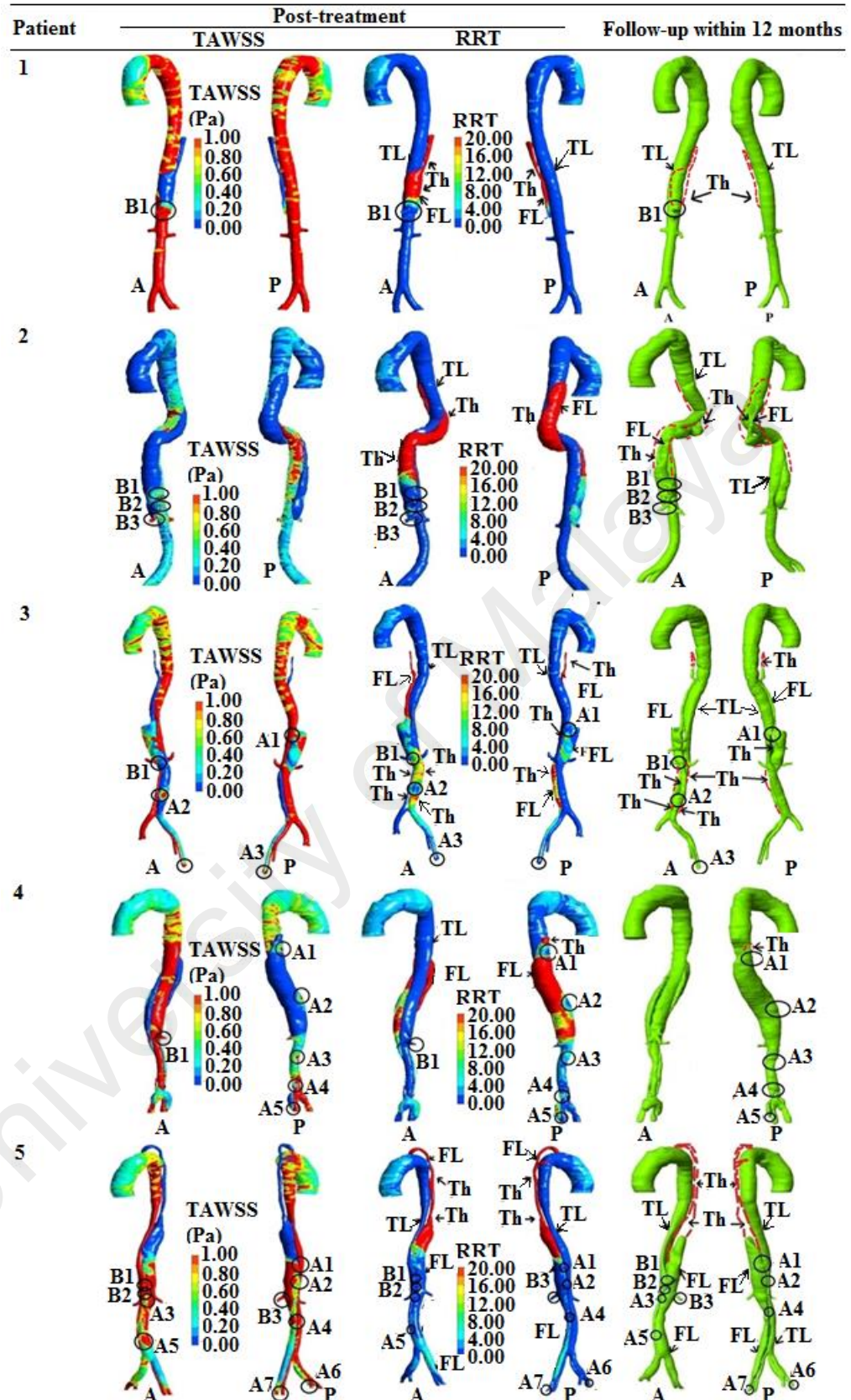


Figure 6.5: TAWSS distributions and RRT contours with subsequent areas of the FL thrombus formation. Th: thrombus, TL: true lumen, FL: false lumen. A: Anterior. P: Posterior. A1: re-entry tear 1; A2: re-entry tear 2; A3: re-entry tear 3; A4: re-entry tear 4, A5, re-entry tear 5, A6: re-entry tear 6, A7, re-entry tear 7. B1: Branch 1, B2: Branch 2: B3: Branch 3 that are partially or fully supplied by FL. The dashed red line is the thrombus region.

### 6.3.5.3 Thrombus growth

As expected, all patients showed thrombus formation at the upper part of the FL within a year (Figure 6.5). The regions of low TAWSS and high RRT for all patients during post-treatment were shown to have been formed into thrombus within a year as shown in Figure 6.5. These findings were comparable with previous studies (Cheng *et al.*, 2013; Menichini *et al.*, 2016). However, the degree of thrombus formation varied between patients and time. Patient 1 developed complete FL thrombosis after six months while only some of the regions with high RRT in patient 2 developed thrombosis within a year (Figure 6.5). Complete thrombosis was only observed after 60 months of follow up (Figure 6.6).

Previously, Menichini and Xu (2016) used a new haemodynamic-based model, which allows the FL surface to change as a function of time when thrombi are formed, and their results were comparable with the longitudinal follow-up results of patient 2 (Figure 6.6). Although this work did not apply the same method as Menichini and Xu (2016), the predictive results of the thrombus growth at the proximal part of the FL over time based on TAWSS and RRT prediction were still comparable with the patients' follow-up results. It was just a matter of time before thrombosis developed in the FL vicinity.

Further, the movement of the flap above the re-entry tear/branch from the FL might also be the reason for slow thrombus formation inside the FL (Sayer *et al.*, 2008). For example, when compared with other patients, patient 1 had the longest stent graft (320 mm), where the stent was inserted right up to the celiac branches. The long stent had probably prevented the movement of the flap above the abdominal branch point, which subsequently prevented blood from flowing inside the FL. Therefore, complete FL thrombosis was seen only after six months. Meanwhile, the upper section of the FL in patient 5 was also observed to develop thrombosis within a year. Unlike patients 1, 2

and 5, very little thrombosis above the re-entry tear points were observed in patients 3 and 4.

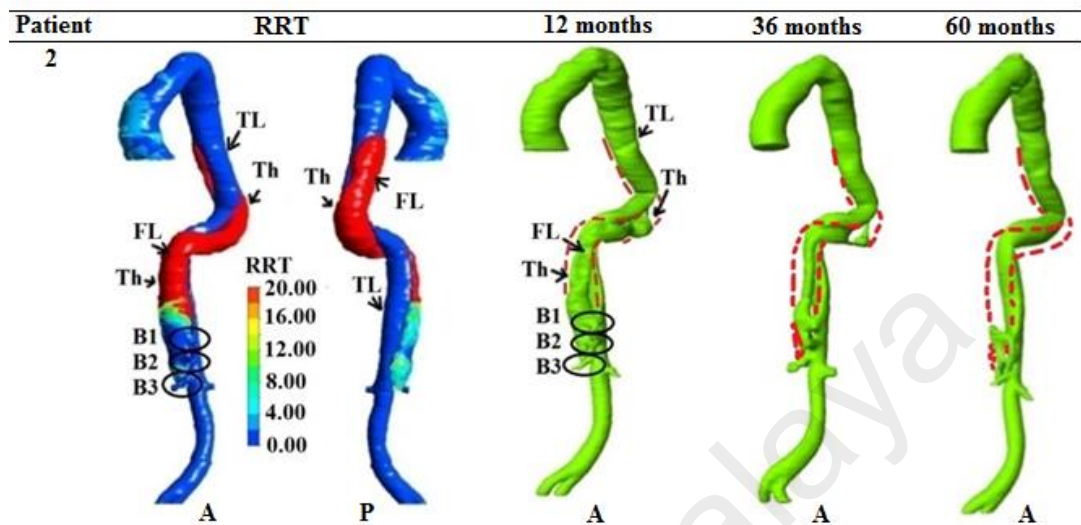


Figure 6.6: RRT contours with subsequent areas of the FL thrombus forming up to 60 months in Patient 2. Th: thrombus, TL: true lumen, FL: false lumen. A:Anterior. P:Posterior. B1:Branch 1, B2:Branch 2, B3:Branch 3 that are partially or fully supplied by the FL. The dashed red line is the thrombus region.

### 6.3.6 Thrombosis between tears

For Group 2 patients that have dissection below the abdominal branches, only patient 3 showed thrombosis in between the re-entry tears below the abdominal branches (Figure 6.5). This region had low level of TAWSS but high RRT (Figure 6.5). The low TAWSS and high RRT regions were influenced by the number and distance of re-entry tears. Patient 3 had few re-entry tears (three) and the distance between the tears were also longer in comparison with patients 4 and 5 (Figure 6.5). For AD patients with fewer and longer distance between tears, a reduced amount of blood would be diverted in the FL (Menichini & Xu, 2016), resulting in lower velocities that caused low WSS distribution and high RRT in between the tears.

The effect of tear distance on the formation of FL thrombosis had been studied by Menichini and Xu (2016) and they found that for models of long distance between tears, thrombosis would be limited to top and bottom areas of the FL only. The results of this

work were not in agreement with theirs (Menichini & Xu, 2016). Even though they observed a high RRT in between the two tears, which was also observed in these results, they found that blood flow in the mid-section of the FL was organised. This allowed normal physiological wall shear rates to occur, which prevented the occurrence of thrombosis in the mid-section of their idealised model (Menichini & Xu, 2016).

However, in the results, although blood flow was seen to be organised in between tears (Figure 6.3), the lowest TAWSS ( $<0.1$  Pa) was also observed in between the tears (Figure 6.5) and this caused activated platelets to adhere to the aortic wall, which resulted in thrombus formation. Compared with Menichini and Xu (2016), the findings of this work should be more relevant as this work had one-year patient follow-up results to validate the CFD analysis (Figure 6.5). Furthermore, the authors employed an idealized two-dimensional (2D) geometry in their work where the tear distance was varied while the other geometric features remained the same (Menichini & Xu, 2016), whereas the patient-specific models employed in this study incorporated several geometric complexities, including non-planar curvature and tortuosity, which would affect the values of local WSS.

Meanwhile, patients 4 and 5 had more re-entry tears (five and seven, respectively) compared with patient 3, and the distance between them were shorter. Due to these conditions, continuous blood flow in and out of the FL that caused low RRT inside the FL was observed below the abdominal branches in both patients 4 and 5 (Figure 6.5). This prevented thrombus formation in between the tears.

### **6.3.7 Vortical structures**

The prediction of FL thrombosis using vortical structures method had been discussed in the previous Chapter 5 without the follow-up images/model to prove the findings. Therefore, in this chapter, the formation of thrombus formation using vortical structures

analysis will be discussed and validate it with the next follow-up scan. To illustrate the thrombus formation using vortical structures in between the re-entry tear (as a continuation from the previous subsections (6.2.6)), patients 3 will be used. The region of interest was shown in a rectangular box as shown in Figure 6.7(F).

Based on Figure 6.7, aggregated vortical structures were found in front of the re-entry tear region during early systole (Figure 6.7(A)) while these vortical structures were found to be slightly reduced in size during peak systole (Figure 6.7(B)). Around the re-entry tear region (around the black circle region as shown in Figure 6.7), vortical structures observed during early systole (Figure 6.7(A)) were found to develop into a ring-shaped pattern during peak systole (Figure 6.7(B)). At the above and below re-entry tear, the spanwise vortical structures started to disappear as compared to early systole, especially at the upper part of the re-entry tear. The interaction between the vortical structures with the boundary layer caused a localized region of high WSS the re-entry tear region.

As compared to peak systole, the ring-shaped vortical structures found around the re-entry tear region expanded and accumulated around, below and above the re-entry tear region during late systole (Figure 6.7(C)) and early diastole (Figure 6.7(D)). The vortical structures seem to stretch during early diastole and had been broken down into several streamwise substructures (Figure 6.7(D)) that distributed to the above (more to inner curvature side) and below the re-entry tear region (as shown in red circle in Figure 6.7 (E)).

The existence of recirculation zones with dominant vortical structures, together with the influence of the high WSS surrounding the re-entry tear, is believed to cause platelet activation (Kamman *et al.*, 2016). The strong jet-like flow through the re-entry tear pushed the reattachment point upstream and downstream and contributed to the growth

of the vortical structures (Ahmed *et al.*, 2016). The growth and accumulation of the vortical structures around, above and below the re-entry tear region continued throughout peak and late systole, causing repeated collision of platelets for a long period of time (Ahmed *et al.*, 2016), and is believed to result in the spontaneous formation of the platelet aggregates (Biasetti *et al.*, 2011). During early diastole, the flow had lost its strength and as a result, the vortical structures were seen to have stretched and had been broken down into several streamwise substructures. The breakup of vortical structures later will release the platelets which were subsequently adhered to the low WSS location at the upper and below part of the FL wall, causing the formation of thrombus.

Based on the above analysis, a tendency of the formation of thrombus was predicted at the above especially at the inner part of the curvature and below the re-entry tear region of the FL wall, over a finite period of time (Figure 6.7(E)). The prediction of the thrombus formation location using vortical structures and WSS contour distribution for Patient 3 was comparable with the results of CTA follow-up scan that was obtained within a year following the repair of the same patient (Figure 6.7(F)).

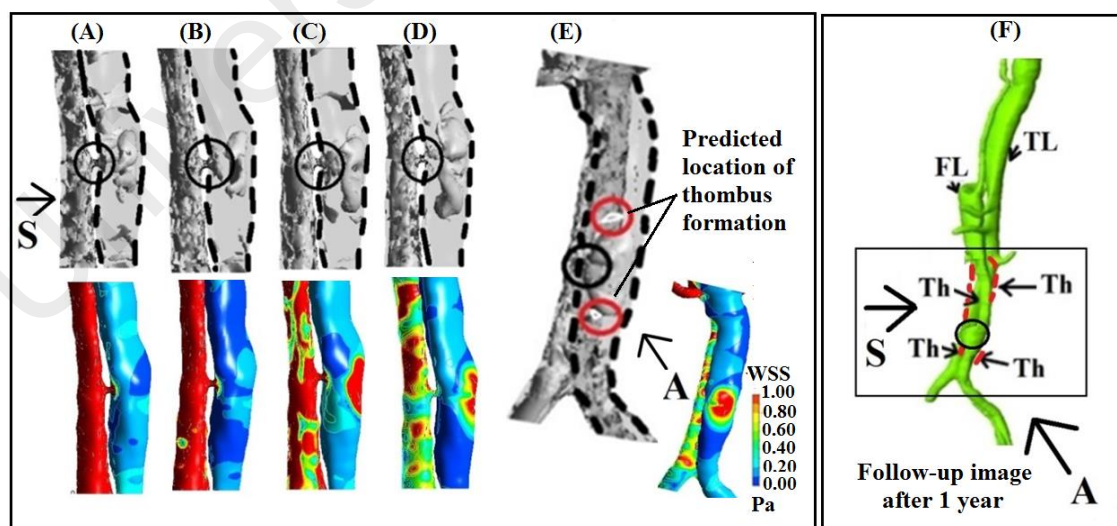


Figure 6.7: Patient 3's vortical structures and WSS contour distribution from side view at (A) early systole; (B) peak systole; (C) late systole and (D) early diastole. (E) from anterior view at early diastole. (F) Area of the FL thrombus formation within one year of follow-up after the repair. The dash red line is the area of thrombus formation. A: Anterior; S: Side view; FL: Th: thrombus. The black circle is the re-entry tear region.

#### **6.4 Significance of this study**

This work provided an insight into predicting the development of complete or incomplete FL thrombosis after the stent graft treatment in patients with Type B aortic dissection using patient-specific models. Compared to imaging data alone, more detailed haemodynamics and their correlation with the anatomical factors are investigated. The findings provided by the predictive model could be used to determine which patients would benefit from the treatment. Previous clinical studies found that complete thrombosis of the FL could occur only when all branches arose from the TL and without presentation of any re-entry tears. However, this work showed that distribution of the re-entry tear/ branches arising from the FL demonstrated an important influence on the formation of FL thrombus. The longitudinal data of the AD patients, i.e. from the CTA images, showed that patients with concentrated re-entry tears had high chances to undergo complete FL thrombosis, which agreed with the observation based on the CFD studies. In addition, the prediction of thrombus formation using TAWSS, RRT and vortical structure distributions was comparable with that shown by the patients' CTA follow-up results. All patients showed thrombus formation at the upper part of the FL within a year. Patients with fewer re-entry tears and longer distance between the tears had thrombosis in between tears. This work also highlighted the importance of including abdominal branches in CFD studies for AD patients; with more blood flowing from the FL into the abdominal branches, blood circulating inside the FL is reduced, thus increasing chances for thrombosis.

#### **6.5 Limitations**

This study implied the pressure profile obtained from clinical data (Vignon-Clementel *et al.*, 2006) as boundary conditions at all the abdominal branches and iliac

arteries. Therefore, the amount of blood flow to the abdominal branches was influenced by the pressure set.

Apart from that, the use of the rigid wall assumption may influence the predicted outcomes of thrombus formation based on TAWSS, particularly at regions below the stented region, which may be affected by the intimal flap movement. Nevertheless, the incorporation of a FSI framework is challenging as the intimal flap at the dissection site is very thin and it is difficult to assign different material properties to each lumen layer. Moreover, a recently published simulation study which compared the rigid wall and fluid structure interaction (FSI) models for a Stanford Type B AD patient had found insignificant differences between both models with respect to the haemodynamics in absolute terms (Alimohammadi *et al.*, 2015). Ongoing studies are conducted to investigate the effect of wall compliance on the haemodynamics in stented patients.

In addition, the number of patients was small, thus strong conclusions could not be drawn. If a larger number of patients were available, the CFD flow analysis might have potential to offer predictive value in differentiating complete and incomplete FL thrombosis. This indirectly will determine individualized patient's outcome.

## **6.6 Summary**

This study suggests that morphologically; patients with a dissection up to the abdominal vicinity with no re-entry tears, as well as branches that are partially supplied by the FL at the end of the dissection are more likely to develop complete FL thrombosis. In CFD analysis, patients with more than 80% thrombus formation in the FL have concentrated communications around the abdominal branches, i.e. at the end of the dissection. For patients with less than 80% FL thrombosis, the re-entry tears are spread out along the dissection, which eventually creates continuous flow activities inside the FL that interrupt thrombosis. Thrombosis is affected by blood flow inside the

FL. Blood circulating inside the FL is influenced by the number of re-entry tears as well as the branches that are partially supplied by the FL. The increased number of re-entry tears will increase the volume of blood circulating inside the FL, which, in turn, reduces the rate of thrombosis. With more blood from the FL going into the branches, circulation inside the FL is reduced, and thrombosis can occur. Based on low TAWSS and high RRT distribution, all patients showed thrombus formation at the upper FL region. The regions with low TAWSS and high RRT are affected by the number of re-entry tears, the FL branches and the distance between them. Thrombosis will occur in the aorta of patients with fewer re-entry tears and longer distance between the tears.

University of Malaya

## CHAPTER 7: CONCLUSIONS AND RECOMMENDATIONS

The findings of each chapter and their contributions are summarized in this chapter. In addition, directions for future works are recommended to expand the research outcomes.

### 7.1 Summary and conclusion

The contribution of this research project can be assessed through the degree of achievement with regards to the objectives of the research. Particularly, the current study has achieved four objectives, which are detailed below:

- i. Have collected and performed image segmentation of CTA scan images of patients with Stanford type B AD who underwent stent graft treatment and examine the luminal changes based on the maximal axial diametric and volumetric measurements.
- ii. Have evaluated the progression of Stanford Type B AD cases after stent graft treatment based on CTA images analysis and identify morphologic characteristics that are related with FL thrombosis.
- iii. Have carried out a preliminary investigation using CFD approach in order to describe the mechanism behind the formation of thrombus and to predict its location in AD patients without stent graft treatment.
- iv. Have investigated the haemodynamic effect and predict thrombus formation location on Stanford Type B AD patient after stent graft treatment using CFD approach.

Based on these objectives, the conclusions are drawn as below:

**i. Reconstruction and measurement of 3D geometry of Stanford Type B AD patients**

The results of this chapter showed the 3D geometry of images reconstructed from the CTA images before and after the stent graft treatment. The 3D geometries of pre-treatment, post-treatment and follow-up images for 13 Stanford Type B AD patients were later used for maximal axial diameter and volume measurements. The results of comparison between the two measurements methods showed that volume measurements should provide supportive information to reflect morphologic changes of both TL and FL. Even though the aorta was divided into three segments, i.e. stented region, distal to stented region up to celiac artery point and abdominal region, and the results were analysed at each of the segments, it was challenging to tell the morphological changes based on maximal axial diameter measurements alone. Diameter measurement had potential to indicate aortic remodelling only at the stented segment of TL as the lumen showed consistent changes along the stent length. Apart from the stented TL segment, the other segments showed inconsistent changes, thus yielding a difference in results between diametric and volumetric measurements. The results may have potential to predict the recovery outcome of patients and facilitate decision-making when further intervention is needed.

**ii. Morphological study of Stanford Type B AD patients after stent graft repair**

The findings of this work showed that the good stent graft treatment outcomes can be achieved through the TL expansion, FL shrinkage as well as complete FL thrombosis. The TL expansion and FL shrinkage can be observed in the stented segment region. However, continues flow into the FL distal to the stent graft region caused FL volumes increase in several patients leaving these segments an area of concern. Besides the

luminal size changes, this study also characterized the thrombus formation into three groups. The details study based on these groups at each segment made this work easier to relate to the anatomical structure with the thrombus development. Several factors had been associated with percentage of FL thrombosis formation. The results showed that the patients with dissection up to abdominal branches without presentation of re-entry tear, and contained abdominal branches that partially supplied by the FL at the end of dissection generated more than 80% complete FL thrombosis. Meanwhile, for patients that had dissection below the abdominal branches and up to iliac arteries with presentation of three and more re-entry tears distal to the stent graft generated more than 50% but less than 80% FL thrombosis. On the other hand, compared to the other patients, patients with less than or equal to 50% FL thrombosis had higher maximal FL diameter at abdominal region observed during pre-treatment. Other circumstances hindered the complete FL thrombosis were the occurrence of SINE, ulcer, as well as chronic type B AD.

**iii. Prediction of thrombus formation in Stanford Type B AD patient: A preliminary study using CFD approach**

This study showed that the evolution of vortical structures throughout a cardiac cycle and their interaction with the WSS provided insight into the potential mechanism behind the development and progression of thrombus in the FL region. In a preliminary study of a case of Stanford Type B AD patients without the stent graft insertion, using the vortical structures method, the formation and thickening of thrombus was likely to occur at the posterior FL wall, distal to the entry tear region.

**iv. Flow pattern analysis in Stanford Type B AD patients after stent-grafting repair**

This work provided an insight into predicting the development of complete or incomplete FL thrombosis and, indirectly, findings could be used to determine which patients would benefit from the treatment. Based on CFD results, patients with more than 80% thrombus formation in the FL basically had concentrated communications at the end of the dissection while for patients with less than 80% FL thrombosis, the re-entry tears were spread out along the dissection distal to the stent graft, which eventually created continuous flow activities inside the FL that interrupted thrombosis. Furthermore, the results of CFD also showed that the thrombosis was affected by blood flow circulating inside the FL. Blood circulating inside the FL was influenced by the number of re-entry tears as well as the branches that were partially supplied by the FL. The increased number of re-entry tears will increase the volume of blood circulating inside the FL, which, in turn, reduces the rate of thrombosis. On the other hand, with more blood from the FL going into the branches, circulation inside the FL will be reduced, and thrombosis can occur. Meanwhile, in terms of low TAWSS and high RRT distribution, all patients showed thrombus formation at the upper FL region. The regions with low TAWSS and high RRT were affected by the number of re-entry tears, the FL branches and the distance between them. Thrombosis will occur in the aorta of patients with fewer re-entry tears and longer distance between the tears.

## 7.2 Directions for future research

### i. CTA image segmentations and measurements

One limitation of the present study is the use of maximal axial diameter measurements. In future, measurement of maximal diameter should be calculated based on perpendicular to the vessel axis (Wever *et al.*, 2000).

Besides that, Volume assessment is time-consuming as it requires additional processing, such as image segmentation and reconstruction. Future work includes the development of an automated segmentation technique to make it more cost-effective. In addition, the analysis was performed using one software only, and different software packages may generate variable results due to the characteristics of their tools. Comparison or assessment of intra-software reproducibility should be considered in further research.

### ii. In terms of CFD

This study implied the pressure profile obtained from clinical data as boundary conditions at all the abdominal branches and iliac arteries (outlets). Therefore, the amount of blood flow to the abdominal branches and iliac arteries were influenced by the pressure set. In future, the more realistic Windkessel model should be set as boundary conditions to imply a more realistic effect of flow rate at branches.

The aortic wall was assumed to be rigid in this work. This is justified to be a reasonable assumption given the fact that the compliance of an aneurysmal blood vessel is significantly reduced due to the lack of elastin (Boussel *et al.*, 2009). Furthermore, Alimohammadi *et al.* (2015) had compared the rigid wall and fluid structure interaction (FSI) in a Stanford Type B AD patient and had shown that in absolute terms of TAWSS, it was clear that the differences between the rigid wall and FSI models were not significant. Moreover, the main difficulty in assuming the wall of aorta and AD to

be elastic is that the vessel wall contains both healthy and diseased tissues, for which the exact material properties are difficult to be ascertained. Therefore, ongoing studies should be conducted to investigate the effect of wall compliance on the haemodynamics in the stented and unstented regions as well as for both healthy and diseased tissue.

The number of patients used in this study is small, thus robust conclusions could not be drawn. To date most CFD studies used only one to eight patients, due to the time taken for each simulation, where it took up to days or weeks for the simulation to complete. Therefore, with the ongoing advanced technology, the issued related with computational time hopefully could be resolved and more patients could be recruited for the simulation. Thus, the CFD flow analysis might have potential to offer predictive value and indirectly will determine individualized patient's outcome.

University of Malaysia

## REFERENCES

- Ahmed, S. B., Dillon-Murphy, D., & Figueroa, C. (2016). Computational study of anatomical risk factors in idealized models of type B aortic dissection. *European Journal of Vascular and Endovascular Surgery*, 52(6): 736-745.
- Alimohammadi, M., Sherwood, J. M., Karimpour, M., Agu, O., Balabani, S., & Díaz-Zuccarini, V. (2015). Aortic dissection simulation models for clinical support: fluid-structure interaction vs. rigid wall models. *Biomedical Engineering Online*, 14(1): 34.
- Ameli-Renani, S., Das, R., & Morgan, R. (2015). Thoracic endovascular aortic repair for the treatment of aortic dissection: Post-operative imaging, complications and secondary interventions. *Cardiovascular and Interventional Radiology*, 38(6): 1391-1404.
- Andacheh, I. D., Donayre, C., Othman, F., Walot, I., Kopchok, G., & White, R. (2012). Patient outcomes and thoracic aortic volume and morphologic changes following thoracic endovascular aortic repair in patients with complicated chronic type B aortic dissection. *Journal of Vascular Surgery*, 56(3): 644-650.
- Auer, J., Berent, R., & Eber, B. (2000). Aortic dissection : Incidence, natural history and impact of surgery. *Journal of Clinical and Basic Cardiology*, 3(3): 151-154.
- Bargellini, I., Cioni, R., Petrucci, P., Pratali, A., Napoli, V., Vignali, C., Ferrari, M., & Bartolozzi, C. (2005). Endovascular repair of abdominal aortic aneurysms: analysis of aneurysm volumetric changes at mid-term follow-up. *Cardiovascular and Interventional Radiology*, 28(4): 426-433.
- Beller, C. J., Labrosse, M. R., Thubrikar, M. J., & Robicsek, F. (2004). Role of aortic root motion in the pathogenesis of aortic dissection. *Circulation*, 109: 763-769.
- Biasseti, J. (2013). *Physics of blood flow in arteries and its relation to intra-luminal thrombus and atherosclerosis*. Doctoral, KTH Royal Institute of Technology, Sweden. (84)
- Biasseti, J., Hussain, F., & Gasser, T. C. (2011). Blood flow and coherent vortices in the normal and aneurysmatic aortas: a fluid dynamical approach intra-luminal thrombus formation. *Journal of The Royal Society Interface*.
- Bluestein, D., Gutierrez, C., Londono, M., & Schoepfoerster, R. T. (1999). Vortex shedding in steady flow through a model of an arterial stenosis and its relevance to mural platelet deposition. *Annals of Biomedical Engineering*, 27(6): 763-773.

- Borghì, A., Wood, N. B., Mohiaddin, R. H., & Xu, X. Y. (2008). Fluid-solid interaction simulation of flow and stress pattern in thoracoabdominal aneurysms : A patient-specific study. *Journal of Fluids and Structures*, 24: 270-280.
- Boussel, L., Rayz, V., Martin, A., Acevedo-Bolton, G., Lawton, M. T., Higashida, R., Smith, W. S., Young, W. L., & Saloner, D. (2009). Phase-contrast magnetic resonance imaging measurements in intracranial aneurysms in vivo of flow patterns, velocity fields, and wall shear stress: Comparison with computational fluid dynamics. *Magnetic Resonance in Medicine*, 61(2): 409-417.
- Braverman, A. C. (2011). Aortic dissection : Prompt diagnosis and emergency treatment are critical. *Cleveland Clinic Journal of Medicine* 78(10): 685-696.
- Carpentier, A., Deloche, A., Fabiani, J. N., Chauvaud, S., Relland, J., Nottin, R., Vouhe, P., Massoud, H., & Dubost, C. (1981). New surgical approach to aortic dissection : flow reversal and thromboexclusion. *The Journal of Thoracic and Cardiovascular Surgery*, 81(5): 659-668.
- Chang, C. P., Liu, J. C., Liou, Y. M., Chang, S. S., & Chen, J. Y. (2008). The role of false lumen size in prediction of in-hospital complications after acute type B aortic dissection. *Journal of the American College of Cardiology*, 52(14): 1170-1176.
- Chen, D., Muller-Eschner, M., Kotelis, D., Bockler, D., Ventikos, Y., & Tengg-Kobligk, H. V. (2013a). A longitudinal study of Type-B aortic dissection and endovascular repair scenarios: Computational analyses. *Medical Engineering & Physics*.
- Chen, D., Muller-Eschner, M., Tengg-Kobligk, H. V., Barber, D., Bockler, D., Hose, R., & Ventikos, Y. (2013b). A patient-specific study of type B aortic dissection: evaluation of true-false lumen blood exchange. *Biomedical Engineering Online*, 12: 1-16.
- Cheng, S. W. K., Lam, E. S. K., Fung, G. S. K., Ho, P., Ting, A. C. W., & Chow, K. W. (2008). A computational fluid dynamic study of stent graft remodeling after endovascular repair of thoracic aortic dissections. *Journal of Vascular Surgery*, 48: 303-310.
- Cheng, Z., Juli, C., Wood, N., Gibbs, R., & Xu, X. (2014). Predicting flow in aortic dissection: comparison of computational model with PC-MRI velocity measurements. *Medical Engineering & Physics*, 36(9): 1176-1184.

- Cheng, Z., Riga, C., Chan, J., Hamady, M., Wood, N. B., Cheshire, N. J., Xu, Y., & Gibbs, R. G. (2013). Initial findings and potential applicability of computational simulation of the aorta in acute type B dissection. *Journal of Vascular Surgery*, 57: 35 S- 43 S.
- Cheng, Z., Tan, F. P. P., Riga, C. V., Bicknell, C. D., Hamady, M. S., Gibbs, R. G. J., Wood, N. B., & Xu, X. Y. (2010). Analysis of flow patterns in a patient-specific aortic dissection model. *Journal of Biomechanical Engineering*, 132: 051007 - 051001 - 051007 -051009.
- Cheng, Z., Wood, N. B., Gibbs, R. G., & Xu, X. Y. (2015). Geometric and flow features of type B aortic dissection: initial findings and comparison of medically treated and stented cases. *Annals of Biomedical Engineering*, 43(1): 177-189.
- Conrad, M. F., Crawford, R. S., Kwolek, C. J., Brewster, D. C., Brady, T. J., & Cambria, R. P. (2009). Aortic remodeling after endovascular repair of acute complicated type B aortic dissection. *Journal of Vascular Surgery*, 50(3): 510-517.
- Cooley, D. A. (1990). Surgical management of aortic dissection. *Texas Heart Institute Journal*, 17(4): 289-301.
- Czermak, B. V., Mallouhi, A., Perkmann, R., Steingruber, I. E., Waldenberger, P., Neuhauser, B., Fraedrich, G., Jung, T., & Jaschke, W. R. (2004). Serial CT volume and thrombus length measurements after endovascular repair of Stanford type B aortic dissection. *Journal of Endovascular Therapy*, 11(1): 1-12.
- Czermak, B. V., Waldenberger, P., Fraedrich, G., Dessel, A. H., Roberts, K. E., Bale, R. J., Perkmann, R., & Jaschke, W. R. (2000). Treatment of Stanford Type B aortic dissection with stent-grafts: Preliminary results. *Radiology*, 217: 544-550.
- Dillon-Murphy, D., Noorani, A., Nordsletten, D., & Figueroa, C. A. (2016). Multi-modality image-based computational analysis of haemodynamics in aortic dissection. *Biomechanics and Modeling in Mechanobiology*, 15(4): 857-876.
- Dong, Z., Fu, W., Wang, Y., Wang, C., Yan, Z., Guo, D., Xu, X., & Chen, B. (2010). Stent graft-induced new entry after endovascular repair for Stanford type B aortic dissection. *Journal of Vascular Surgery*, 52(6): 1450-1457.
- Doyle, B. J., & Norman, P. E. (2016). Computational biomechanics in thoracic aortic dissection: today's approaches and tomorrow's opportunities. *Annals of Biomedical Engineering*, 44(1): 71-83.

- Elefteriades, J. A., Hartleroad, J., Gusberg, R. J., Salazar, A. M., Black, H. R., Kopf, G. S., Baldwin, J. C., & Hammond, G. L. (1992). Long term experience with descending aortic dissection : The complication specific approach. *Annals of Thoracic Surgery*, 53: 11-21.
- Erbel, R., Alfonso, F., Boileau, C., Eber, D. B., Haverich, A., Rakowski, H., Struyven, J., Radegran, K., Sechtem, U., Taylor, J., & Zollikofer, C. (2001). Diagnosis and management of aortic dissection. *European Heart Journal*, 22: 1642-1681.
- Evangelista, A., Salas, A., Ribera, A., Ferreira-González, I., Cuellar, H., Pineda, V., González-Alujas, T., Bijmens, B., Permanyer-Miralda, G., & Garcia-Dorado, D. (2012). Long-term outcome of aortic dissection with patent false lumen predictive role of entry tear size and location. *Circulation*, 125(25): 3133-3141.
- Fan, Y., Cheng, S. W. K., Qing, K. X., & Chow, K. W. (2010). Endovascular repair of type B aortic dissection : A study by computational fluid dynamics. *J. Biomedical Science and Engineering*, 3: 900-907.
- Fung, G. S. K., Lam, S. K., Cheng, S. W. K., & Chow, K. W. (2008). On stent-graft models in thoracic aortic endovascular repair : A computational investigation of the hemodynamic factors. *Computers in Biology and Medicine*, 38: 484-489.
- Ganten, M. K., Weber, T. F., Von Tengg-Kobligk, H., Böckler, D., Stiller, W., Geisbüsch, P., Kauffmann, G. W., Delorme, S., Bock, M., & Kauczor, H. U. (2009). Motion characterization of aortic wall and intimal flap by ECG-gated CT in patients with chronic B-dissection. *European Journal of Radiology*, 72(1): 146-153.
- Gao, F., Watanabe, M., & Matsuzawa, T. (2006). Stress analysis in a layered aortic arch model under pulsatile blood flow. *Biomedical Engineering online* 5(25).
- Gijsen, F. J. H., Van de Vosse, F. N., & Janssen, J. D. (1999). The influence of the non-Newtonian properties of blood on the flow in large arteries: steady flow in a carotid bifurcation model. *Journal of Biomechanics*, 32: 601-608.
- Golledge, J., & Eagle, K. A. (2008). Acute aortic dissection. *Lancet*, 372: 55-66.
- Guan, J., Chu, B., Chang, Y., & Qiao, A. (2009). *Two-dimensional computational simulation of bypassed aortic dissection with a blind false lumen*. Paper presented at the 2nd International Conference on Biomedical Engineering and Informatic, Tianjin, China.
- Guan, J., Chu, B., Zhang, Y., Zeng, K., & Qiao, A. (2010). Three-dimensional computational simulation of bypassed aortic dissection. *IEEE*.

- Hiratzka, L. F., Bakris, G. L., Beckman, J. A., Bersin, R. M., Carr, V. f., Casey Jr, D. E., Eagle, K. A., Hermann, L. K., Isselbacher, E. M., Kazerooni, E. A., Kouchoukos, N. T., Lytle, B. W., Milewicz, D. M., Reich, D. L., Sen, S., Shinn, J. A., Svensson, L. G., & Williams, D. M. (2010). 2010 ACCF/AHA/AATS/ACR/ASA/SCA/SCAI/SIR/STS/SVM Guidelines for the Diagnosis and Management of Patients With Thoracic Aortic Disease .A Report of the American College of Cardiology Foundation/American Heart Association Task Force on Practice Guidelines, American Association for Thoracic Surgery, American College of Radiology, American Stroke Association, Society of Cardiovascular Anesthesiologists, Society for Cardiovascular Angiography and Interventions, Society of Interventional Radiology, Society of Thoracic Surgeons, and Society for Vascular Medicine. *Circulation*, *121*: e266-e369.
- Hogendoorn, W., Hunink, M., Schlösser, F. J., Moll, F. L., Sumpio, B. E., & Muhs, B. E. (2014). A clinical decision model for selecting the most appropriate therapy for uncomplicated chronic dissections of the descending aorta. *Journal of Vascular Surgery*.
- Hou, G., Tsagakis, K., Wendt, D., Stühle, S., Jakob, H., & Kowalczyk, W. (2010). *Three-phase numerical simulation of blood flow in the ascending aorta with dissection*. Paper presented at the V European Conference on Computational Fluid Dynamics ECCOMAS CFD 2010, Lisbon, Portugal.
- Hughes, G. C., Ganapathi, A. M., Keenan, J. E., Englum, B. R., Hanna, J. M., Schechter, M. A., Wang, H., & McCann, R. L. (2014). Thoracic endovascular aortic repair for chronic DeBakey IIIb aortic dissection. *The Annals of Thoracic Surgery*, *98*(6): 2092-2098.
- Ince, H., & Nienaber, C. A. (2007). Diagnosis and management of patients with aortic dissection. *Heart*, *93*: 266-270.
- Jeong, J., & Hussain, F. (1995). On the identification of a vortex. *Journal of Fluid Mechanics*, *285*: 69-94.
- Juang, D., Braverman, A. C., & Eagle, K. (2008). Aortic dissection. *Circulation*, *118*: e507-e510.
- Kamman, A. V., Van Herwaarden, J. A., Orrico, M., Nauta, F. J., Heijmen, R. H., Moll, F. L., & Trimarchi, S. (2016). Standardized protocol to analyze computed tomography imaging of type B aortic dissections. *Journal of Endovascular Therapy*, *23*(3): 472-482.

- Karmonik, C., Bismuth, J., Davies, M. G., Shah, D. J., Younes, H. K., & Lumsden, A. B. (2011a). A computational fluid dynamics study pre- and post-stent graft placement in an acute type B aortic dissection. *Vascular and Endovascular Surgery*, 45(2): 157-164.
- Karmonik, C., Bismuth, J., Redel, T., Anaya-Ayala, J. E., Davies, M. G., Shah, D. J., & Lumsden, A. B. (2010). *Impact of tear location on hemodynamics in a type B aortic dissection investigated with computational fluid dynamics*. Paper presented at the 32nd Annual International Conference of the IEEE EMBS, Buenos Aires, Argentina.
- Karmonik, C., Bismuth, J., Shah, D. J., Davies, M. G., Purdy, D., & Lumsden, A. B. (2011b). Computational study of haemodynamic effects of entry- and exit- tear coverage in a DeBakey Type III aortic dissection : Technical report. *European Journal of Vascular Endovascular Surgery*, 42: 172-177.
- Karmonik, C., Partovi, S., Müller-Eschner, M., Bismuth, J., Davies, M. G., Shah, D. J., Loebe, M., Böckler, D., Lumsden, A. B., & Tengg-Kobligk, H. V. (2012). Longitudinal computational fluid dynamics study of aneurysmal dilation in a chronic DeBakey type III aortic dissection. *Journal of Vascular Surgery*, 56: 260-263.
- Karthikesalingam, A., Holt, P. J. E., Hinchliffe, R. J., Thompson, M. M., & Loftus, I. M. (2010). The diagnosis and management of aortic dissection. *Vasc Endovascular Surg*, 44(165): 165-169.
- Khan, I. A., & Nair, C. K. (2002). Clinical, diagnostic, and management perspectives of aortic dissection. *Chest*, 122(1): 311-328.
- Khanafer, K., & Berguer, R. (2009). Fluid-structure interaction analysis of turbulent pulsatile flow within a layered aortic wall as related to aortic dissection. *Journal of Biomechanics*, 42: 2642-2648.
- Khoynezhad, A., Walot, I., Kruse, M. J., Rapae, T., Donayre, C. E., & White, R. A. (2010). Distribution of intimomedial tears in patients with type B aortic dissection. *Journal of Vascular Surgery*, 52(3): 562-568.
- Kim, K. M., Donayre, C. E., Reynolds, T. S., Kopchok, G. E., Walot, I., Chauvapun, J. P., & White, R. A. (2011). Aortic remodeling, volumetric analysis, and clinical outcomes of endoluminal exclusion of acute complicated type B thoracic aortic dissections. *Journal of Vascular Surgery*, 54(2): 316-325.
- Kim, T. H., Ko, Y. G., Kwon, S. W., Choi, D., Lee, D. Y., Shim, W. H., & Hyon, M. S. (2014). Large false lumen area is a predictor of failed false lumen volume

reduction after stent-graft repair in type B aortic dissection. *Journal of Endovascular Therapy*, 21(5): 697-706.

Kusagawa, H., Shimono, T., Ishida, M., Suzuki, T., Yasuda, F., Yuasa, U., Onoda, K., Yada, I., Hirano, T., & Takeda, K. (2005). Changes in false lumen after transluminal stent-graft placement in aortic dissections six years' experience. *Circulation*, 111(22): 2951-2957.

Lam, S. K., Fung, G. S. K., Cheng, S. W. K., & Chow, K. W. (2008). A computational study on the biomechanical factors related to stent graft models in the thoracic aorta. *Medical & Biological Engineering & Computing*, 46: 1129-1138.

Lee, M., Lee, D. Y., Kim, M. D., Lee, M. S., Won, J. Y., Park, S. I., Yoon, Y. N., Lee, S., Choi, D., & Ko, Y.-G. (2013). Outcomes of endovascular management for complicated chronic type B aortic dissection: effect of the extent of stent graft coverage and anatomic properties of aortic dissection. *Journal of Vascular and Interventional Radiology*, 24(10): 1451-1460.

Leshnower, B. G., Szeto, W. Y., Pochettino, A., Desai, N. D., Moeller, P. J., Nathan, D. P., Jackson, B. M., Woo, E. Y., Fairman, R. M., & Bavaria, J. E. (2013). Thoracic endografting reduces morbidity and remodels the thoracic aorta in DeBakey III aneurysms. *The Annals of Thoracic Surgery*, 95(3): 914-921.

Liffman, K., Lawrence-Brown, M., Semmens, J. B., Bui, A., Rudman, M., & Hartley, D. E. (2001). Analytical modeling and numerical simulation of forces in an endoluminal graft. *Journal of Endovascular Therapy*, 8: 358-371.

Litmanovich, D., Bankier, A. A., Cantin, L., Raptopoulos, V., & Boiselle, P. M. (2009). CT and MRI in diseases of the aorta. *American Journal of Roentgenology*, 193(4): 928-940.

Loerakker, S., Cox, L. G. E., Van Heijst, G. J. F., de Mol, B. A. J. M., & Van de Vosse, F. N. (2008). Influence of dilated cardiomyopathy and a left ventricular assist device on vortex dynamics in the left ventricle. *Computer Methods in Biomechanics and Biomechanical Engineering*, 11(6): 649-660.

Manning, B. J., Dias, N., Manno, M., Ohrlander, T., Malina, M., Sonesson, B., Resch, T., & Ivancev, K. (2009). Endovascular treatment of acute complicated type B dissection: morphological changes at midterm follow-up. *Journal of Endovascular Therapy*, 16(4): 466-474.

Marui, A., Mochizuki, T., Mitsui, N., Koyama, T., Kimura, F., & Horibe, M. (1999). Toward the best treatment for uncomplicated patients with type B acute aortic

dissection : A consideration for sound surgical indication. *Circulation*, 100(II-275-Ii-280).

Mehta, R. H., Bossone, E., Evangelista, A., O'gara, P. T., Smith, D. E., Cooper, J. V., Oh, J. K., Januzzi, J. L., Hutchison, S., Gilon, D., Pape, L. A., Nienaber, C. A., Isselbacher, E. M., & Eagle, K. A. (2004). Acute Type B Aortic Dissection in Elderly Patients: Clinical Features, Outcomes, and Simple Risk Stratification Rule. *The Annals Thoracic Surgery*, 77: 1622-1629.

Menichini, C., Cheng, Z., Gibbs, R. G., & Xu, X. Y. (2016). Predicting false lumen thrombosis in patient-specific models of aortic dissection. *Journal of The Royal Society Interface*, 13(124): 20160759.

Menichini, C., & Xu, X. Y. (2016). Mathematical modeling of thrombus formation in idealized models of aortic dissection: initial findings and potential applications. *Journal of Mathematical Biology*, 73(5): 1205-1226.

Midulla, M., Moreno, R., Baali, A., Chau, M., Negre-Salvayre, A., Nicoud, F., Pruvo, J. P., Haulon, S., & Rousseau, H. (2012). Haemodynamic imaging of thoracic stent-grafts by computational fluid dynamics (CFD): presentation of a patient-specific method combining magnetic resonance imaging and numerical simulations. *European Radiology*, 22: 2094-2102.

Mohan, I. V., Harris, P. L., Marrewijk, C. J., Laheij, R. J., & How, T. V. (2002). Factors and forces influencing stent graft migration after endovascular aortic aneurysm repair. *Journal of Endovascular Therapy*, 9: 748-755.

Morris, L., Delassus, P., Callanan, A., Walsh, M., Wallis, F., Grace, P., & McGloughlin, T. (2005). 3-D Numerical Simulation of blood flow through models of the human aorta. *Journal of Biomechanical Engineering*, 127(5): 767-775.

Morris, L., Delassus, P., Grace, P., Wallis, F., Walsh, M., & McGloughlin, T. (2006). Effects of flat, parabolic and realistic steady flow inlet profiles on idealised and realistic stent graft fits through abdominal aortic aneurysm (AAA). *Medical Engineering and Physics*, 28: 19-26.

Nerem, R., Seed, W. A., & Wood, N. B. (1972). An experimental study of the velocity distribution and transition to turbulence in the aorta. *Journal of Fluid Mechanics*, 52: 137-160.

Olufsen, M. S., Charles S. Peskin, Won Yong Kim, Pedeson, E. M., Nadim, A., & Larsen, J. (2000). Numerical simulation and experimental validation of blood

flow in arteries with structured-tree outflow conditions. *Annals of Biomedical Engineering*, 28: 1281-1299.

Palma, J. H., Almeida, D. R., Carvalho, A. C., Andrade, J. C. S., & Buffolo, E. (1997). Surgical treatment of acute type B aortic dissection using an endoprosthesis. *The Annals of Thoracic Surgery*, 63: 1081-1084.

Panneton, J. M., Teh, S. H., Cherry Jr, K. J., Hofer, J. M., Gloviczki, P., & Andrews, J. C. (2000). Aortic fenestration for acute or chronic aortic dissection : An uncommon but effective procedure. *Journal of Vascular Surgery*, 32: 711-721.

Parr, A., Jayaratne, C., Buttner, P., & Golledge, J. (2011). Comparison of volume and diameter measurement in assessing small abdominal aortic aneurysm expansion examined using computed tomographic angiography. *European Journal of Radiology*, 79(1): 42-47.

Patterson, B. O., Vidal-Diez, A., Karthikesalingam, A., Holt, P. J., Loftus, I. M., & Thompson, M. M. (2015). Comparison of aortic diameter and area after endovascular treatment of aortic dissection. *The Annals of Thoracic Surgery*, 99(1): 95-102.

Pierakos, O., & Vlachos, P. P. (2006). The effect of vortex formation on left ventricular filling and mitral valve efficiency. *Journal of Biomechanical Engineering*, 128: 527-539.

Qiao, A., Gu, Z., & Meng, X. (2008). *Simulation of hemodynamics in bypassed aortic dissection*. Paper presented at the The 2nd International Conference on Bioinformatics and Biomedical Engineering, Shanghai.

Qin, Y.-L., Deng, G., Li, T. X., Jing, R. W., & Teng, G. J. (2012). Risk factors of incomplete thrombosis in the false lumen after endovascular treatment of extensive acute type B aortic dissection. *Journal of Vascular Surgery*, 56(5): 1232-1238.

Qin, Y. L., Wang, F., Li, T. X., Ding, W., Deng, G., Xie, B., & Teng, G. J. (2016). Endovascular repair compared with medical management of patients with uncomplicated type B acute aortic dissection. *Journal of the American College of Cardiology*, 67(24): 2835-2842.

Qing, K.-x., Yiu, W.-k., & Cheng, S. W. (2012). A morphologic study of chronic type B aortic dissections and aneurysms after thoracic endovascular stent grafting. *Journal of Vascular Surgery*, 55(5): 1268-1276.

- Quint, L. E., Platt, J. F., Sonnad, S. S., Deeb, G. M., & Williams, D. M. (2009). Aortic intimal tears: detection with spiral computed tomography. *Journal of Endovascular Therapy*, 10(3), 505-510.
- Raz, S., Einav, S., Alemu, Y., & Bluestein, D. (2007). DPIV prediction of flow induced platelet activation-Comparison to numerical predictions. *Annals of Biomedical Engineering*, 35(4): 493-504.
- Rodriguez, J. A., Olsen, D. M., Lucas, L., Wheatley, G., Ramaiah, V., & Diethrich, E. B. (2008). Aortic remodeling after endografting of thoracoabdominal aortic dissection. *Journal of Vascular Surgery*, 47(6): 1188-1194.
- Rudenick, P. A., Bijmens, B. H., García-Dorado, D., & Evangelista, A. (2013). An in vitro phantom study on the influence of tear size and configuration on the hemodynamics of the lumina in chronic type B aortic dissections. *Journal of Vascular Surgery*, 57(2): 464-474.
- Rudenick, P. A., Bordone, M., Bijmens, B. H., Soudah, E., Onate, E., Garcia-Dorado, D., & Evangelista, A. (2010). *A multi-method approach towards understanding the pathophysiology of aortic dissections - the complementary role of in silico, in vitro and in vivo information*. Paper presented at the STACOM -CESC 2010, LNCS 6364, Berlin.
- Sayer, D., Bratby, M., Brooks, M., Loftus, I., Morgan, R., & Thompson, M. (2008). Aortic morphology following endovascular repair of acute and chronic type B aortic dissection: implications for management. *European Journal of Vascular and Endovascular Surgery*, 36(5): 522-529.
- Schoder, M., Czerny, M., Cejna, M., Rand, T., Stadler, A., Sodeck, G. H., Gottardi, R., Loewe, C., & Lammer, J. (2007). Endovascular repair of acute type B aortic dissection: long-term follow-up of true and false lumen diameter changes. *The Annals of Thoracic Surgery*, 83(3): 1059-1066.
- Shahcheraghi, N., Dwyer, H. A., Cheer, A. Y., Barakat, A. I., & Rutaganira, T. (2002). Unsteady and three-dimensional simulation of blood flow in the human aortic arch. *Journal of Biomechanical Engineering*, 124: 378-387.
- Shinohara, T., Suzuki, K., Okada, M., Shiigai, M., Shimizu, M., Maehara, T., & Ohsuzu, F. (2003). Soluble elastin fragments in serum are elevated in acute aortic dissection. *Arteriosclerosis, Thrombosis, and Vascular Biology*, 23(1839-1844).
- Simon, C., Liu, W., Wong, R. H., Underwood, M., & Wang, D. (2016). The potential of computational fluid dynamics simulation on serial monitoring of hemodynamic

change in type B aortic dissection. *Cardiovascular and Interventional Radiology*, 39(8): 1090-1098.

- Song, S. W., Kim, T. H., Lim, S. H., Lee, K. H., Yoo, K. J., & Cho, B. K. (2014). Prognostic factors for aorta remodeling after thoracic endovascular aortic repair of complicated chronic DeBakey IIIb aneurysms. *The Journal of Thoracic and Cardiovascular Surgery*, 148(3): 925-933. e921.
- Stanley, G. A., Murphy, E. H., Knowles, M., Ilves, M., Jessen, M. E., Dimaio, J. M., Modrall, J. G., & Arko, F. R. (2011). Volumetric analysis of type B aortic dissections treated with thoracic endovascular aortic repair. *Journal of Vascular Surgery*, 54(4): 985-992.
- Steingruber, I. E., Chemelli, A., Glodny, B., Hugl, B., Bonatti, J., Hiemetzbeger, R., Jaschke, W., & Czermak, B. V. (2008). Endovascular repair of acute type B aortic dissection: midterm results. *Journal of Endovascular Therapy*, 15(2): 150-160.
- Sueyoshi, E., Sakamoto, I., & Uetani, M. (2009). Growth rate of affected aorta in patients with type B partially closed aortic dissection. *The Annals of Thoracic Surgery*, 88(4): 1251-1257.
- Sun, Z., & Chaichana, T. (2016). A systematic review of computational fluid dynamics in type B aortic dissection. *International Journal of Cardiology*, 210: 28-31.
- Suzuki, T., Mehta, R. H., Ince, H., Nagai, R., Sakomura, Y., Weber, F., Sumiyoshi, T., Bossone, E., Trimarchi, S., Cooper, J. V., Smith, D. E., Isselbacher, E. M., Eagle, K. A., & Nienaber, C. A. (2003). Clinical profiles and outcomes of acute type B aortic dissection in the current era: Lessons from the International Registry of Aortic Dissection (IRAD). *Circulation*, 108: II-312-II-317.
- Svensson, L. G., Kouchoukos, N. T., & Miller, D. C. (2008). Expert consensus document on the treatment of descending thoracic aortic disease using endovascular stent-grafts. *The Annals of Thoracic Surgery*, 85: S1-45.
- Tan, F. P. P., Borghi, A., Mohiaddin, R. H., Wood, N. B., Thom, S., & Xu, X. Y. (2009). Analysis of flow patterns in a patient-specific thoracic aortic aneurysm model. *Computers and Structures*, 87: 680-690.
- Tang, A. Y. S., Fan, Y., Cheng, S. W. K., & Chow, K. W. (2012). Biomechanical factors influencing type B thoracic aortic dissection : Computational fluid dynamics study. *Engineering Applications of Computational Fluid Mechanics* 6(4): 622-632.

- Thrumurthy, S., Karthikesalingam, A., Patterson, B., Holt, P., Hinchliffe, R., Loftus, I., & Thompson, M. (2011). A systematic review of mid-term outcomes of thoracic endovascular repair (TEVAR) of chronic type B aortic dissection. *European Journal of Vascular and Endovascular Surgery*, 42(5): 632-647.
- Thrumurthy, S. G., Karthikesalingam, A., Patterson, B. O., Holt, P. J. E., & Thompson, M. M. (2012). The diagnosis and management of aortic dissection. *BMJ*, 344.
- Tolenaar, J. L., Kern, J. A., Jonker, F. H., Cherry, K. J., Tracci, M. C., Angle, J. F., Sabri, S., Trimarchi, S., Strider, D., & Alaiwaidi, G. (2014). Predictors of false lumen thrombosis in type B aortic dissection treated with TEVAR. *Annals of Cardiothoracic Surgery*, 3(3): 255-263.
- Trimarchi, S., Nienaber, C. A., Rampoldi, V., Myrmel, T., Suzuki, T., Bossone, E., Tolva, V., Deeb, M. G., Upchurch, G. R., Cooper, J. V., Fang, J., Isselbacher, E. M., Sundt, T. M., & Eagle, K. A. (2006). Role and results of surgery in acute type B aortic dissection: Insights from the International Registry of Acute Aortic Dissection (IRAD). *Circulation*: I-357-I-364.
- Trimarchi, S., Tolenaar, J. L., Jonker, F. H., Murray, B., Tsai, T. T., Eagle, K. A., Rampoldi, V., Verhagen, H. J., van Herwaarden, J. A., & Moll, F. L. (2013). Importance of false lumen thrombosis in type B aortic dissection prognosis. *The Journal of Thoracic and Cardiovascular Surgery*, 145(3): S208-S212.
- Tsai, T. T., Evangelista, A., Nienaber, C. A., Myrmel, T., Meinhardt, G., Cooper, J. V., Smith, D. E., Suzuki, T., Fattori, R., & Llovet, A. (2007). Partial thrombosis of the false lumen in patients with acute type B aortic dissection. *New England Journal of Medicine*, 357(4): 349-359.
- Tsai, T. T., Nienaber, C. A., & Eagle, K. A. (2005). Acute aortic syndrome. *Circulation*, 112: 3802-3813.
- Tsai, T. T., Schlicht, M. S., Khanafer, K., Bull, J. L., Valassis, D. T., Williams, D. M., Berguer, R., & Eagle, K. A. (2008). Tear size and location impacts false lumen pressure in an ex vivo model of chronic type B aortic dissection. *Journal of Vascular Surgery* 47: 844-851.
- Tse, K. W., Chiu, P., Lee, H. P., & Ho, P. (2011). Investigation of hemodynamics in the development of dissecting aneurysm within patient-specific dissecting aneurysmal aortas using computational fluid dynamics (CFD) simulations. *Journal of Biomechanics*, 44: 827-836.
- Van Doormaal, M. A., Kazakidi, A., Wylezinska, M., Hunt, A., Tremoleda, J. L., Protti, A., Bohraus, Y., Gsell, W., Weinberg, P. D., & Ethier, C. R. (2012).

Haemodynamics in the mouse aortic arch computed from MRI-derived velocities at the aortic root. *Journal of The Royal Society Interface*: 1-11.

- Vignon-Clementel, I. E., Figueroa, C. A., Jansen, K. E., & Taylor, C. A. (2006). Outflow boundary conditions for three-dimensional finite element modeling of blood flow and pressure in arteries. *Computer Methods in Applied Mechanics and Engineering*, 195(29): 3776-3796.
- Wen, C. Y., Yang, A. S., Tseng, L. Y., & Chai, J. W. (2010). Investigation of pulsatile flowfield in healthy thoracic aorta models. *Annals of Biomedical Engineering*, 38(2): 391-402.
- Weng, S. H., Weng, C. F., Chen, W. Y., Huang, C. Y., Chen, I., Chen, C. K., Hsu, C. P., & Shih, C. C. (2013). Reintervention for distal stent graft-induced new entry after endovascular repair with a stainless steel-based device in aortic dissection. *Journal of vascular surgery*, 57(1): 64-71.
- Wever, J., Blankensteijn, J., Mali, W. T. M., & Eikelboom, B. (2000). Maximal aneurysm diameter follow-up is inadequate after endovascular abdominal aortic aneurysm repair. *European Journal of Vascular and Endovascular Surgery*, 20(2): 177-182.
- Won, J. Y., & Lee, D. Y. (2006). Problems encountered during and after stent-graft treatment of aortic dissection. In H. Roussesau, P. Verhoye & F. Heautot (Eds.), *Thoracic Aortic Diseases*: Springer.

## LIST OF PUBLICATIONS AND PAPERS PRESENTED

### Journal Articles:

1. Wan Ab Naim, W. N., Ganesan, P. B., Sun, Z., Chee, K. H., Hashim, S. A., & Lim, E. (2014). A perspective review on numerical simulations of hemodynamics in aortic dissection. *The Scientific World Journal*, 2014.
2. Wan Ab Naim, W. N., Ganesan, P. B., Sun, Z., Liew, Y. M., Qian, Y., Lee, C. J., Jansen, S., Hashim, S. A., & Lim, E. (2016). Prediction of thrombus formation using vortical structures presentation in Stanford type B aortic dissection: a preliminary study using CFD approach. *Applied Mathematical Modelling*, 40(4): 3115-3127.
3. Wan Ab Naim, W. N., Ganesan, P. B., Sun, Z., Lei, J., Jansen, S., Hashim, S.A., Ho, T.K., & Lim, E. (2018). Flow pattern analysis in Stanford Type B aortic dissection patients after stent-grafting repair: Comparison between complete and incomplete false lumen thrombosis. *International Journal for Numerical Methods in Biomedical Engineering*.

### Proceedings:

1. Wan Ab Naim, W.N., Ganesan, P.B., Sun, Z., Lei, J., Jansen, S., & Lim, E. (2016). Comparison between diametric and volumetric changes in true lumen for Stanford Type B aortic dissection patients. Poster presentation at the 16th International Conference on Biomedical Engineering (ICBME 2016) in National University of Singapore, Singapore.